

OXIDATION STATES OF TRACE ELEMENTS IN SYNTHETIC CORUNDUM



A Thesis Submitted in Partial Fulfillment of the Requirements
for the Degree of Master of Science in Earth Sciences

Department of Geology

Faculty of Science

Chulalongkorn University

Academic Year 2019

Copyright of Chulalongkorn University

ระดับออกซีเดชันของมลทินในพลอยสังเคราะห์



วิทยานิพนธ์นี้เป็นส่วนหนึ่งของการศึกษาตามหลักสูตรปริญญาวิทยาศาสตรมหาบัณฑิต
สาขาวิชาโลกศาสตร์ ภาควิชาธรณีวิทยา
คณะวิทยาศาสตร์ จุฬาลงกรณ์มหาวิทยาลัย
ปีการศึกษา 2562
ลิขสิทธิ์ของจุฬาลงกรณ์มหาวิทยาลัย

Thesis Title	OXIDATION STATES OF TRACE ELEMENTS IN SYNTHETIC CORUNDUM
By	Miss Ontima Yamchuti
Field of Study	Earth Sciences
Thesis Advisor	Assistant Professor WARUNTORN KANITPANYACHAROEN, Ph.D.
Thesis Co Advisor	Associate Professor CHAKKAPHAN SUTTHIRAT, Ph.D.

Accepted by the Faculty of Science, Chulalongkorn University in Partial
Fulfillment of the Requirement for the Master of Science

..... Dean of the Faculty of Science
(Professor POLKIT SANGVANICH, Ph.D.)

THESIS COMMITTEE

..... Chairman
(Associate Professor SRILERT CHOTPANTARAT, Ph.D.)

..... Thesis Advisor
(Assistant Professor WARUNTORN KANITPANYACHAROEN,
Ph.D.)

..... Thesis Co-Advisor
(Associate Professor CHAKKAPHAN SUTTHIRAT, Ph.D.)

..... Examiner
(Associate Professor SANTI PAILOPLEE, Ph.D.)

..... External Examiner
(Associate Professor Visut Pisutha-Armond, Ph.D.)

อรธิตา แยมซุติ : ระดับออกซิเดชันของมลทินในพลอยสังเคราะห์. (

OXIDATION STATES OF TRACE ELEMENTS IN SYNTHETIC CORUNDUM) อ.ที่

ปรึกษาหลัก : ผศ. ดร.วรัญทร คณิตปัญญาเจริญ, อ.ที่ปรึกษาร่วม : รศ. ดร.จักรพันธ์

สุทธิรัตน์

คอร์ันดัมในธรรมชาติ และ ที่สังเคราะห์ขึ้น มีสีที่หลายหลากแตกต่างกันเนื่องจากธาตุมลทินให้สีและไม่ให้สีภายในโครงสร้าง แม้จะมีงานวิจัยมากมายเกี่ยวกับธาตุมลทินในคอร์ันดัมตามธรรมชาติ แต่สำหรับองค์ประกอบของธาตุมลทินในคอร์ันดัมสังเคราะห์นั้นยังมีการศึกษาไม่มากนัก งานวิจัยนี้จึงมีวัตถุประสงค์เพื่อหาปริมาณธาตุมลทิน และ ระบุสถานะการเกิดออกซิเดชันที่เกี่ยวข้องกับการเกิดสีในคอร์ันดัมสังเคราะห์ โดยได้ทำการตรวจสอบตัวอย่างคอร์ันดัมจำนวน 15 ตัวอย่าง ในกลุ่ม 3กลุ่มสีคือ สีแดง สีน้ำเงิน และ สีเหลือง ที่สังเคราะห์โดยกระบวนการหลอมเหลวด้วยเปลวไฟ ทำการวิเคราะห์ด้วยเทคนิคขั้นสูง โดยผลจากการทดลอง X-ray Diffraction บ่งชี้ว่าคอร์ันดัมสังเคราะห์ที่นำมาเป็นตัวอย่างสำหรับการวิจัยนี้มีองค์ประกอบของผลึกเป็น Al_2O_3 และ ผลการทดลองจาก Electron Probe Micro-Analyzer, UV-Vis-NIR spectroscopy และ X-ray Absorption Near Edge Structure spectrometry พบว่า Cr^{3+} เป็นองค์ประกอบธาตุร่องรอยที่สำคัญก่อให้เกิดสีแดงในคอร์ันดัม โดยปริมาณเพียงเล็กน้อยของ Cr^{3+} เมื่อเข้าไปแทนที่ในบางตำแหน่งของ Al^{3+} ภายในโครงสร้างของคอร์ันดัมก่อให้เกิดสีแดง โดยการเปลี่ยนระดับพลังงานของอิเล็กตรอนเดี่ยวใน d -orbital จากพลังงานต่ำไปยังพลังงานสูง ตามทฤษฎี crystal field ทำให้เกิดการดูดกลืนช่วง 552-580 nm และที่น่าสนใจเมื่อตรวจพบว่าปริมาณของ V^{3+} ส่งผลให้เกิดสีม่วงในตัวอย่างคอร์ันดัมสังเคราะห์ นอกจากนี้การถ่ายโอนประจุระหว่าง Fe^{2+} และ Ti^{4+} นำไปสู่การดูดกลืนแสงในช่วง 576-590 nm ซึ่งเป็นช่วงการดูดกลืนที่ทำให้เกิดสีน้ำเงินในคอร์ันดัมสังเคราะห์ สีน้ำเงิน สำหรับคอร์ันดัมสังเคราะห์สีเหลืองพบว่าองค์ประกอบที่สำคัญ ได้แก่ Cr^{3+} และ Ni โดยแนวโน้ม Ni จะเป็นธาตุที่ก่อให้เกิดสีเหลือง จากช่องว่างที่เกิดขึ้นในตำแหน่งของออกซิเจนภายในโครงสร้าง หรือ ศูนย์กลางการเกิดสีแบบหลุมอิเล็กตรอน เป็นสาเหตุการดูดกลืนในช่วง 402-420 nm

สาขาวิชา โลกศาสตร์

ลายมือชื่อนิสิต

ปีการศึกษา 2562

ลายมือชื่อ อ.ที่ปรึกษาหลัก

ลายมือชื่อ อ.ที่ปรึกษาร่วม

5872153323 : MAJOR EARTH SCIENCES

KEYWORD:

Ontima Yamchuti : OXIDATION STATES OF TRACE ELEMENTS
IN SYNTHETIC CORUNDUM. Advisor: Asst. Prof. WARUNTORN
KANITPANYACHAROEN, Ph.D. Co-advisor: Assoc. Prof. CHAKKAPHAN
SUTTHIRAT, Ph.D.

Natural and synthetic corundums have various colors due to trace elements in their structures. Despite the abundance of research on impurities in natural corundum, little is known about trace elements in synthetic corundum. This project is aimed to quantify trace elements and identify their oxidation states related to coloration in red, blue, and yellow synthetic corundums. A total of 15 corundums, synthesized by melt growth process, were investigated by advanced analytical techniques. X-ray diffraction results indicate that all synthetic corundums contain crystalline Al_2O_3 . Measurements from Electron Probe Micro-Analyzer, UV-Vis-NIR, and X-ray Absorption Near Edge Structure spectrometry suggest that Cr^{3+} is significant trace element in red samples. A small amount of Cr^{3+} substitutes in some Al^{3+} sites in corundum structure. Cr^{3+} has unpaired electrons, which can be excited and cause light absorption around 552-580 nm, resulting in red color. Interestingly, a high amount of V^{3+} is detected in a few red samples and contributed to a unique purple shade. In addition, the electron charge transfer between Fe^{2+} and Ti^{4+} pair leads to the absorption around 576-590 nm, causing blue light transmission. Yellow samples have Ni and Cr^{3+} as major trace elements. Ni is likely the cause of yellow color due to a vacancy in oxygen position or trapped electron hole color center, leading to light absorption around 402-420 nm in synthetic samples.

Field of Study: Earth Sciences

Student's Signature

Academic Year: 2019

Advisor's Signature

Co-advisor's Signature

ACKNOWLEDGEMENTS

This thesis cannot succeed without the support from these individuals. Therefore, I would like to appreciate all of them.

First, I would like to thank you, my advisor, Asst. Prof. Dr. Waruntorn Kanitpanyacharoen for hard working and advised me not only for work but also teach me about life and inspire me to be the better person. Moreover, I would like to thank you, my co-advisor, Assoc. Prof. Dr. Chakkaphan Sutthirat for advised me about gemstone and give me a chance to do this research. I really appreciate both of you from my sincere gratitude.

Second, I would like to thank you Department of geology, Chulalongkorn University for XRD and EPMA measurement. Indispensable the beamline 8 stations, Synchrotron light research institute (SLRI), Thailand for XANES measurement and The Gem and Jewelry Institute of Thailand (GIT) for UV-VIS-NIR measurement. Includes all staff persons to help this research.

Next, I would like to thank you Silpakorn University for preaching me everything before.

Finally, I would like to thank you, my family and my friends. For my lovely family thank you so much for your support and always trust me it that means a lot. For my friends, I don't know how to thank you for your support and kindness towards me, including assistance and always beside me on my bad day. The thing made me grateful thank you from my deep in heart.

Ontima Yamchuti

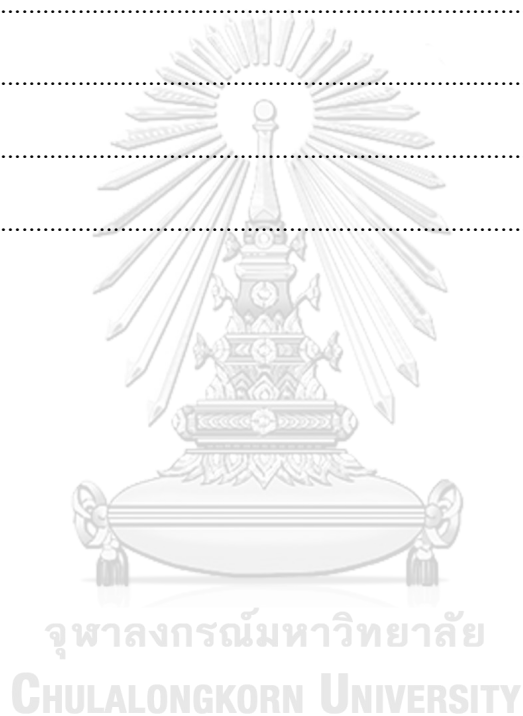
TABLE OF CONTENTS

	Page
.....	iii
ABSTRACT (THAI).....	iii
.....	iv
ABSTRACT (ENGLISH).....	iv
ACKNOWLEDGEMENTS.....	v
TABLE OF CONTENTS.....	vi
LIST OF TABLES.....	x
LIST OF FIGURES.....	xii
CHAPTER 1 Introduction.....	1
1.1. Introduction.....	1
1.2 Research objectives.....	5
1.3 Scope of study.....	5
CHAPTER 2.....	6
Literature Review.....	6
2.1 The cause of color.....	6
2.1.1 Crystal field theory.....	7
2.1.2 Charge transfer.....	9
2.1.3 Color center.....	11
2.2 Previous works.....	13
2.2.1 Red synthetic corundums.....	13
2.2.2 Blue synthetic corundums.....	15

2.2.3 Yellow synthetic corundums.....	16
CHAPTER 3.....	19
Methodology	19
3.1 X-Ray Diffraction (XRD).....	19
3.1.1 Theory of XRD	19
3.1.2 Experimental conditions for XRD.....	20
3.2 UV-Vis-NIR spectroscopy	21
3.2.1 Theory of UV-Vis-NIR	21
3.2.2 Experimental conditions for UV-Vis-NIR	21
3.3 Electron Probe Micro-Analyzer (EPMA).....	22
3.3.1 Theory of EPMA.....	22
3.3.2 Experimental conditions for EPMA.....	22
3.4 X-ray Absorption Near Edge Structure spectrometry (XANES).....	23
3.4.1 Theory of XANES.....	23
3.4.2 Experimental conditions for XANES	25
CHAPTER 4.....	27
Results.....	27
4.1 Red synthetic corundum	27
4.1.1 XRD Experiment	27
4.1.2 EPMA Experiment.....	28
4.1.3 UV-Vis-NIR Experiment	30
4.1.4 XANES Experiment.....	33
4.2 Blue synthetic corundum	36
4.2.1 EPMA Experiment.....	36

4.2.2 UV-Vis-NIR Experiment	39
4.2.3 XANES Experiment	41
4.3 Yellow synthetic corundum	43
4.3.1 EPMA Experiment	43
4.3.2 UV-Vis-NIR Experiment	46
4.3.3 XANES Experiment	48
Chapter 5	50
Discussion	50
5.1 Red synthetic corundum	50
5.1.1 Type and oxidation state of trace elements	50
5.1.2 Cause of red color	52
5.1.3 Comparison with previous studies	56
5.2 Blue synthetic corundum	57
5.2.1 Type and oxidation state of trace elements	57
5.2.2 Cause of blue color	59
5.2.3 Comparison with previous studies	60
5.3 Yellow synthetic corundum	61
5.3.1. Type and oxidation state of trace elements	61
5.3.2 Cause of yellow color	62
5.3.3 Comparison with previous studies	63
Chapter 6	66
Conclusion	66
6.1 Red synthetic corundums	66
6.2 Blue synthetic corundum samples	66

6.3 Yellow synthetic corundum samples	67
6.4 Further study.....	67
APPENDIX.....	68
APPENDIX A	68
APPENDIX B	69
APPENDIX C	72
APPENDIX D.....	73
APPENDIX E.....	76
REFERENCES	77
VITA.....	85



LIST OF TABLES

	Page
Table 1 The standards of XANES experiment	26
Table 2 The average amount of trace elements (wt%) based on six spot analyses in each red synthetic corundum (R1-R5).....	29
Table 3 The average atomic proportion of red synthetic corundum R1-R5.....	29
Table 4 A comparison of UV-Vis-NIR absorption of Cr ³⁺ and V ³⁺ between previous studies and this study.....	33
Table 5 The average amount of trace elements (wt%) based on six spot analyses in each blue synthetic corundum (B1-B5).	37
Table 6 The average atomic proportion of blue synthetic corundum B1-B5.	38
Table 7 A comparison of UV-Vis-NIR absorptions of Fe ²⁺ -Ti ⁴⁺ pair between previous studies and this study.....	41
Table 8 Average EPMA analyses based on selective six spot analyses in each yellow synthetic corundum (Y1-Y5).	44
Table 9 Average atomic proportions of major and trace elements in synthetic yellow corundum samples Y1-Y5.....	45
Table 10 A comparison of UV-Vis-NIR absorption values of Cr ³⁺ , Ni ²⁺ , and Ni ³⁺ between previous studies and this study.....	48
Table 11 The range of absorption color in visible light	52
Table 12 Comparison the oxidation state of trace elements in red synthetic corundum samples between previous studies and this study.	57
Table 13 Comparison the oxidation state of trace elements in blue synthetic corundum samples between previous studies and this study.	61

Table 14 Comparison the oxidation state of trace elements in yellow synthetic corundum samples between previous studies and this study.	65
--	----



LIST OF FIGURES

	Page
Figure 1 A comparison between of natural corundum (a) and synthetic corundum samples (b).....	2
Figure 2 A diagram of flame fusion or Verneuil process to make synthetic corundum	3
Figure 3 The Al_2O_3 lattice in corundum. The blue circle is the aluminum (Al) atom and the red circles are oxygen (O) atoms. (Bristow et al., 2014).....	7
Figure 4 The splitting of d-orbital diagram in octahedron structure. Δ_0 refer to crystal field splitting energy. Available from: chem.libretexts.org.....	8
Figure 5 The color change in sapphire (a) Bluish color in daylight (b) Violetish red in incandescent light. (Gübelin et al., 1992).....	9
Figure 6 The electron charge transfer diagram in sapphire. Credit from: Na-Phattalung et al., 2018.....	10
Figure 7 The transition from the ground state to the excited state in blue sapphire. (Nassau, 1987).....	10
Figure 8 A) Normal structure of fluorite and B) an electron replacing F ion to create electron color center. Available from: webexhibits.org.....	11
Figure 9 A) Normal structure of quartz (SiO_2) and B) an electron missing caused by irradiation to create hole color center. Available from: webexhibits.org.....	12
Figure 10 The alexandrite effect in synthetic corundum (a) bluish purple in daylight (b) red-purple in incandescent light. Available from: alexandrite.net	15
Figure 11 The synthetic corundum by Verneuil technique. Available from: ruby-sapphire.com	18
Figure 12 Synthetic corundum samples (a) red sample set (R1-R5), (b) blue sample set (B1-B5), (c) yellow sample set (Y1-Y5).....	19

Figure 13 Schematic diagram of X-ray diffraction (XRD). Available from: met.reading.ac.uk.....	20
Figure 14 A diagram of UV-Vis-NIR spectroscopy (UV-Vis-NIR) Available from: saif.iitm.ac.in.....	21
Figure 15 Mode of Electron probe micro-analyzer (EPMA) (Chatterjee, 2012).....	22
Figure 16 Synthetic corundum samples in epoxy resin showing different spots of the analysis; six different spots for the red samples (white spots), twelve different spots for the blue samples (yellow spots at the rim and grey spots at the inner of the boule), and twelve different spots for yellow samples (black spots at the rim and the grey spots at the inner of the boule).....	23
Figure 17 Model of synchrotron light of XANES. Available from: ssrl.slac.stanford.edu	24
Figure 18 A diagram of XANES results. Available from: cei.washington.edu	25
Figure 19 X-ray diffraction patterns of red (bottom), blue (middle), and yellow (top) samples show similarly the main peaks of corundum (Al_2O_3).....	27
Figure 20 Red synthetic corundum samples: R1 (deep red); R2 (pinkish red); R3 (pinkish red); R4 (pinkish red); R5 (purplish red).....	28
Figure 21 Atomic proportions of Cr and V in the red samples (R1-R5) from EPMA analyses.	30
Figure 22 UV-Vis-NIR absorption spectra (O-ray) of red samples: (a) R1 in deep red, (b) R2 in pinkish red, (c) R3 in pinkish red, (d) R4 in pinkish red, and (e) R5 in purplish red.	32
Figure 23 XANES absorption edges of red samples (a) R1, (b) R2, (c) R3, (d) R4, and (e) R5. The solid red line represents the absorption of samples, the dash-dotted line represents the absorption of the standard CrO_3 (Cr^{6+}), and the dash line represents the absorption of the standard Cr_2O_3 (Cr^{3+}). The main absorption edge is marked by a gray vertical line.....	35

Figure 24 Blue synthetic sapphire samples: B1 (pale blue); B2 (pale blue); B3 (blue); B4 (pale blue); B5 (deep blue).....	36
Figure 25 Atomic proportions of Ti and Fe in the blue samples (B1-B5) from EPMA analyses.	39
Figure 26 UV-Vis-NIR absorption spectra (O-ray) of blue synthetic corundum samples: (a) pale blue B1, (b) pale blue B2, (c) blue B3, (d) pale blue B4, and (e) deep blue B5.	40
Figure 27 XANES absorption near edge of blue samples (a) B1, (b) B2, (c) B3, (d) B4, and (e) B5; the solid blue line represents the absorption of samples, dotted line represents the absorption of the standard Ti_2O_3 (Ti^{3+}), dash-dotted line represents the absorption of the standard TiO_2 (Ti^{4+}) (anatase), and dash line represents the absorption of the standard TiO_2 (Ti^{4+}) (rutile). The main absorption edge is marked by a gray vertical line.	42
Figure 28 Yellow synthetic corundum samples: Y1 (pale yellow); Y2 (orangish yellow); Y3 (orangish yellow); Y4 (yellow); Y5 (orangish yellow).	43
Figure 29 Atomic proportions of Cr and Ni in the yellow samples (Y1-Y5) from EPMA experiment.....	46
Figure 30 UV-Vis-NIR absorption spectra (O-ray) of yellow samples: (a) pale yellow Y1, (b) orangish yellow Y2, (c) orangish yellow Y3, (d) yellow Y4, and (e) orangish yellow Y5.....	47
Figure 31 XANES absorption of yellow samples (a) Y1, (b) Y2, (c) Y3, (d) Y4, and (e) Y5. The solid line represents the absorption of yellow samples, the dotted line represents the absorption of the standard Fe_2O_3 (Fe^{3+}), dash-dotted line represents the absorption of the standard Fe_3O_4 (Fe^{2+} , Fe^{3+}), and the dashed line represents the absorption of the standard FeO_2 (Fe^{2+}). Main edge peak is also marked by a gray vertical line.	49
Figure 32 Complementary wheel Available from: faculty.sites.uci.edu	52

Figure 33 The structure of corundum: blue circle represents Al atom and red circle represents O atom (Bristow et al., 2014).....	53
Figure 34 The corundum structure of corundum: (a) Al_2O_3 in octahedral structure (b) regular octahedral (c) irregular octahedral (Nassau, 1987).	53
Figure 35 The splitting of d-orbitals in octahedral structure. Available from: chemistry.stackexchange.com.....	54
Figure 36 Color change apparent in the red synthetic corundum sample (R5): (a) side view in daylight, (b) top view showing bluish purple in daylight, and (c) top view showing purplish red in incandescent light.....	55
Figure 37 Comparison the amount of V^{3+} in red corundum between natural and synthetic (Muhlmeister et al., 1998).....	56
Figure 38 The Al site in corundum structure occupied by Fe^{2+} and Ti^{4+} (Nassau, 1987).	60
Figure 39 (a) The spectrum of yellow synthetic corundum by trapped hole involving Mg^{2+} and Fe^{3+} (Hughes et al., 2017) (b) the spectrum of yellow samples (Y3, Y4, and Y5).....	64

CHAPTER 1

Introduction

1.1. Introduction

Corundum (Al_2O_3) is commonly found in igneous and metamorphic rocks. Its hardness is 9 on Mohs scale, only second to diamond. Corundum also has a wide variety of colors depending on the localities and characteristics of trace elements. Red corundum, or commercially known as ruby, is one of the most popular colors due to its beauty and scarcity. Other color varieties include blue and yellow, which are known as blue sapphire and yellow sapphire, respectively. Different colors in corundum are due to the presence of various types of trace elements or transition metal impurities in corundum structure (Calligaro and Poirot and Querre, 1999). For example, reddish purple corundum contains chromium or vanadium as major trace elements (Sun and Palke and Renfro, 2015; Sutherland and Zaw and Meffre and Yui and Thu, 2014; Zaw and Sutherland and Yui and Meffre and Thu, 2015). Yellow corundum, can have various impurities such as iron and magnesium (Kanouo et al., 2016; Mungchamnankit and Kittiauchawal and Kaewkhao and Limsuwan, 2012; Nassau, 2001). The presence of iron with other metals such as titanium can also give blue shades in corundum (Emmett et al., 2003; Ferguson and Fielding, 1971; Soonthornantikul and Atikarnsakul and Weeramonkhonlert, 2016). The abundance and oxidation state of transition metals can largely influence the specific color of corundum (Gorghinian et al., 2013).

Although corundums can be found in many places around the world, not all regions produce the colors that are high qualities. The origins of corundum can largely influence on price and demand due to their unique characteristics such as distinctive color, inclusions, and history. There are several popular sources of high-quality ruby and sapphire such as Kashmir, Myanmar, Sri Lanka, Thailand, Australia, Madagascar, and Vietnam (Shor and Weldon, 2009). Among corundum localities, classic Kashmir sapphires display lush, velvety blue color while Burmese Mogok rubies exhibit vivid red colors and medium-to-dark tones, sometimes described as “pigeon’s blood red” (Shor and Weldon, 2009). Many shades of sapphire and ruby can be found in riverbeds and alluvial deposits in many countries, but the specimens from Kashmir and Mogok

have been known as the world's rarest and costliest colored corundums (Harlow and Bender, 2013; Shor and Weldon, 2009).

In addition to natural deposits, corundum can be synthesized in a laboratory (Figure 1). Synthetic corundum has the same chemical, optical, and physical characteristics as natural corundum. Synthetic corundum can be made in various colors since the late 1800s (Nassau, 1972). The synthetic corundum can be made in specific color with consistency given the right ingredients, time, and facilities (Nassau, 1980). There are two main approaches to create synthetic gems – melt or solution process. The main difference between these two processes is that the chemical composition of melt is the same as the composition of the resulting crystal while the chemical composition of solution is different from that of the resulting crystal.



Figure 1 A comparison between of natural corundum (a) and synthetic corundum samples (b)

Note: the natural corundum. Available from: gia.edu.

The most common way to make synthetic corundum is flame fusion or Verneuil technique which is also considered a melt process (Keck and Levin and Broder and Lieberman, 1954; Ueltzen, 1993; Verneuil, 1904). This process involves dropping very fine-powdered of aluminium oxide with a mixture of high-temperature H_2 and O_2 gases flame (Kurlov, 2016), where it melts and falls onto a rotating pedestal to produce a synthetic crystal. A small amount of various metal oxides is added for color creation such as chromium oxide for a red ruby, or ferric oxide for a yellow sapphire. The melted droplets, which are infused with metal oxides, are then allowed to crystallize

into the boule (Figure 2). Flame fusion method is widely used and the least expensive way to make synthetic corundum and spinel (Carr and Nisevich, 1977; Winchell, 1944). Although corundums produced by this technique are chemically and physically similar to natural corundums, exact colors of corundum remains challenging to reproduce.

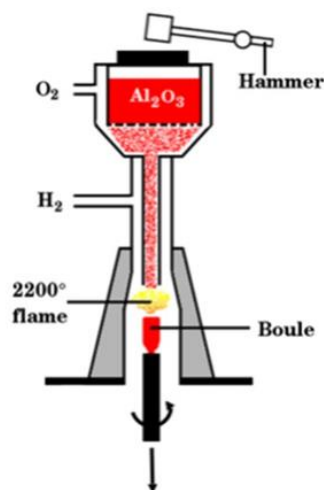


Figure 2 A diagram of flame fusion or Verneuil process to make synthetic corundum Available from: [gemologyproject](http://gemologyproject.com)

Another common method to synthesize corundum is called flux growth, which is a solution process. This method was first created by Chatham Created Gems, Inc. Because of problems with synthesis, flux-grown blue sapphires have not been sold as faceted gemstones. The first successful synthesis by the flux method is orange sapphire in 1982 (Kane, 1982). Flux growth refers to the growth of crystal from molten solvent of aluminium oxide at high temperature. As the dissolved aluminium oxide solution gradually cools down, synthetic corundum crystals form. The flux allows the growth to continue below the melting temperature of the solute materials. The reduction of growth temperature allows growing better quality crystals. This is the main advantage of the flux growth. Growing a synthetic corundum by the flux method requires significant amount of time and resources (Subashini and Govindarajan, 2017). Consequently, synthetic corundum is available at many price levels, from very affordable to very expensive (Weldon, 2002). The demand of synthetic gemstone has been increased worldwide (Grynberg and Sengwaketse and Motswapong, 2014) due to

its cost-effectiveness and various industrial applications. Other common synthetic gemstones include diamond, ruby, sapphire, and emerald. These synthetic gemstones can be made by various laboratory methods such as melt growth process or Verneuil technique, solution growth, and chemical vapor deposition (CVD) (Nassau, 1990).

Although corundums produced by synthetic processes are chemically and physically quite similar to natural corundums, exact colors of corundum are challenging to reproduce. In addition, the characteristics of trace elements such as type, volume, and oxidation state vary in different colors of synthetic corundums. In general, there are several theories that explain the presence of color in corundums such as the crystal field theory, electron charge transfer, and color center.

The crystal field theory happens when the electrons receive the excited energy (visible light in this case) and move to the excited state in the structure. In red corundum, Cr^{3+} substitutes some of the Al^{3+} ions in the Al_2O_3 lattice; the unpaired electrons will move up to the specific excited state and move back to the ground state, giving the specific absorption of the yellow-green and violet portions of white light that give yielding red color (Nassau, 1978).

Electron charge transfer between ions of two impurities can only happen through the absorption of energy. When the energy required for that transition is equivalent to the energy near the visible range of light, it will result in color (Nassau, 2001). For corundum, the effect of transition between Fe^{2+} and Ti^{4+} , the intervalence charge transfer from $\text{Ti}^{4+}\text{-Fe}^{2+}$ to $\text{Ti}^{3+}\text{-Fe}^{3+}$ gives blue color (Na-Phattalung and Limpijumnong and T-Thienprasert and Yu, 2018). Moreover, color center refers to imperfections in crystals; this can happen due to unpaired electrons in the imperfect crystal absorb the energy and move to the excited state then produce colors. Thus, a vacancy site in the crystal that is filled by unpaired electrons is called "color center". Another case is called "hole color center" when an electron missing from a location, that makes the crystal has a "hole" and some elements may substitute. When the electrons receive the energy of radiation, they can absorb such energy and move the exciting state. This leaves a hole and different energy levels become available to the

unpaired electron on the ion causing absorption and color (Nassau, 1978; Nassau, 2001).

To better understand the causes of colors in synthetic corundums, this study focuses on the investigation of different oxidation states of trace elements. This study thus aims to use advanced analytical techniques such as X-Ray Diffraction (XRD), UV-Vis-NIR spectroscopy, Electron Probe Micro-Analyzer (EPMA), and X-ray Absorption Near Edge Structure spectrometry (XANES) to investigate composition, trace element, and their oxidation states that relate to the cause of color in synthetic corundum.

1.2 Research objectives

1.2.1 Identify the type and amount of trace element in synthetic, red, blue and yellow corundums

1.2.2 Describe the oxidation states of trace element and the potential cause of color in the synthetic corundums

1.3 Scope of study

A total of fifteen corundums, in red, blue, and yellow, synthesized by Verneuil technique from Aziz import & export Co, LTD. are used in this study. Each color set has five samples which were analyzed under the same experimental conditions for quantifying amounts of trace elements and identifying their oxidation states. The analytical methods include X-Ray Diffraction (XRD), Electron probe micro-analyzer (EPMA), UV-Vis-NIR spectroscopy (UV-Vis-NIR) and X-ray absorption near edge structure spectrometry (XANES). XRD and EPMA were carried out at Chulalongkorn University; UV-Vis-NIR was engaged at The Gems and Jewelry Institute of Thailand; XANES was completed at Synchrotron Light Research Institute, Thailand. These results are used to identify oxidation states of trace elements in each color variety.

CHAPTER 2

Literature Review

Gemstones are known for having various colors, depending on the type and amount of trace elements. The color of a gemstone largely impacts its price and reflects its scarcity. For example, red corundum, which is widely known as ruby has a wide range of color from bright red to dark reddish-brown. The most sought-after color is deep blood red with a slightly bluish hue, which is called “pigeon’s blood”. The pigeon’s blood ruby is found in a few areas of Myanmar and is the world’s most expensive ruby (Zaw and Sutherland and Yui and Meffre and Thu, 2015). The ancient mines of Mogok in the Mandalay region were famous for producing 90 percent of the world’s rubies (Zaw and Sutherland and Yui and Meffre and Thu, 2015). The most expensive ruby ever sold is from Myanmar due to its exceptional coloring (Harlow and Bender, 2013). However, many rubies on the market are from Thailand, and these ruby have a brownish hue (Shor and Weldon, 2009). Other colored corundums such as blue sapphire, yellow sapphire, etc. also have a wide range of shades and prices. Therefore color is one of the most important characteristics of corundum. This study aims to investigate the oxidation state of metal impurities in synthetic ruby and sapphire and to better understand the cause of color in synthetic corundums.

2.1 The cause of color

Color in corundum depends on various factors such as the intrinsic constituents, impurities, defects, and specific structures. In general, there are three main types of color in minerals: idiochromatic, allochromatic, and pseudochromatic. Idiochromatic mineral is the mineral in which color occurs from a major ingredient (Nassau, 1978). Allochromatic mineral is the mineral in which color formation is caused by impurity. Coloring of a pseudochromatic mineral occurs by the physical optical effects to produce the color (Nassau, 1978). The color in the mineral comes from the differential absorption and transmission of light or wavelengths. The human eye can respond to the color of a limited range of wavelength from about 350-750 nm. This range is the wavelength of visible light (Loeffler and Burns, 1976). The color occurred

in corundum is categorized in allochromatic because pure crystal form of corundum (Al_2O_3) is colorless (Nassau, 1987). The color of corundum is thus caused by the absorption of specific wavelengths of light by impurities in corundum. While some wavelengths were absorbed, allowing other wavelengths to pass through the corundum, the wavelengths that pass give the color to the corundum. The causes of color in corundum can be divided into three different theories: crystal field theory, charge transfer, and color center.

2.1.1 Crystal field theory

Crystal field theory describes the relationship between the five d -orbitals and ligands arranged around a transition metal ion. In corundum, an aluminum atom is surrounded by six oxygen atoms in octahedral coordination (Figure 3).

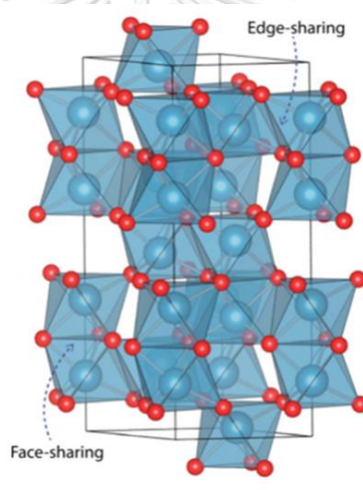


Figure 3 The Al_2O_3 lattice in corundum. The blue circle is the aluminum (Al) atom and the red circles are oxygen (O) atoms. (Bristow et al., 2014).

Under specific conditions, the aluminum can be replaced by transition metals such as V, Cr, Mn, Fe, Co, Ni, and Cu (Loeffler and Burns, 1976). These transition metals have incompletely filled d -orbitals. When the six oxygens are at the tips of the octahedron, the energy of the five d -orbitals can split into two groups, known as low- and high-energy orbitals. The difference in energy between two d -orbitals is called the crystal field splitting energy (Figure 2). The level of crystal field splitting energy depends on several factors such as the strength and nature of the bonding, and the oxidation state of transition elements.

In rubies, when Cr^{3+} substitutes some of the Al^{3+} ions, the ideal Al_2O_3 lattice is distorted, resulting in changes of Al-O distances and bonding strength. The substitution by transition metal can significantly change the strength of the crystal field splitting energy. Due to the electron configuration of Cr^{3+} is $1s^2 2s^2 2p^6 3s^2 3p^6 3d^3$, there are three unpaired electrons in the $3d$ shell. When exposed to the visible light, these unpaired electrons can absorb specific photon energy, which is equivalent to the crystal field splitting energy. As a result, these electrons are thus excited and move between low- and high-energy d -orbital (Nassau, 1978). This process is called $d-d$ transition, which is a unique characteristic of transition metals. When the metal cation exists in the structure, it makes distribution of six electrons in corundum structure change. Consequently, the energy of d -orbital increase due to electrostatic repulsions which cause the splitting of d orbital into two groups: low energy (d_{xy} , d_{xz} , and d_{yz}) and high energy ($d_{x^2-y^2}$ and d_{z^2}) (Burns, 1993). Therefore transmission of energy between the energy gap of low energy and high energy in d -orbital cause the specific absorption in corundum and produce red color (Lancashire, 2019; Rückamp et al., 2005). (Figure 4)

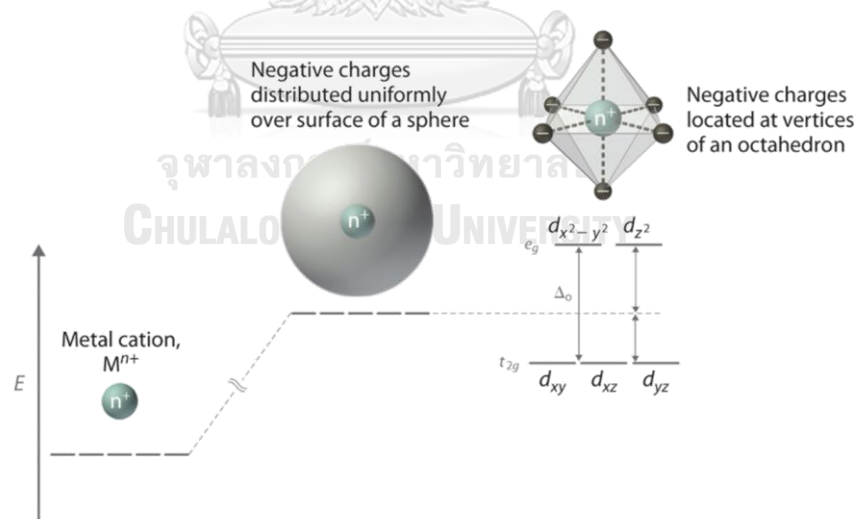


Figure 4 The splitting of d -orbital diagram in octahedron structure. Δ_0 refer to crystal field splitting energy. Available from: chem.libretexts.org

In some cases of crystal field theory, corundum has a wide range of absorption that is red and blue-green. This situation in corundum occurs by V^{3+} which makes the color change in minerals depending on the different light (daylight and incident light) called 'alexandrite effect' (Figure 5) (Gübelin and Schmetzer, 1982).



Figure 5 The color change in sapphire (a) Bluish color in daylight (b) Violetish red in incandescent light. (Gübelin et al., 1992).

2.1.2 Charge transfer

Charge transfer is a part of Molecular Orbital Theory. The metal-metal charge transfers can be either 'heteronuclear' or 'homonuclear'. A heteronuclear charge transfer is the transference of ions in different elements while a homonuclear transfer occurs with the same element. The process of charge transfer is the movement of electrons from the transition metal ions to other ions. When two different transition elements exist in different position in crystal structure, the electrons exchange is occur which cause the visible color. (Nassau, 1978; Nassau and Valente, 1987).

In general, if corundum only has titanium (Ti) impurities in the structure, it will appear colorless. If a corundum crystal has only iron (Fe) impurities, it will have a pale yellow color. If both impurities are present together, it will appear a deep blue color. In the case of blue sapphire, the Al_2O_3 structure has Fe and Ti impurities in the structure. The oxidation states of Fe and Ti can exist in two combinations: $Fe^{2+}-Ti^{4+}$ and $Fe^{3+}-Ti^{3+}$ (Nassau, 1978). In sapphire, the transfer occurs because the Fe^{2+} ion has one more electron in its outer shell than the Ti^{4+} ion. The electron is attracted to the

Ti^{4+} ion. When the electron orbits the Ti^{4+} ion, it transfers between ions, causing the Ti^{4+} to become Ti^{3+} and the Fe^{2+} to become Fe^{3+} (Nassau, 1978) (Figure 6).

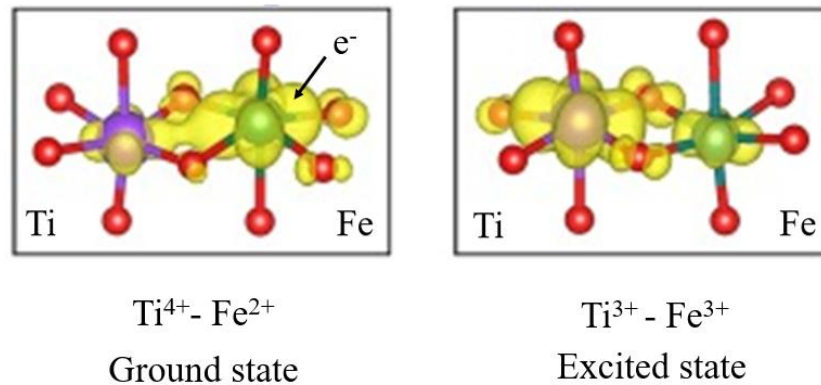


Figure 6 The electron charge transfer diagram in sapphire. Credit from: Na-Phattalung et al., 2018

The process of intervalence charge transfer (Na-Phattalung et al., 2018; Nassau, 1980) occurs from the lower energy ($Fe^{2+}-Ti^{4+}$) to higher energy ($Fe^{3+}-Ti^{3+}$). The transition involves the absorption of energy, producing the absorption band (Figure 7). The required energy corresponds to the absorption of yellow light, so the result is that the sapphire has a blue color (Nassau and Valente, 1987).

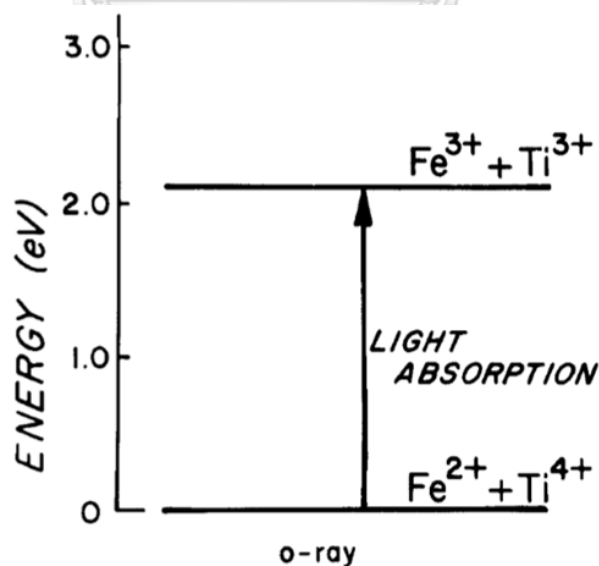


Figure 7 The transition from the ground state to the excited state in blue sapphire. (Nassau, 1987).

In addition to heteronuclear charge transfer in blue corundum, there is homonuclear charge transfer with the same element in two different sites. For example, a change involving only Fe would be from $\text{Fe}^{2+}\text{-Fe}^{3+}$ to $\text{Fe}^{3+}\text{-Fe}^{2+}$ that occurs in hydrated iron phosphate vivianite (Nassau, 1978). Normally, the hydrated iron phosphate vivianite has only Fe^{2+} and appears colorless. Through oxidation-reduction, some Fe^{2+} to Fe^{3+} change transfer becomes possible and the result gives a deep blue color (Nassau, 1978). In addition, the charge transfer between metal-metal happens in other minerals such as the aquamarine iolite via Fe^{2+} to Fe^{3+} or the blue kyanite via $\text{Fe}^{2+}\text{-Ti}^{4+}$ (Loeffler and Burns, 1976).

2.1.3 Color center

Color center is one of the most widely accepted causes of color. Color center is a type of defect in the regular spacing of the crystal structure, and “electron color center” is when electrons fill in the vacancy caused by the defect (Nassau, 1980). The cause of color center can occur for two reasons.

The first reason is when the crystal with negative ions missing (Figure 8B) from its usual position (Figure 8A) and replaced by electrons. This can occur during crystal growth or due to radiation. The electron color center is produced when an electron occupies the empty position. That unpaired electron can move to the excited state, where the energy is controlled by the same factors in the crystal field described above (Nassau, 1978). This gives color in the crystal. For example, purple fluorite (CaF_2) creates an electrons color center by fluorite called F-center (Nassau, 1980, 2001).

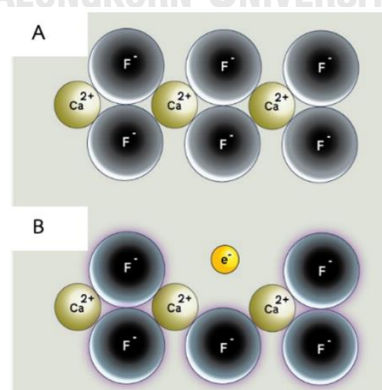


Figure 8 A) Normal structure of fluorite and B) an electron replacing F ion to create electron color center. Available from: webexhibits.org

The second reason referred to "hole color center", occurs when an electron is missing from an electrons pair in the crystal (Figure 9) (Nassau, 1978). Due to there is no unpaired electron in the structure, the crystal usually does not give a color (Figure 9a). When the crystal is irradiated with X-ray, gamma rays, or exposed to radioactivity, one of the pair of electrons in the crystal can be ejected from its position, leaving an unpaired electron "hole" (Figure 9b). That unpaired electron can move to the exciting energy and absorbed energy which produce color (Loeffler and Burns, 1976; Nassau, 1978).

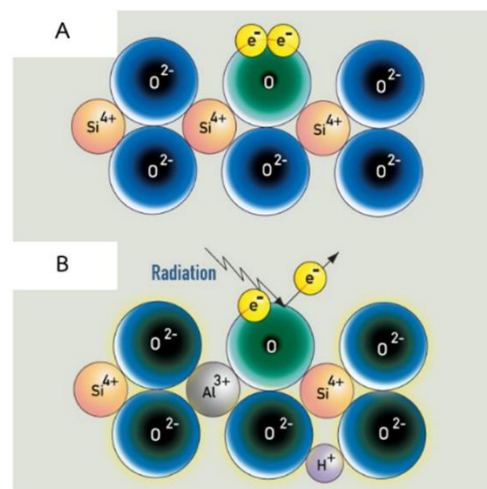


Figure 9 A) Normal structure of quartz (SiO₂) and B) an electron missing caused by irradiation to create hole color center. Available from: webexhibits.org

The color center can cause color in a variety of minerals and give different colors depending on the impurities. For example, halite when Cl⁻ lattice vacancies are filled with electrons, gives a blue color. Smoky quartz occurs when Al³⁺ substitutes for Si⁴⁺, and radiation ejects one of electrons from an O²⁻ and leaves a hole color center to give a brown color (Nassau, 1978). Similarly, Fe³⁺ substituting for Si⁴⁺ gives purple in amethyst (Loeffler and Burns, 1976). In addition, the study by Pisutha-Armond (2006) suggests that synthetic corundum can be turned to yellow by inserting Fe, though the color fades. However, with doped treatment of Mg and/or Be, a stable yellow color in synthetic corundum is given. They concluded the result of the cause of color in the study is trapped hole color center (Pisutha-Armond and Hager and Atichat and Wathanakul, 2006).

2.2 Previous works

Synthetic corundum can be made by different processes such as flame fusion (Verneuil process), crystal pulling (Czochralski process), flux growth technique, and hydrothermal growth. Although the corundum has many colors, the popular colors are red (ruby), blue, and yellow (sapphire), respectively.

2.2.1 Red synthetic corundums

Red corundum or ruby was the first successful synthetic corundum and has been manufactured since late 1800s (Weldon, 2002). Natural ruby contains <1% of trivalent chromium (Cr^{3+}), which contributes to its red color (Muhlmeister and Emmanue and Shigley and Devouard and Laurs, 1998; Nassau, 1978). A previous study by Schmetzer and Peretti, (2000) suggests that Mn^{3+} is the cause of reddish-orange in red synthetic corundum, which was produced by hydrothermal synthesis. The synthesis occurs with the mix of water with the main element to produce the color in solution with the application of heat and pressure, the crystal will crystallize slowly and formed to corundum (Laurs and Devouard and Shigley and Fritsch and Muhlmeister, 1998). Schmetzer (1999) suggest Cr^{3+} is the cause of color in synthetic ruby by hydrothermal synthesis, and Cr^{3+} can provide the pink shade in synthetic sapphire (Schmetzer and Peretti, 1999). In addition, the Czochralski-pulled, Flame-fusion and floating zone techniques use Cr_2O_3 (Cr^{3+}) as the impurity to give the red color (Muhlmeister and Emmanue and Shigley and Devouard and Laurs, 1998).

Considering the amount of elements in natural and synthetic ruby, the synthetic ruby was found that, the amount of V and Ga especially Fe are the lowest in melt-grown technique. While the flame-fusion technique has high Ti (nearly 0.05 wt%), V (nearly 0.02 wt%) and Cr is the highest component contained in measurement of the synthetic ruby (2.41 wt%). Natural rubies show high Fe (0.299-0.72 wt%) and low V (up to 0.007 wt%) but the rubies from Myanmar show high amount of V (up to 0.171 wt%) (Muhlmeister and Emmanue and Shigley and Devouard and Laurs, 1998). It can conclude the difference between natural and synthetic rubies can be determined by the amount of trace elements they each contain. For example, synthetic rubies have little amounts of Ga and Fe, which is much different from the natural. (Saeseaw and Pardieu and Weeramongkhonlert and Sangsawong and Moyal, 2015).

For studying corundum, especially ruby, many techniques are used to identify measure important elements in the ruby. One of widely used techniques is UV-Vis-NIR spectroscopy, UV-Vis-NIR is the technique for investigating the light absorption of the elements in a crystal. The result of absorption is called a spectrum. The spectra can be used to determine the color and type of element in a sample (Martin and Pretzel, 1991). The results of UV-Vis-NIR of rubies shows the range of absorbance in two peaks. The first peak shows the absorption with 405- 415 nm and another peak shows at 548-560 nm (Duroc-Danner, 2002; Emmett et al., 2003; Kane, 1982). Although the examination has different absorptions, all absorbance was interpreted to represents Cr^{3+} in synthetic ruby.

In addition, ruby has other techniques to investigate the element related to the color or important elements that produce the color in natural red corundum. Because X-ray absorption near edge structure (XANES) technique is a powerful technique in the study of electronic structure around the absorbing atom and can be used to determine oxidation state of element in minerals. The peak positions of the absorption line by XANES spectrum are strongly sensitive to valence state that can define the oxidation state of elements (Klysubun, 2017).

The study compared two corundum: Indian natural ruby and flame fusion synthetic ruby. The result showed the absorption energy at 6010 eV that represent Cr^{3+} for natural ruby (Wongkokua and Pongkrapan and Dararutana and T-Thienprasert and Wathanakul, 2009). When measuring the synthetic ruby by the same technique, they found the absorption at 5990 eV that represent Cr^{3+} (Wongkokua and Pongkrapan and Dararutana and T-Thienprasert and Wathanakul, 2009). Another study by XANES technique of synthetic ruby calculated the transition probability of the Cr in synthetic ruby. They found that the change of electron in 3d states of Cr move the state, under the influence of the octahedral ligand field, or called the crystal field, which is the cause of color. The results showed the absorption of Cr in synthetic ruby at 5999 eV (Parikh et al., 2002).

Moreover, in a synthetic ruby the color can change when the crystal has a high value of V. The color change is called "Alexandrite Effect". Alexandrite effect is the color change of a gemstone. The different color happens under the different light

between daylight and incandescent light (Gübelin and Schmetzer, 1982). In natural red corundum, the color change to green in daylight and pink in incandescent light due to the alexandrite effect (Gübelin and Schmetzer, 1982). Most gemstones described as synthetic alexandrite are actually synthetic corundum laced with vanadium (V). The alexandrite effect in synthetic corundum has the color change from bluish purple in daylight to red-purple in incandescent light (Figure 10) (Smith, 2000).



Figure 10 The alexandrite effect in synthetic corundum (a) bluish purple in daylight (b) red-purple in incandescent light. Available from: alexandrite.net.

2.2.2 Blue synthetic corundums

Corundum has a variety of colors, one of the most popular blues is called sapphire. In the previous studies have a study about the cause of color in blue synthetic corundum or synthetic sapphire. That makes the measurement the different method to detected the elements be the cause of color in synthetic sapphire.

In the UV-Vis-NIR spectroscopy experiment, the synthetic sapphire has the absorbance around 576-590 nm presence of $\text{Fe}^{2+}\text{-Ti}^{4+}$ pair (Emmett et al., 2003; Soonthorntantikul and Atikarnsakul and Weeramonkhonlert, 2016). Kadleiková et al., (2001) suggested the Raman spectra to detected trace elements in synthetic sapphire. The results show the high value of Fe^{2+} , Fe^{3+} , Ti^{4+} , Ti^{3+} , V^{3+} , and Cr^{3+} in synthetic sapphire (Kadleiková and Breza and Veselý, 2001). In addition, the other study suggested that $\text{Ti}^{4+}\text{-Fe}^{2+}$ pair is the important element to coloration of blue color in sapphire (Ferguson and Fielding, 1971; Kurlov and Rossolenko and Abrosimov and Lebbou, 2010; Monarumit and Wongkokua and Satitkune, 2016). The synthetic

corundum has strong absorptions at 580 and 700 nm that represent $Ti^{4+}-Fe^{2+}$. Notice that synthetic corundum has high intensity of Ti and Fe, which gives blue color. The blue color maybe occur by the pair of $Ti^{4+}-Fe^{2+}$ located on nearest-neighbor Al sites in corundum that called Intervalence Charge Transfer (IVCT), the IVCT is the cause of blue color in synthetic corundum (Emmett et al., 2003).

Nassau (2001) suggested that the charge transfer occurs in blue corundum between Fe^{2+} and Ti^{4+} , and intervalence charge transfer from $Ti^{4+}-Fe^{2+}$ to $Ti^{3+}-Fe^{3+}$ in natural blue corundum (Na-Phattalung and Limpijumnong and T-Thienprasert and Yu, 2018). The correlation between Ti and Fe occur in natural and synthetic. In blue corundum the highest impurity is Ti (Nikolskaya and Terekhova and Samoilovich, 1978). In XANES experiment, the measurement iron (Fe) and titanium (Ti) in synthetic blue corundum shows the absorption of Fe at 7124 eV, represent Fe^{3+} and Ti at 4984 eV, represent Ti^{4+} (Wongrawang and Monarumit and Thammajak and Wathanakul and Wongkokua, 2016). In addition, the absorption of XANES was measured for investigated the impurities for calculated structural relaxations in corundum, the result shows the absorption of Fe at 7130 eV in blue sapphire (Gaudry et al., 2005).

Seemingly, titanium (Ti) is the important impurity in blue corundum. In general, titanium dioxide (TiO_2) occurs in nature as well known minerals such as rutile, anatase, and brookite. The most widespread of titanium dioxide bearing ore around the world are rutile (Bourikas and Hiemstra and Van Riemsdijk, 2001). Rutile and anatase are polymorph which have same crystal system in tetragonal and anatase can transform to rutile under high temperature (Mila et al., 2000).

2.2.3 Yellow synthetic corundums

The yellow corundum in natural and synthetic have varieties of cause of color such as $Fe^{3+}-Fe^{3+}$, Mg^{2+} , Ni^{3+} , $Mg^{2+}-Fe^{3+}$ (Mungchamnankit and Kittiauchawal and Kaewkhao and Limsuwan, 2012; Pisutha-Arnond and Hager and Atichat and Wathanakul, 2006; Wang and Lee and Kroger and Cox, 1983). The yellow in corundum occur with many causes such as the color center by iron or containing ion on the surface (iron or nickel) in natural corundum or addition of the elements (nickel or/and others) in synthetic corundum (Nassau and Valente, 1987). In addition, the color in yellow corundum can occur because the combination between elements: Cr and Fe

gives orangish yellow (Hughes, 1997). Commonly, iron (Fe) is important metal showed in natural yellow corundum measured by UV-Vis-NIR (Emmett et al., 2003; Peretti and Günther, 2002; Soonthorntantikul and Atikarnsakul and Weeramonkhonlert, 2016) and the absorption peak showed at 377, 388 and 450 nm that represent Fe^{3+} .

The cause of color in synthetic corundum suggested by Pisutha-Arnond (2006), is the Mg^{2+} trapped hole color center related/paired with Fe^{3+} . The result of this study concluded Mg was involved in stabilizing the color center together with Fe can provide the stable yellow color (Pisutha-Arnond and Hager and Atichat and Wathanakul, 2006). Apart from Fe, nickel (Ni) was found in synthetic yellow corundum (Mungchamnankit and Kittiauchawal and Kaewkhao and Limsuwan, 2012). Color formation in synthetic can occur by addition of elements (nickel or/and other) into corundum and have been the heat treatment to produce the yellow color (Nassau and Valente, 1987). Moreover both elements Fe and Ni had chemical properties to give yellow color (Thomas and Mashkovtsev and Smirnov and Maltsev, 1997). Some reports said that the color formation in yellow corundum in natural and synthetic by trapped-hole mechanism often possess an orange or reddish orange hue (Lu, 2013). The UV-Vis-NIR absorption below ~ 500 nm, originating from trapped holes associated with Mg and Cr associated with yellow color at 450 nm (Lu, 2013).

There is a possibility that the color formation in yellow corundum depends on the trace elements that are inside because the yellow color can coloration by many elements. All previous studies mentioned Fe in natural yellow corundum significantly (Emmett et al., 2003; Soonthorntantikul and Atikarnsakul and Weeramonkhonlert, 2016) and Ni, Mg and Fe in the synthetic corundum (Mungchamnankit and Kittiauchawal and Kaewkhao and Limsuwan, 2012; Nassau and Valente, 1987; Pisutha-Arnond and Sutthirat and Artichart and Wathanakul and Suksawee, 2012; Wang and Lee and Kroger and Cox, 1983). The interesting is that there are other elements combined with iron or not, in the produce the yellow colored in synthetic corundum.

Nowadays, the synthesis of synthetic gemstones can be made by various laboratory methods such as melt growth process or Verneuil technique, solution growth, and chemical vapor deposition (CVD) as mentioned above. This study focus on the Verneuil technique or flame fusion because this technique is the first synthetic

gemstone process, which was developed mainly for corundum and is still widely used this day (Nassau, 1990). The characteristic of synthetic corundum by Verneuil technique is the curved growth lines which may be caused by the growth of boules in an uncontrolled atmosphere with a huge drop in temperature (thermal gradient) between the growing crystal and surrounding atmosphere that makes the color of synthetic corundum inhomogeneous, which rim shows intense color more than center. Sometimes, gas bubbles in the synthetic corundum are presented which are caused by an excess of oxygen during the synthesis process (Figure 11) (Hughes, 1997).

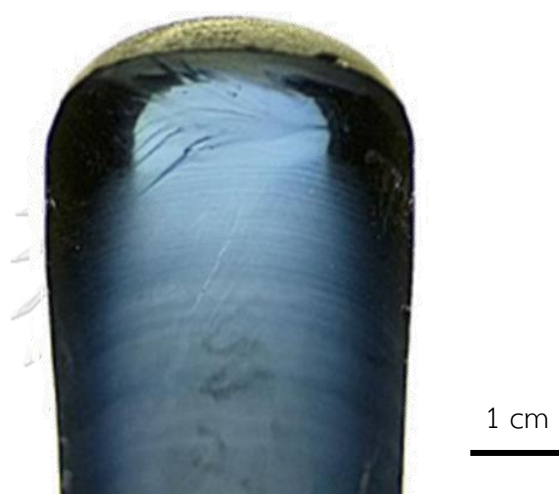


Figure 11 The synthetic corundum by Verneuil technique. Available from: ruby-sapphire.com.

CHAPTER 3

Methodology

The samples used in the study are synthetic corundums synthesized by the melt grown process or Verneuil technique. A total of fifteen synthetic corundum samples were used in this study, they have the sizes ranging from 1-1.5 cm (Figure 12). There are three colors in which each color set contains five samples. All samples were analyzed by X-Ray Diffraction (XRD), Electron Probe Micro-Analyzer (EPMA), UV-Vis-NIR spectroscopy (UV-Vis-NIR) and X-ray Absorption Near Edge Structure spectrometry (XANES) which details of these analytical techniques are reported below.

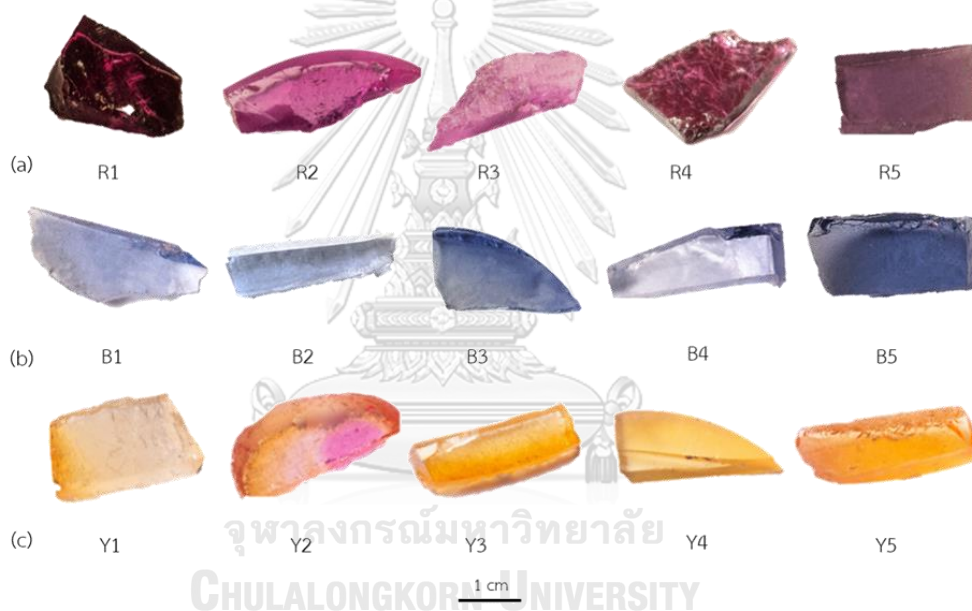


Figure 12 Synthetic corundum samples (a) red sample set (R1-R5), (b) blue sample set (B1-B5), (c) yellow sample set (Y1-Y5).

3.1 X-Ray Diffraction (XRD)

3.1.1 Theory of XRD

XRD is a technique for characterizing crystalline materials. It provides information on structures, phases, preferred crystal orientations, and other structural parameters such as average grain size, crystallinity, strain, and crystal defects (Bunaciu and Udriștioiu and Aboul-Enein, 2015). X-ray diffraction peaks are produced by interference beam of X-rays scattered at specific angles from each set of lattice planes

in a sample. The result of scattered X-rays corresponds to electromagnetic radiation in the wavelength range is 1\AA (Figure 13). The interaction of the incident rays with the sample produces the following relationship called Bragg's law (Bunaciu and Udriștioiu and Aboul-Enein, 2015).

$$n\lambda = 2d \sin\theta \quad (1)$$

, where n is an integer, λ is the wavelength, d is the distance between atomic layers in a crystal, and θ is the reflect of X-ray beams at certain angles in the crystals faces.

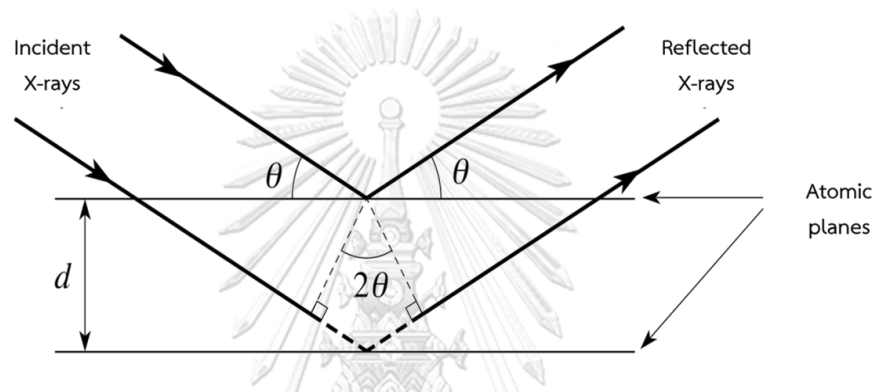


Figure 13 Schematic diagram of X-ray diffraction (XRD). Available from: met.reading.ac.uk

3.1.2 Experimental conditions for XRD

Synthetic corundum sample was firstly ground into very fine powder. The XRD experiments were done by Bruker model D8 Advance: Bruker AXS, based at the Geology Department, Chulalongkorn University. $\text{Cu K}\alpha$ radiation with an energy of 40 keV were used in the XRD experiment. The diffraction angles (2θ) were set between 5° – 70° with increment of 0.02 degree and scanning speed of 0.5 degree per min (1 sec per step). Diffraction profiles were analyzed by Diffracting Plus software for mineral identification.

3.2 UV-Vis-NIR spectroscopy

3.2.1 Theory of UV-Vis-NIR

UV-Vis-NIR is a tool used to measure intensity within the spectrum range from ultraviolet (UV) to visible light (Vis) and near infrared (NIR) that is absorbed by the sample placed in the tool. The selective wavelength of light may be absorbed due to the amount and type of particular substance in the sample. When the sample's molecules are exposed to light in the range of ultraviolet or UV light, the optimum energy of the electrons in the atoms is absorbed by the electrons and then transferred to the energy level (Martin and Pretzel, 1991). When measuring the amount of light passing or reflected from a sample relative to light from a source at wavelengths, according to the Beer-Lambert's law, the absorbance of the substance varies with the amount of molecules absorbed (Figure 14). This technique can be used to identify the types and quantities of substances present in the sample (Martin and Pretzel, 1991).

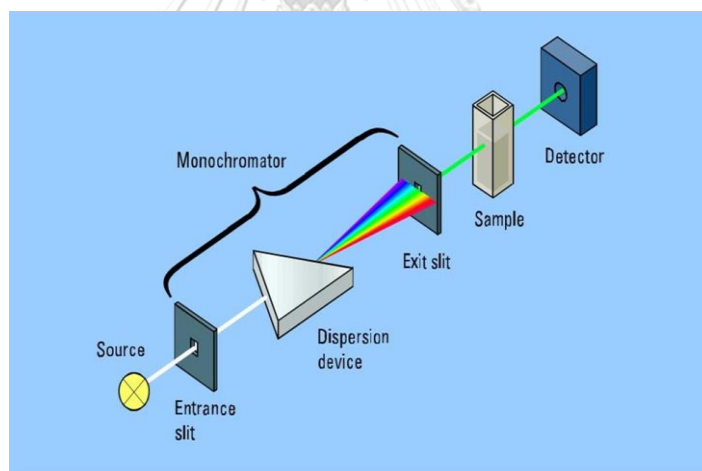


Figure 14 A diagram of UV-Vis-NIR spectroscopy (UV-Vis-NIR) Available from: sajf.iitm.ac.in

3.2.2 Experimental conditions for UV-Vis-NIR

Samples were cut into small pieces (~1-1.5 cm) and polished with flat surface. UV-Vis-NIR absorption spectroscopy was used for this research to investigate the light absorption of the synthetic corundums sample. The measurements were performed on PerkinElmer Lambda 1050 spectrophotometer operated at Data interval 3 nm, scan speed 500 nm/minute, source UV: Deuterium Vis-NIR: Tungsten, Detectors UV-

Vis: PMT and NIR: InGaAs. Gems were inspected at The Gem and Jewelry Institute of Thailand (GIT).

3.3 Electron Probe Micro-Analyzer (EPMA)

3.3.1 Theory of EPMA

EPMA has been considered as a suitable method to analyze the major and minor of elements by using electron beams (Batanova and Sobolev and Magnin, 2018). EPMA has important modes: Back-Scattered electrons (BSE), Secondary Electrons (SE), Characteristic X-rays, and Cathodoluminescence (CL) (Figure 15). The analysis with EPMA technique, electrons moving from the source of electrons or the electron gun, which is made from tungsten (W) or Ce-Bix. After being stimulated by a high potential voltage from the anode focused by a condenser lens and an objective lens so that moves parallel to the EPMA camera's column and combines the focal point to bombard the surface of the specimen. The signal from the interaction signals can be used as data for both structural and chemical analysis of samples. The sample is required to be polished and carbon-coated for EPMA analysis (Chatterjee, 2012).

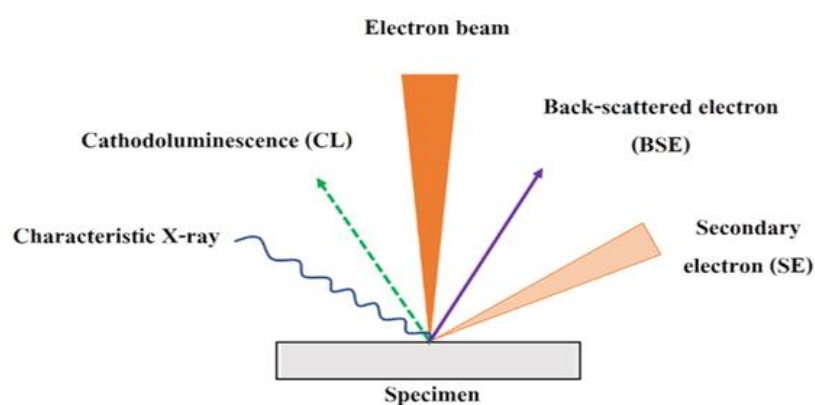


Figure 15 Mode of Electron probe micro-analyzer (EPMA) (Chatterjee, 2012)

3.3.2 Experimental conditions for EPMA

Samples were cut into small pieces (~1-1.5 cm), and embedded in epoxy resin then polished into cylinders with flat surface. The cylinders were coated with a thin layer of carbon to increase electron conductivity. The measurements were done with JEOL model JXA 8100, which was equipped with 5 wavelength dispersive

spectrometers. The experiments were conducted with 20 keV acceleration voltages and 20 nA filament current. Beam spot measuring time for Al_2O_3 5 sec and trace elements 10 sec. Various standard materials were selected to analyze the chemical composition of Al_2O_3 , TiO_2 , V_2O_5 , Ga_2O_3 , FeO , Cr_2O_3 , and MgO oxides. Each sample was analyzed at six different spots for red samples. Blue and yellow samples included into two sections: rim (six spots) and inner of the boule (six spots) because two colors of samples are not homogeneous (Figure 16).



Figure 16 Synthetic corundum samples in epoxy resin showing different spots of the analysis; six different spots for the red samples (white spots), twelve different spots for the blue samples (yellow spots at the rim and grey spots at the inner of the boule), and twelve different spots for yellow samples (black spots at the rim and the grey spots at the inner of the boule).

3.4 X-ray Absorption Near Edge Structure spectrometry (XANES)

3.4.1 Theory of XANES

XANES is a technique for investigation absorption near edge energy when giving energy (synchrotron radiation) to electrons in the deep energy layer (core electrons). Then the electron will absorb the energy and move to vacant orbital in higher energy state within the atom (Henderson and De Groot and Moulton, 2014) (Figure 17). The synchrotron radiation is released from the electrons that curve at a

speed close to the speed of light. When electrons are high-speed curves result in relativity, that electrons emit light this makes it that the light emitted from several points in the arc comes simultaneously (Henderson and De Groot and Moulton, 2014). As a result, synchrotron light is a small cone of high intensity because synchrotron light is emitted from free electrons. Wavelengths of light cover the wavelength range from infrared to X-rays. It can be used for a variety of applications including observation the oxidation state of elements (Klysubun, 2017). The result shows the absorption spectrum and this part of the spectrum called XANES (Figure 18). Seemingly, XANES is an important tool for the characterization of minerals because the particular assets of XANES spectroscopy are its element specificity (Henderson and De Groot and Moulton, 2014).

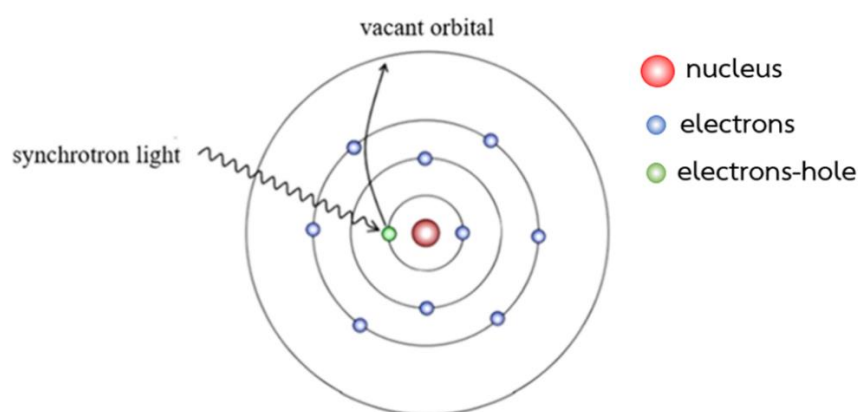


Figure 17 Model of synchrotron light of XANES. Available from: ssrl.slac.stanford.edu

CHULALONGKORN UNIVERSITY

XANES is a subset of X-ray Absorption Spectroscopy (XAS), XAS is the absorption of a photon. In this process, an electron interacts with the field of an incident X-ray to acquire a time-dependent acceleration (Henderson and De Groot and Moulton, 2014). The probability of an excitation sharply increases when the energy of the incident photon reaches the binding energy of a core-electron it called edge. XANES is sensitive to electronic structure information, which may be analyzed in three sections such as pre-edge, main-edge and multiple scattering region (Figure 18). The pre-edge feature is affected by the coordination geometry of the central atom. This study focuses on main-edge because this feature defines the absorption at the edge of metals (Bhale and Sharma and Mishra and Parsai, 2015). The oxidation

state may be assigned according to the energy of the edge position or shifts in accordance with electron density of metals. The multiple scattering regions are the energy of coordination shells are interrogated beyond the edge as the emitted photoelectron scatters off neighboring atoms (Henderson and De Groot and Moulton, 2014).

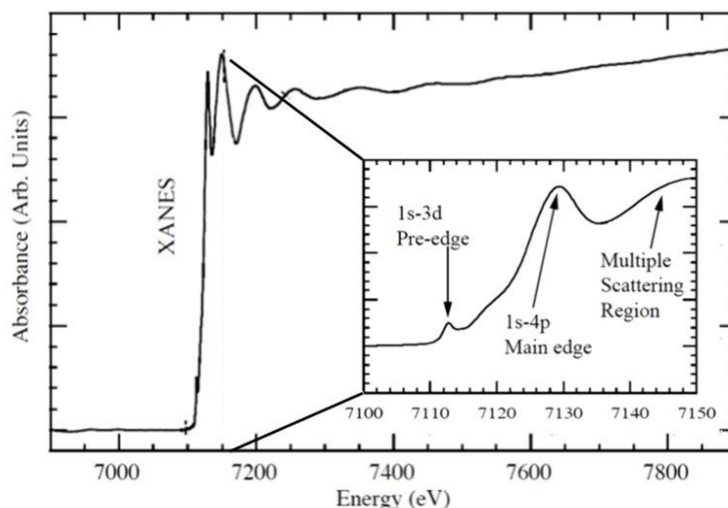


Figure 18 A diagram of XANES results. Available from: cei.washington.edu

3.4.2 Experimental conditions for XANES

XANES measurement was carried out in the transmission mode at the BL8: XAS beamline at the Synchrotron Light Research Institute (SLRI). The same samples were ground into fine powder for XANES experiment. The spectra were recorded at room temperature in a photon (X-ray) energy region of the Cr K-edge (5889 eV to 6189 eV), Ti K-edge (4866 eV to 5166 eV) and Fe K-edge (7012 eV to 7312 eV). The photon energies were scanned by Ge (220) double crystal monochromator and calibrated against the K-edge of Cr foil (5989 eV; precision ± 0.3 eV). For the Cr foil, Cr_2O_3 and CrO_3 were used as the standard in red synthetic corundums (R1-R5). The calibration of Ti standards was done at the K-edge of Ti (4986 eV; precision ± 0.2 eV) with Ti foils of, Ti_2O_3 , TiO_2 (anatase), TiO_2 (rutile) for blue synthetic corundums. The K-edge of Fe (7112 eV; precision ± 0.3 eV) was used to calibrate Fe foil standards, including Fe_2O_3 , Fe_3O_4 , and FeO for yellow synthetic corundums (Table 1). Three spectra were acquired for

each sample and analyzed for pre-edge absorption energy through Athena software (Klysubun, 2017).

Table 1 The standards of XANES experiment

Samples	Trace elements	Main-edge energy (eV)
Red	Cr_2O_3 (Cr^{3+})	6009
	CrO_3 (Cr^{6+})	5992
Blue	Ti_2O_3 (Ti^{3+})	4976
	TiO_2 (Ti^{4+}) _{anatase}	4982
	TiO_2 (Ti^{4+}) _{rutile}	4979
Yellow	FeO (Fe^{2+})	7130
	Fe_3O_4 (Fe^{2+} , Fe^{3+})	7132
	Fe_2O_3 (Fe^{3+})	7134

CHAPTER 4

Results

The results are divided according to the color of synthetic corundum samples, starting from red, blue, and yellow, respectively.

4.1 Red synthetic corundum

4.1.1 XRD Experiment

In the XRD experiment, all samples show the similar diffraction pattern (Figure 19). High X-ray intensity peaks observed at 25.56° , 35.19° , 37.78° , 43.38° and 57.56° indicate diffraction from (012), (104), (110), (113), and (116) planes of Al_2O_3 or corundum in all samples. Results from X-Ray Diffraction (XRD) method, Electron Probe Micro-Analyzer (EPMA), UV-Vis-NIR Spectrophotometer, and X-ray Absorption Near Edge Structure (XANES) experiments are shown in samples. A minor amount of impurities (<1%) are detected in at $\sim 44.50^\circ$ and $\sim 61.00^\circ$ and cannot be resolved with this method. Other analytical methods such as EPMA is then used to further quantify chemical composition.

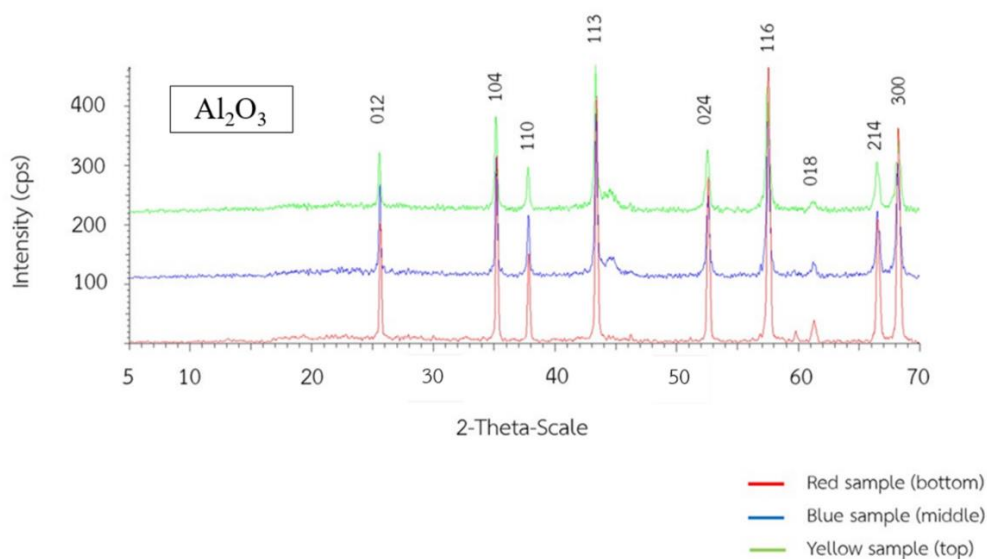


Figure 19 X-ray diffraction patterns of red (bottom), blue (middle), and yellow (top) samples show similarly the main peaks of corundum (Al_2O_3).

4.1.2 EPMA Experiment

EPMA results are used to investigate the type and average amount of trace elements in red synthetic corundum samples. The average weight percentage of oxides is based on six spots analyses in each sample (Table 2). The samples were divided into three groups based on the color: deep red (R1), pinkish red (R2-R4), and purplish red (R5) (Figure 20).

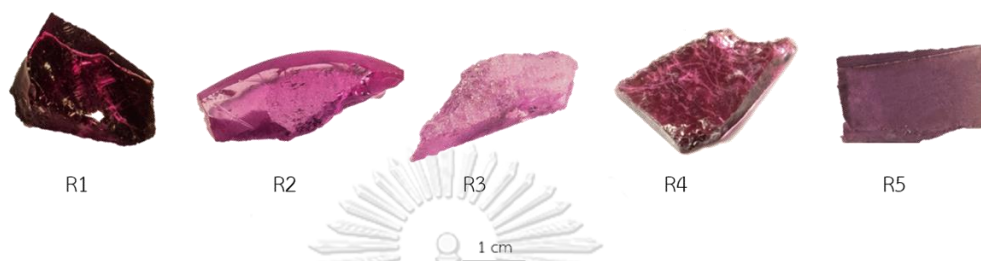


Figure 20 Red synthetic corundum samples: R1 (deep red); R2 (pinkish red); R3 (pinkish red); R4 (pinkish red); R5 (purplish red).

All red samples R1-R5 contain Al_2O_3 as a major component. In addition to Al_2O_3 , Cr_2O_3 is another main component in samples R1-R4 while V_2O_3 is present in a significant portion in sample R5 (Table 2). EPMA results were further calculated to determine the atomic proportion (based on 3 oxygen atoms) of each element (cation) in the sample (Table 3). Sample R1, deep red sample, contains the highest amount of Cr with the average of 0.0092 (Table 3). In the pinkish red group, there are three samples e.g. R2, R3, and R4, which have moderately high average amount of Cr at 0.0030, 0.0027, and 0.0067, respectively (Table 3). On the other hand, sample R5 has the lowest amount of Cr at the average of 0.0010 and the highest proportion of V at 0.0084, which gives rise to a purple shade in this sample. All individual EPMA spot analyses of all red samples can be found in Appendix A.

Table 2 The average amount of trace elements (wt%) based on six spot analyses in each red synthetic corundum (R1-R5).

Oxides	Average amount (wt%)				
	R1 (Deep red)	R2 (Pinkish red)	R3 (Pinkish red)	R4 (Pinkish red)	R5 (Purplish red)
Al ₂ O ₃	99.160	99.140	98.960	98.990	99.070
Cr ₂ O ₃	0.680	0.220	0.200	0.470	0.080
FeO	0.020	0.010	0.010	0.010	0.040
Ga ₂ O ₃	0.030	0.030	0.050	0.030	0.050
TiO ₂	0.020	0.020	0.010	0.030	0.030
V ₂ O ₃	0.020	0.020	0.020	0.030	0.610
NiO	0.020	0.010	0.020	0.010	0.020
MgO	ND	ND	0.001	ND	ND
Total	99.950	99.450	99.271	99.570	99.990

* ND: Not detected

Table 3 The average atomic proportion of red synthetic corundum R1-R5.

Elements	Average atomic proportion				
	R1 (Deep red)	R2 (Pinkish red)	R3 (Pinkish red)	R4 (Pinkish red)	R5 (Purplish red)
Al	1.9900	1.9963	1.9966	1.9931	1.9896
Cr	0.0092	0.0030	0.0027	0.0063	0.0010
Fe	0.0000	0.0001	0.0000	0.0001	0.0002
Ga	0.0002	0.0002	0.0003	0.0002	0.0003
Ti	0.0002	0.0002	0.0001	0.0002	0.0003
V	0.0001	0.0001	0.0001	0.0001	0.0084
Ni	0.0002	0.0001	0.0001	-	0.0003
Mg	-	-	-	-	-
Total	2.0000	2.0000	2.0000	2.0000	2.0000

From EPMA results, Cr and V show significant atomic proportions, which could be related to the color of red sample. These elements were compared to investigate the relationship between color and elements in red samples (Figure 21). Figure 21 displays a comparison of atomic proportion between Cr and V in red samples. Sample R5, which appears purplish red, has the highest amount of V compared to those of other samples. Conversely, R1 has the highest amount of Cr, leading to the deepest red color. In the group of pinkish red, samples R2 and R3 have similar amount of Cr, thus give moderate shade of pinkish red color. In contrast, sample R4 has the highest amount of Cr in the group thus appears as darker pinkish red. It can be concluded that the red color of the sample corresponds to the amount of Cr found in the sample. It can be explained that the amount of trace elements, particularly Cr, are contributed to different shades of red colors (Figure 21).

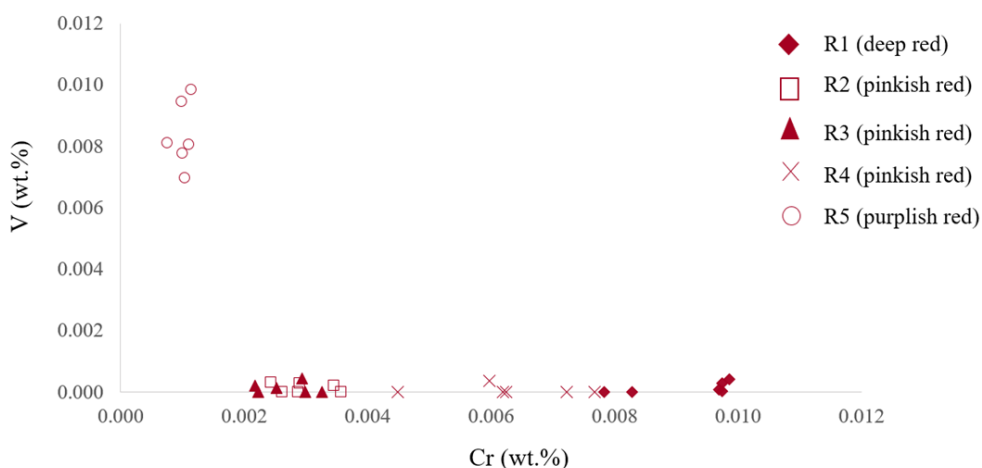
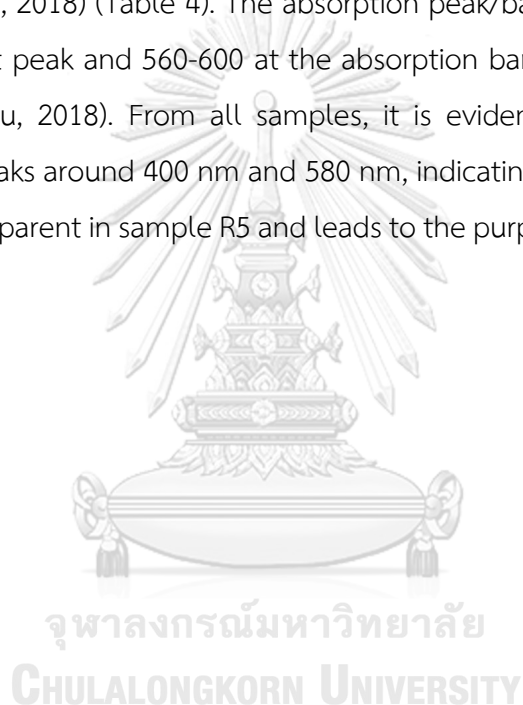


Figure 21 Atomic proportions of Cr and V in the red samples (R1-R5) from EPMA analyses.

4.1.3 UV-Vis-NIR Experiment

UV-Vis-NIR experiment is used to determine the type of trace elements and its oxidation state. Only O-ray measurements are included in this study due to the small sample size. Samples R1-R5 generally show two strong absorption positions (Figure 22, Table 4). The first absorption peak in all samples occurs in a range of 393-414 nm. The second absorption peak occurs around 552-580 nm in all samples, except for sample R5 which displays a wide absorption band at 558 nm. Sample R2 shows clear

absorption peaks at 414 nm and 564 nm that represent Cr^{3+} (Figure 22b). However, the absorption peak in samples R1, R3, and R4 include noticeable noises which were probably caused by detection limit of measurement due to intensity or thickness of sample, and the error of UV-Vis-NIR spectroscopy. The second absorption peaks at 552-580 are thus better used to indicate the presence of Cr^{3+} . Sample R5 clearly shows the first absorption peak at 393 nm and the second absorption band at 558 nm (Figure 22e). The first absorption peak around 400 nm in R5 is possibly due to the presence of Cr^{3+} and V^{3+} based on previous studies (Emmett et al., 2003; Schmetzer and Peretti, 2000; Shen and Lu, 2018) (Table 4). The absorption peak/band of V is around 400 and 500 nm at the first peak and 560-600 at the absorption band (Schmetzer and Peretti, 2000; Shen and Lu, 2018). From all samples, it is evident that red samples show absorption two peaks around 400 nm and 580 nm, indicating the presence of Cr^{3+} . The presence of V is apparent in sample R5 and leads to the purple shade in red corundum.



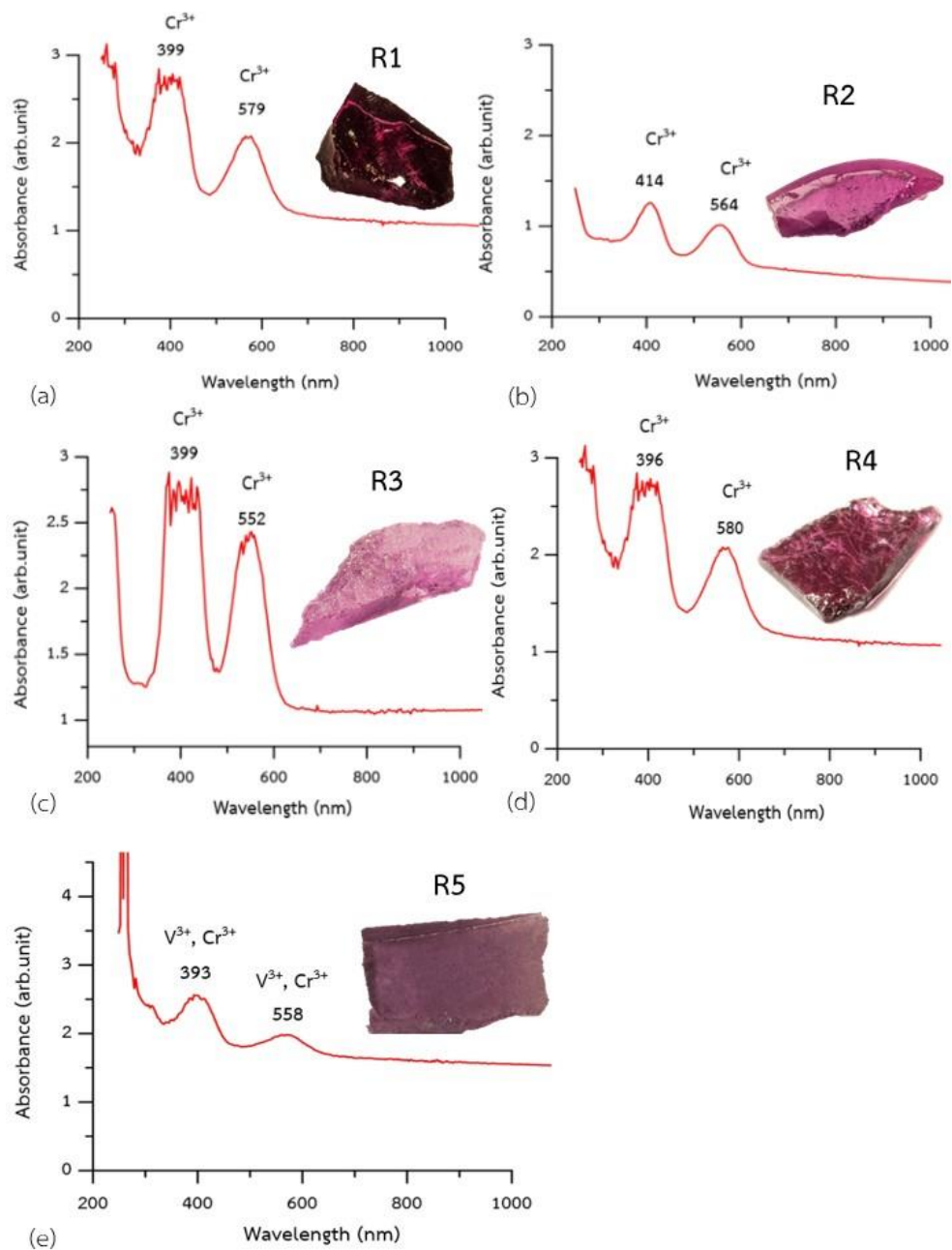


Figure 22 UV-Vis-NIR absorption spectra (O-ray) of red samples: (a) R1 in deep red, (b) R2 in pinkish red, (c) R3 in pinkish red, (d) R4 in pinkish red, and (e) R5 in purplish red.

Table 4 A comparison of UV-Vis-NIR absorption of Cr³⁺ and V³⁺ between previous studies and this study.

Elements	Wavelength (nm)		References	Remarks
	1 st peak	2 nd band		
Cr ³⁺	399-414	552-580	This study	Samples R1, R3, and R4 have noticeable noises in 1 st peak
Cr ³⁺ , V ³⁺	393	558	This study	Only sample R5
Cr ³⁺	400	550	Emmett et al., 2003; Shen and Lu, 2018	
Cr ³⁺	405	580	Schmetzer and Peretti, 2000	
Cr ³⁺	405-410	560	Schwarz et al., 2008	
V ³⁺	400	560	Shen and Lu, 2018 Schmetzer and Peretti, 2000	
V ³⁺	500	600	2000	

4.1.4 XANES Experiment

EPMA and UV-Vis-NIR results clearly indicate the presence of Cr as the major trace element in red samples. This is the reason why Cr was selected to be determined for its oxidation states in XANES experiment. V is a minor trace element in purplish red R5 sample but is not available as the standard in XANES measurement. The oxidation state is thus determined based on Cr₂O₃ (Cr³⁺) and CrO₃ (Cr⁶⁺) standards which were calibrated prior to the sample measurement. XANES spectra consist of three absorption zones: a pre-edge, a main edge, and a post-edge. The edge refers to each absorption taken from an element-specific core-electron excitation energy. The main edge thus can be used to determine the oxidation state and can be shifted up to 5 eV. The main absorption edge of Cr³⁺ and Cr⁶⁺ standards in this study are 6009 eV and 5992 eV, respectively. Samples R1-R5 show fairly consistent main absorption edges around 6009-6010 eV (marked by gray vertical solid line), which are closely similar to

the main absorption edge of Cr^{3+} standard (black dash line) (Figure 23). The main edge of samples R1 and R5 is at 6009 eV (Figure 23a, 23e) and slightly lower than those of samples R2, R3, and R4 at 6010 eV (Figure 23b, 23d). From XANES absorption results, it can be summarized that the main absorption edge of red samples closely resembles to the main edge of Cr^{3+} in Cr_2O_3 standard (dash line). XANES results are consistent with EPMA and UV-Vis-NIR observations, indicating Cr^{3+} as the main trace element in red synthetic corundums in this study.



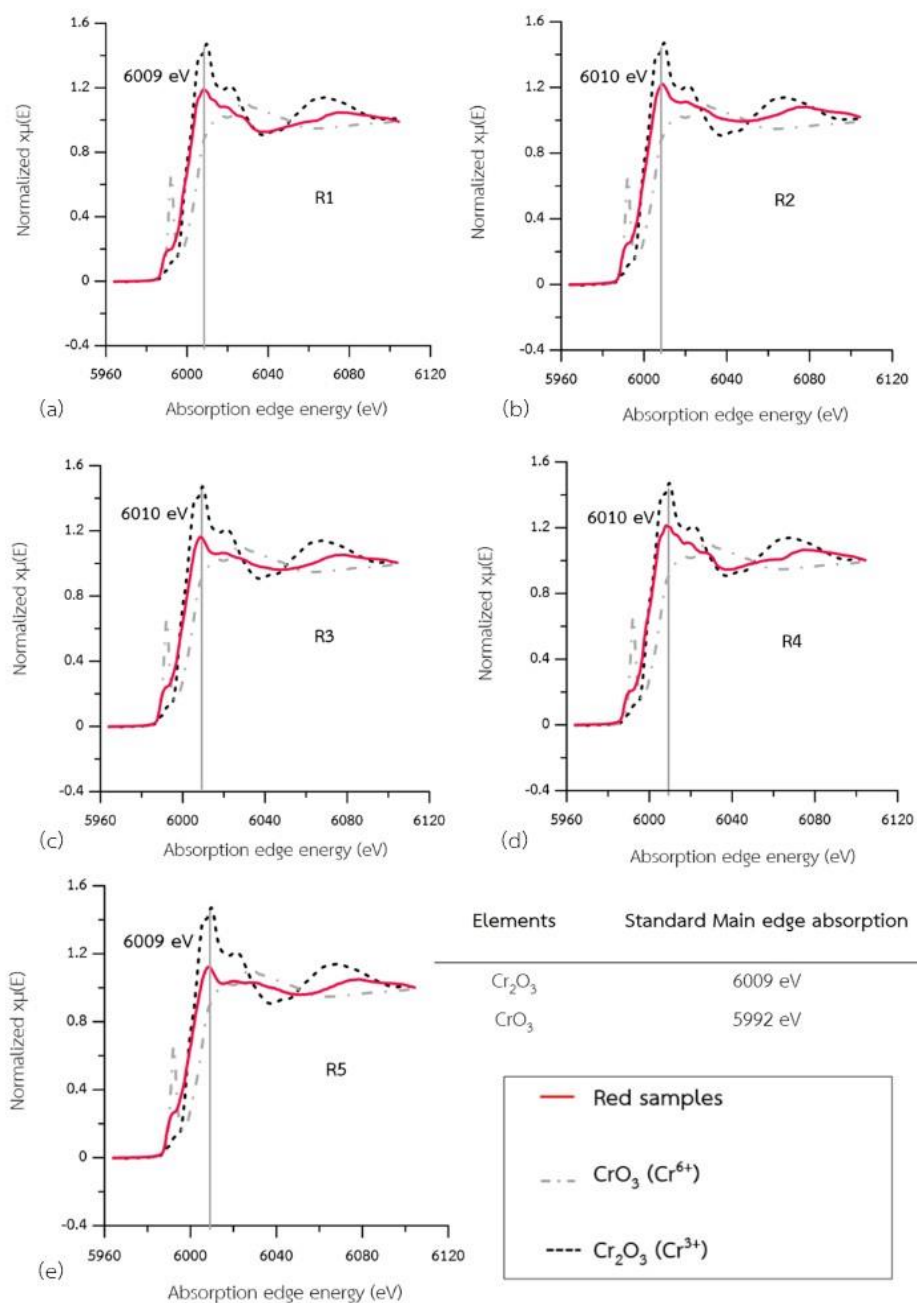


Figure 23 XANES absorption edges of red samples (a) R1, (b) R2, (c) R3, (d) R4, and (e) R5. The solid red line represents the absorption of samples, the dash-dotted line represents the absorption of the standard CrO_3 (Cr^{6+}), and the dash line represents the absorption of the standard Cr_2O_3 (Cr^{3+}). The main absorption edge is marked by a gray vertical line.

4.2 Blue synthetic corundum

Blue samples are first analyzed for their compositions by XRD experiment (Figure 19) and confirmed that their mineralogical compositions are corundum. Blue samples (B1-B5) are further determined for trace elements and oxidation states by using the EPMA, UV-Vis-NIR, and XANES.

4.2.1 EPMA Experiment

Blue samples were divided into three groups based on the color of samples: deep blue (B5), blue (B3), and pale blue (B1, B2, and B4) (Figure 24). In EPMA experiment, blue samples were measured in different twelve spots and the average amount of oxides is displayed in Table 5. The results show that Al_2O_3 is a major component in all blue samples as it is the main component of corundum. Apart from Al_2O_3 , TiO_2 shows a significant amount in most samples (Table 5). Therefore, six spots that found with a significant amount of TiO_2 were selected to calculate atomic proportion of compositional elements.

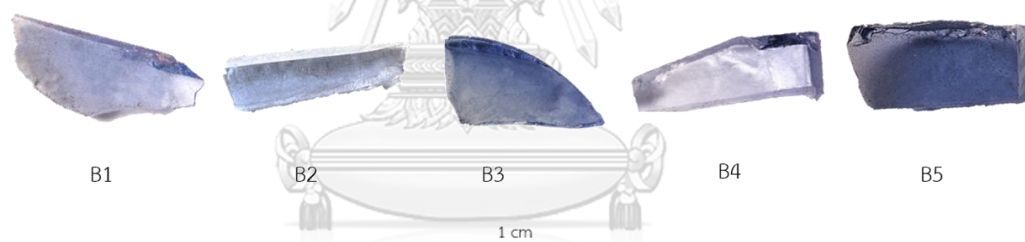


Figure 24 Blue synthetic sapphire samples: B1 (pale blue); B2 (pale blue); B3 (blue); B4 (pale blue); B5 (deep blue).

The average atomic proportion of cations based on these six spot analyses are shown in Table 4.5. The deep blue sample (B5) shows average amount of Ti at 0.0010 and Fe at 0.0002 (Table 6). Sample B3 is blue color which has average amount of Ti and Fe at 0.0015 and 0.0002, respectively (Table 6). The group of pale blue, consisting of sample B1, B2, and B4, shows relatively high average amount of Ti at 0.0016, 0.0015, and 0.0012, respectively while the average amount of Fe in the pale blue group is the same at 0.0002 for sample B1 and B2 except sample B4 show less average amount of Fe at 0.0001 (Table 6). The results illustrate that shades of color in blue samples are directly proportional to the amount of Fe. Sample B4 which has pale blue color

displays less amount of Fe than other samples. On the other hands, other samples having the average amount of Fe at 0.0002 tend to have more intense shades of blue color than the samples B4. These EPMA results suggests that the amount of Fe influences the shade of blue color in synthetic corundum. Full EPMA analyses of all blue samples can be found in Appendix B-C.

Table 5 The average amount of trace elements (wt%) based on six spot analyses in each blue synthetic corundum (B1-B5).

Oxides	Average oxide (wt%)				
	Samples				
	B1 (Blue)	B2 (Pale blue)	B3 (Pale blue)	B4 (Pale blue)	B5 (Deep blue)
Al ₂ O ₃	98.913	98.509	98.653	98.579	98.916
Cr ₂ O ₃	0.003	0.007	0.005	0.007	0.003
FeO	0.012	0.011	0.013	0.008	0.014
Ga ₂ O ₃	0.030	0.015	0.032	0.015	0.017
TiO ₂	0.128	0.115	0.117	0.094	0.079
V ₂ O ₃	0.004	0.007	0.010	0.043	0.036
NiO	0.008	0.011	0.018	0.003	0.020
MgO	0.001	ND	0.002	0.001	ND
Total	99.099	98.675	98.849	98.749	99.085

* ND: Not detected

Table 6 The average atomic proportion of blue synthetic corundum B1-B5.

Elements	Average atomic proportion				
	Samples				
	B1 (Blue)	B2 (Pale blue)	B3 (Pale blue)	B4 (Pale blue)	B5 (Deep blue)
Al	1.9972	1.9975	1.9971	1.9974	1.9976
Cr	-	0.0001	0.0001	0.0001	-
Fe	0.0002	0.0002	0.0002	0.0001	0.0002
Ga	0.0003	0.0002	0.0004	0.0002	0.0002
Ti	0.0016	0.0015	0.0015	0.0012	0.0010
V	0.0001	0.0001	0.0001	0.0006	0.0005
Ni	0.0001	0.0001	0.0002	-	0.0003
Mg	-	-	0.0001	-	-
Total	1.9996	1.9996	1.9997	1.9997	1.9998

Regarding to the averages of atomic proportion based on 3 oxygen atoms, Ti and Fe are compared to investigate the dominant elements in blue samples (Figure 25). The result shows that Ti and Fe is dominant elements in blue synthetic corundum samples. The result indicates that the highest Ti whereas, Fe are generally present in a very small amount in all blue samples.

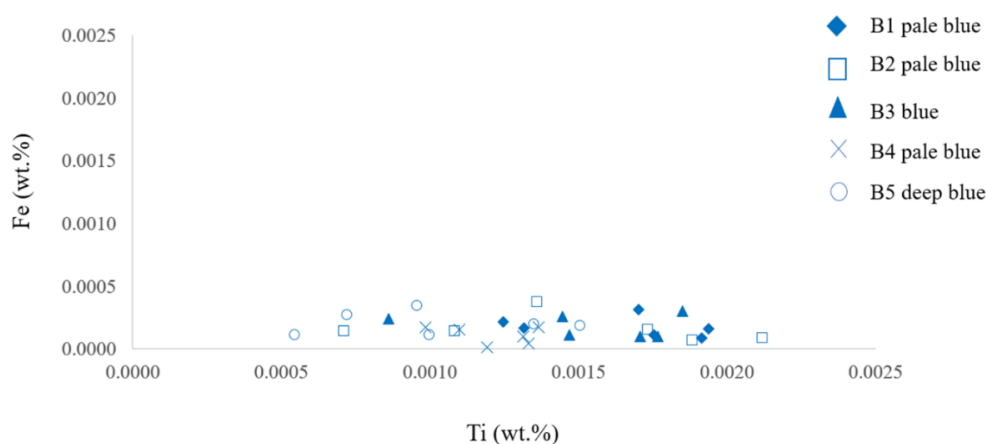


Figure 25 Atomic proportions of Ti and Fe in the blue samples (B1-B5) from EPMA analyses.

4.2.2 UV-Vis-NIR Experiment

UV-Vis-NIR spectroscopic investigation of blue synthetic corundums shows the absorption peaks of specific trace elements. Only O-ray spectra are present due to the small size of samples which can only be measured on one direction vertical the *c*-axis. Sample B4 shows clearly the 1st absorption peak at 400 nm (Figure 26d) that could represent Fe³⁺. Sample B2 shows clearly the 1st peak at 390 nm of Fe³⁺ (Figure 26b). Sample B5 shows the 1st absorption peak around 380 nm that represents Fe³⁺ (Figure 26e). While samples B1 and B3 show resemble of 1st peak at 380 nm (Figure 26a, 26c) represent of Fe³⁺. However, all samples show clearly absorption band at 576-590 nm which represents the absorptions of Fe²⁺-Ti⁴⁺ pair, (Figure 26a-e). The absorption of blue synthetic samples in this study are indicated based on the absorption values in blue corundums reported in previous studies (Table 7). It is evident that all samples show clearly the absorption band of Fe²⁺-Ti⁴⁺ pair and Fe³⁺ absorption at the 1st peak. Especially some sample has pale color contains have clearly peak at the 1st absorption in the UV-Vis-NIR spectra.

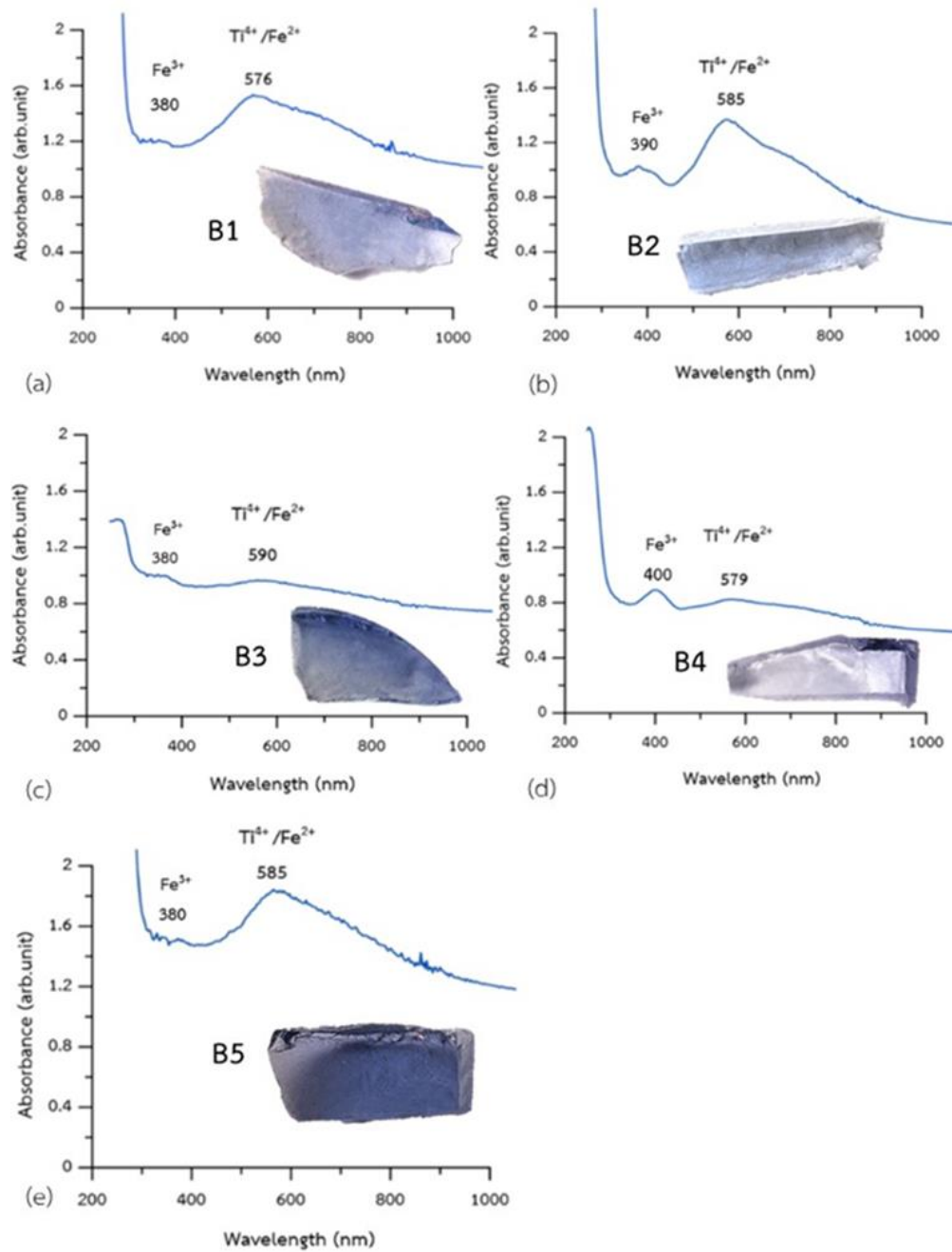


Figure 26 UV-Vis-NIR absorption spectra (O-ray) of blue synthetic corundum samples: (a) pale blue B1, (b) pale blue B2, (c) blue B3, (d) pale blue B4, and (e) deep blue B5.

Table 7 A comparison of UV-Vis-NIR absorptions of Fe²⁺-Ti⁴⁺ pair between previous studies and this study.

Elements	Wavelength (nm)			References
	1 st peak	2 nd band	3 rd band	
Fe ²⁺ -Ti ⁴⁺		576-590		This study
Fe ³⁺	380-400			This study
Fe ³⁺	388, 398			Shen and Lu, 2018
Fe ²⁺ -Ti ⁴⁺		700		Emmett et al., 2003; Schwarz et al., 2008
Fe ²⁺ -Ti ⁴⁺		570		Shen and Lu, 2018; Amphon and Thanasuthipitak, 2016
Fe ²⁺ -Ti ⁴⁺		550-600	680-750	Sutherland et al., 1998

4.2.3 XANES Experiment

Results from UV-Vis-NIR and EPMA experiments suggest that Ti and Fe are the major trace elements in the blue samples. In particular, the highest amount of Ti recorded by EPMA experiment; therefore, it was selected to be determined for its oxidation state by XANES. The samples B1-B5 show the main absorption edge around 4987-4989 eV. These main edges are fairly consistent across all samples, indicating the oxidation state of Ti⁴⁺ (Figure 27). Samples B1, B4, and B5 reveal the main edge at 4989 eV while samples B2 and B3 show the main edge slightly shifted to 4987 eV (Figure 27). The main edge of samples B1, B2, and B4 are fairly consistent between main absorption edge of Ti⁴⁺ (rutile) and Ti⁴⁺ (anatase). While sample B3 similar to main absorption edge of Ti⁴⁺ (rutile) standard (dash line). and sample B5 clearly similar to main absorption edge of Ti⁴⁺ (anatase) standard (dash-dotted line). However, XANES absorption results can indicate that the most main absorption edge of blue samples. These samples closely resemble to the main absorption edge of Ti⁴⁺ in TiO₂ (anatase) standard (dash-dotted line).

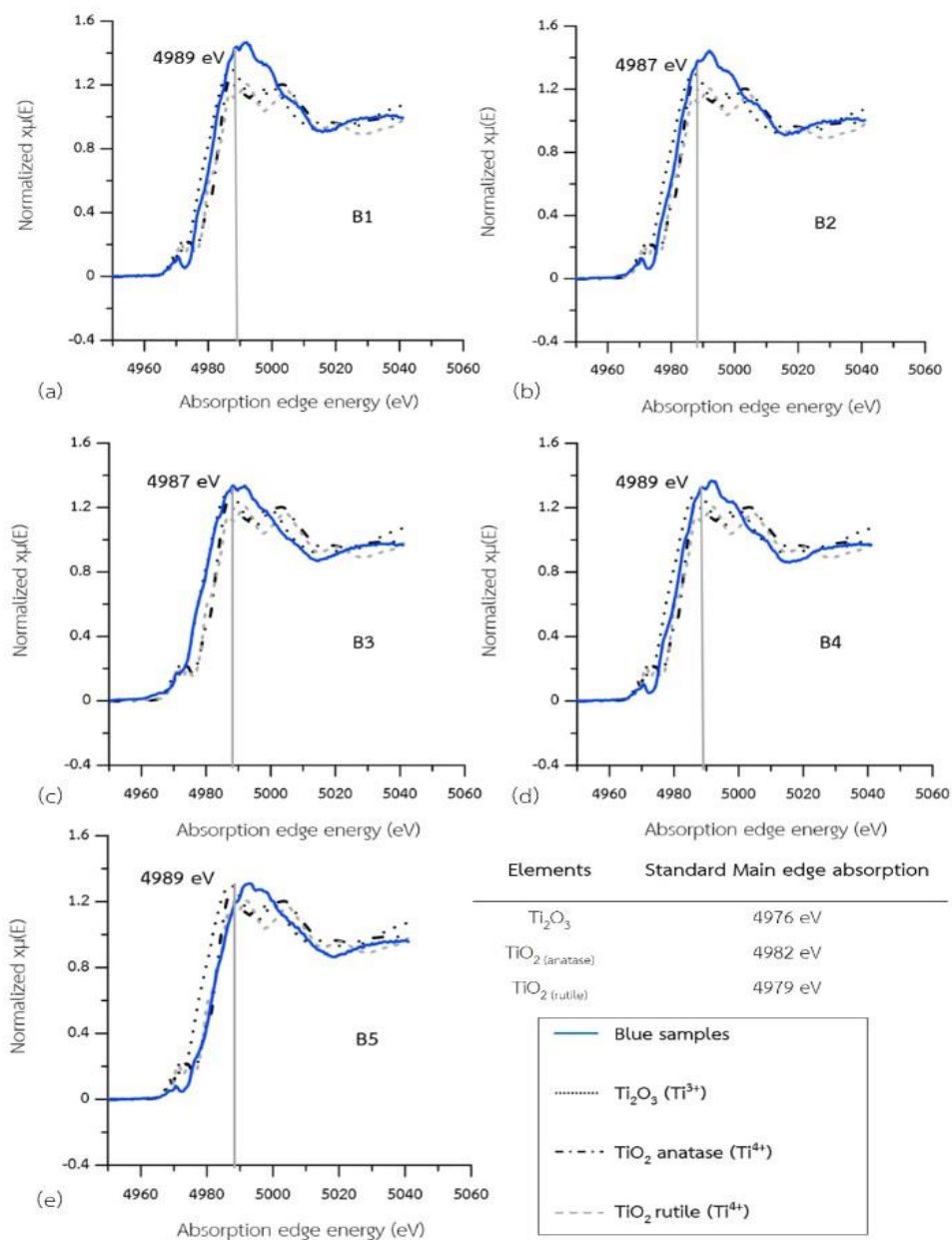


Figure 27 XANES absorption near edge of blue samples (a) B1, (b) B2, (c) B3, (d) B4, and (e) B5; the solid blue line represents the absorption of samples, dotted line represents the absorption of the standard Ti₂O₃ (Ti³⁺), dash-dotted line represents the absorption of the standard TiO₂ (Ti⁴⁺) (anatase), and dash line represents the absorption of the standard TiO₂ (Ti⁴⁺) (rutile). The main absorption edge is marked by a gray vertical line.

4.3 Yellow synthetic corundum

Yellow synthetic corundum samples were initially analyzed for mineralogical characteristic by XRD technique (Figure 19). XRD result identifies the main composition of these samples as corundum. The yellow samples (Y1-Y5) are further analyzed to determine the type, weight oxides, and oxidation state of trace elements using EPMA, UV-Vis-NIR, and XANES experiments, respectively.

4.3.1 EPMA Experiment

Yellow samples were divided into three groups based on their colors: yellow (Y4), orangish yellow (Y2, Y3, and Y5) and pale yellow (Y1) (Figure 28). In EPMA experiment, yellow samples were measured in different twelve spots and six spots were selected based on significant amount of elements that possibly the cause of color in yellow synthetic corundums.



Figure 28 Yellow synthetic corundum samples: Y1 (pale yellow); Y2 (orangish yellow); Y3 (orangish yellow); Y4 (yellow); Y5 (orangish yellow).

The averaged oxide compositions are displayed in Table 8. All yellow samples Y1-Y5 show that Al_2O_3 is the major component. In addition to Al_2O_3 , Cr_2O_3 and NiO show significant amounts in all samples (Table 8). Six spots with higher amounts of CrO_3 and NiO were selected to calculate the atomic proportions. The average atomic proportions of cations based on 3 oxygen atoms of these samples are shown in Table 9. Yellow sample Y4 shows average proportions of Cr and Ni at 0.0005 and 0.0002, respectively. Orangish yellow samples, Y2, Y3 and Y5 show high average amounts of Cr at 0.0009, 0.0005 and 0.0004, respectively and these samples show an equal proportion of Ni at 0.0002. The pale yellow sample Y1, shows average amount of Cr at 0.0002 and highest Ni at 0.0004. Full range of EPMA analyses of yellow synthetic corundum samples are collected in Appendix D-E.

Table 8 Average EPMA analyses based on selective six spot analyses in each yellow synthetic corundum (Y1-Y5).

Oxides	Average oxide (wt%)				
	Samples				
	Y1 (Pale yellow)	Y2 (Orangish yellow)	Y3 (Orangish yellow)	Y4 (yellow)	Y5 (Orangish yellow)
Al ₂ O ₃	99.074	99.207	98.610	98.546	98.692
Cr ₂ O ₃	0.018	0.068	0.037	0.034	0.030
FeO	0.012	0.005	0.009	0.003	0.003
Ga ₂ O ₃	0.017	0.009	0.022	0.028	0.022
TiO ₂	0.003	ND	0.001	0.016	ND
V ₂ O ₃	0.006	0.004	0.003	0.001	ND
NiO	0.031	0.012	0.016	0.017	0.019
MgO	ND	0.001	0.001	ND	0.002
Total	99.160	99.305	98.699	98.645	98.769

* ND: Not detected

Table 9 Average atomic proportions of major and trace elements in synthetic yellow corundum samples Y1-Y5.

Elements	Average atomic proportion				
	Samples				
	Y1 (Pale yellow)	Y2 (Orangish yellow)	Y3 (Orangish yellow)	Y4 (yellow)	Y5 (Orangish yellow)
Al	1.9990	1.9988	1.9990	1.9988	1.9993
Cr	0.0002	0.0009	0.0005	0.0005	0.0004
Fe	0.0002	0.0001	0.0001	-	-
Ga	0.0002	0.0001	0.0002	0.0003	0.0002
Ti	-	-	-	0.0002	-
V	0.0001	0.0001	-	-	-
Ni	0.0004	0.0002	0.0002	0.0002	0.0002
Mg	-	-	-	-	-
Total	2.0002	2.0001	2.0001	2.0000	2.0001

Based on average atomic proportions, Cr is recognized to be the most abundant trace element in all yellow samples, with a range of 0.0002-0.0009 atoms. In addition to Cr, Ni is also recorded in these synthetic samples. Figures 29 compare the atomic proportions of Cr and Ni. The component of Cr has the highest amount in yellow synthetic samples that possibly leading to the orangish yellow color (Figure 29).

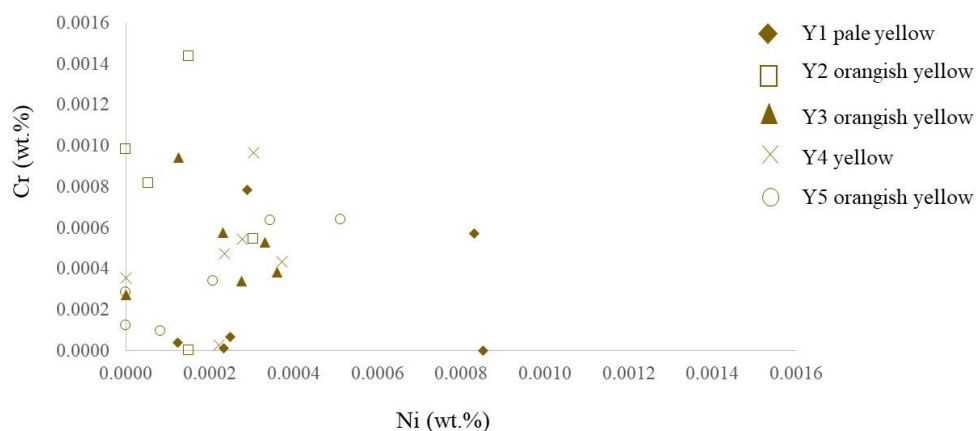


Figure 29 Atomic proportions of Cr and Ni in the yellow samples (Y1-Y5) from EPMA experiment.

4.3.2 UV-Vis-NIR Experiment

The result of the yellow synthetic corundum measurement from UV-Vis-NIR shows the absorption peaks of trace element in samples. Samples Y3 and Y4 show only one absorption peak at 417 nm and 402 nm, which can be due to the presence of Ni^{2+} and Ni^{3+} (Figure 30c, 30d). Samples Y1, Y2, and Y5 show two absorption positions, these samples show 1st absorption peak at 420 nm, 399 nm, and 405 nm respectively, that represent Cr^{3+} , Ni^{2+} , and Ni^{3+} (Figure 30a, 30b, 30e). In addition to the 1st absorption peak, sample Y1, Y2, and Y5 shows 2nd absorption peak at 570 nm, 531 nm, and 550 nm that indicate the presence of Cr^{3+} (Figure 30a, 30b, 30e). In this study, the absorption peaks of yellow samples were indicated based on the absorption values in corundum reported in previous studies (Table 10). It is evident that all samples show the absorption of Ni^{2+} , and Ni^{3+} , while some sample has Cr^{3+} absorption in UV-Vis-NIR experiment.

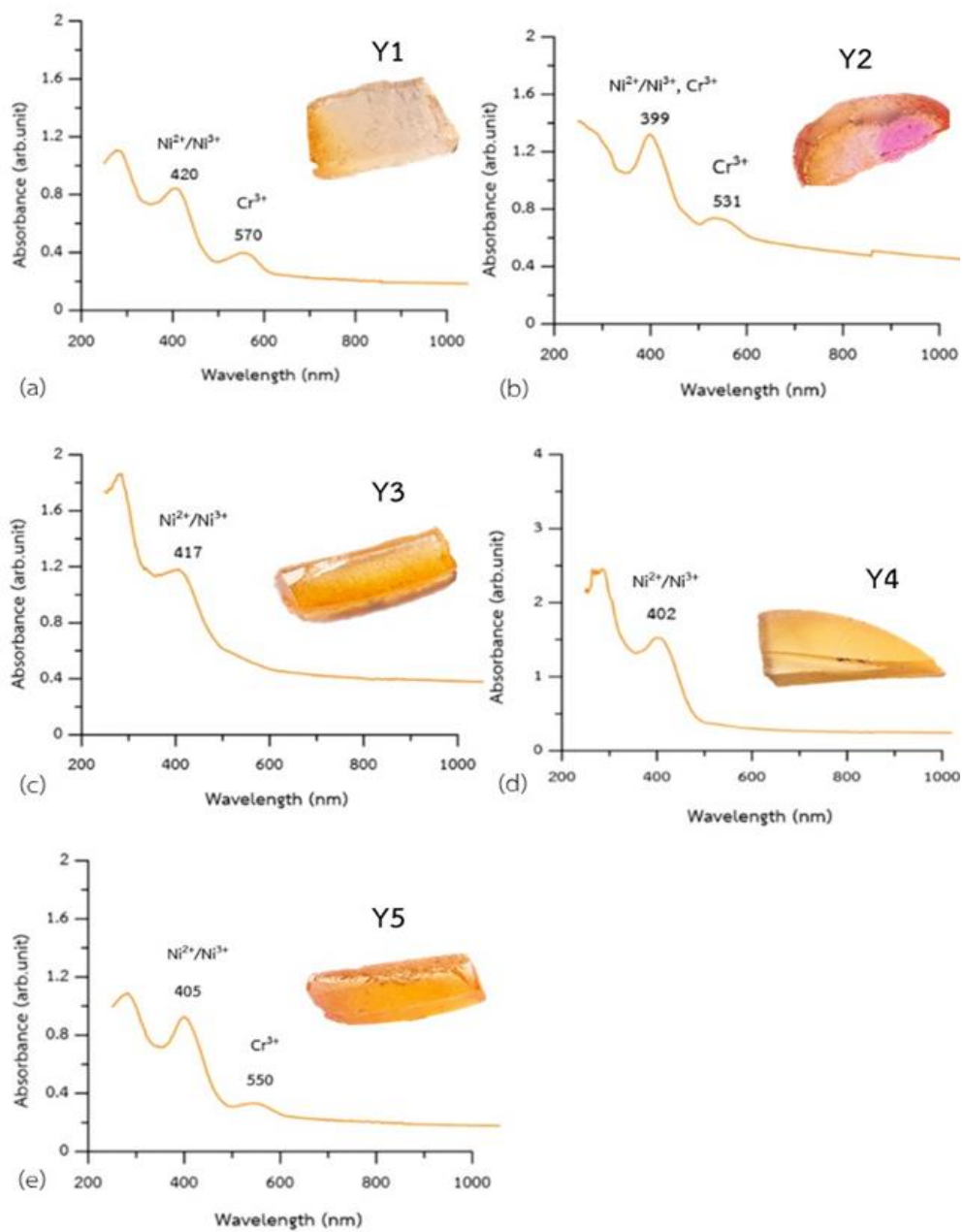


Figure 30 UV-Vis-NIR absorption spectra (O-ray) of yellow samples: (a) pale yellow Y1, (b) orangish yellow Y2, (c) orangish yellow Y3, (d) yellow Y4, and (e) orangish yellow Y5.

Table 10 A comparison of UV-Vis-NIR absorption values of Cr^{3+} , Ni^{2+} , and Ni^{3+} between previous studies and this study.

Elements	Wavelength (nm)		References	Remarks
	1 st peak	2 nd band		
Ni^{2+} or Ni^{3+}	399-420		This study	All samples
Cr^{3+}		530-570	This study	Only sample Y1, Y2, and Y5
Cr^{3+}	400	550	Emmett et al., 2003; Shen and Lu, 2018	
Cr^{3+}	405	580	Schmetzer and Peretti, 2000	
Cr^{3+}	405-410	560	Schwarz et al., 2008	
Ni^{3+}	400		Thomas et al., 1997	
Ni^{2+}	380,420	580-620	Thomas et al., 1997	

4.3.3 XANES Experiment

Based on EPMA and UV-Vis-NIR results, major trace elements in yellow synthetic corundums are Cr and Ni. According on our results of red synthetic corundum, the presence of Cr_2O_3 leads to red color. While Ni detected in EPMA and UV-Vis-NIR experiments but Ni standard was not available for our experiment in the XANES laboratory. Thus, Fe was selected as a representative to measure the oxidation states instead. The XANES spectrum of Fe_3O_4 standard was compared to that of FeO and Fe_2O_3 as shown in Figure 31. The spectra are smeared out due to the limited flux and finite energy resolution of synchrotron X-ray. However, the difference in the absorption edge position in the three standards confirms that the energy resolution is sufficient to resolve the change in the oxidation state of Fe ions. In the measurement, the samples Y1-Y5 show the absorption energy around 7132 eV, which is closely similar to the absorption of Fe^{2+} and Fe^{3+} in Fe_3O_4 standard (Figure 31). However, the shape of absorption edge is quite different from the Fe standards without the clearly main edge.

While only trace amount of Fe was measured in EPMA experiment and the Fe-related absorption peak was not detected in UV-Vis-NIR experiment. Therefore, the results of XANES experiment may not be helpful to understand the color formation of yellow synthetic samples.

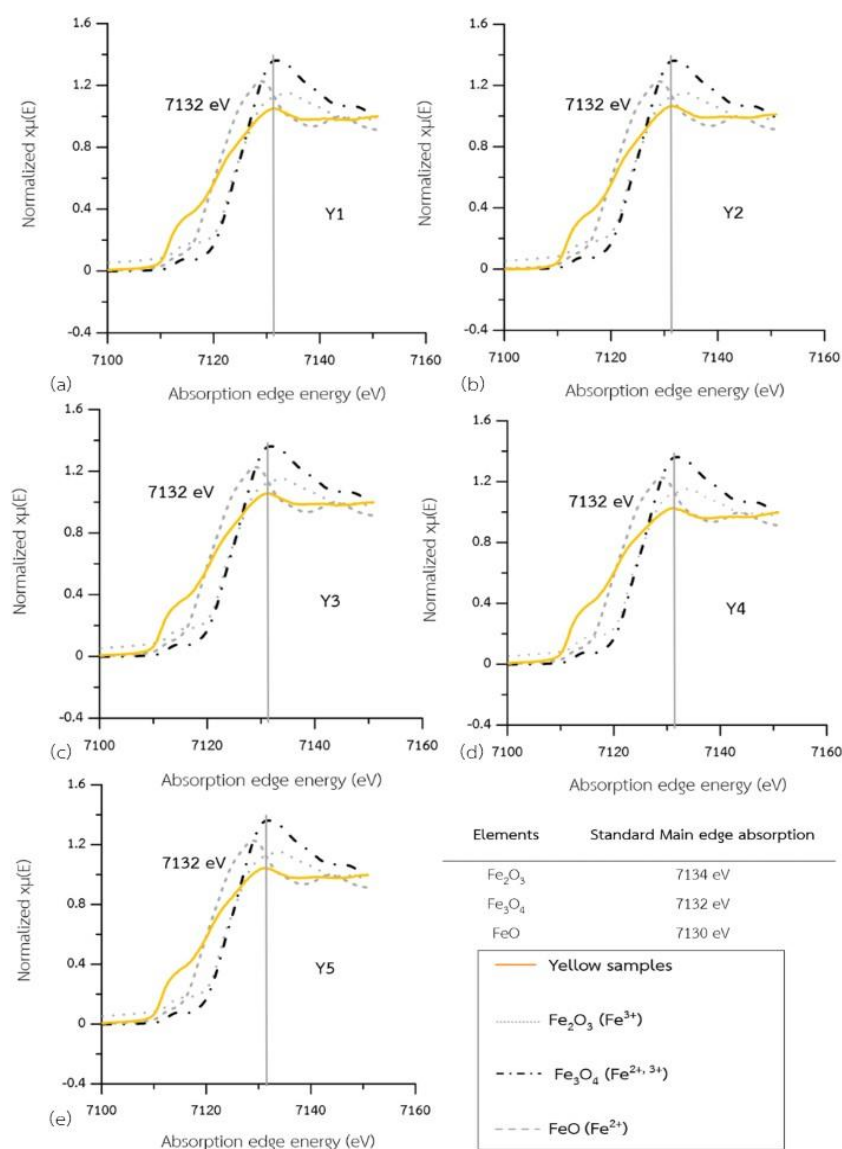


Figure 31 XANES absorption of yellow samples (a) Y1, (b) Y2, (c) Y3, (d) Y4, and (e) Y5. The solid line represents the absorption of yellow samples, the dotted line represents the absorption of the standard Fe₂O₃ (Fe³⁺), dash-dotted line represents the absorption of the standard Fe₃O₄ (Fe²⁺, Fe³⁺), and the dashed line represents the absorption of the standard FeO₂ (Fe²⁺). Main edge peak is also marked by a gray vertical line.

Chapter 5

Discussion

To understand the cause of color in synthetic corundum, the oxidation states of trace elements were determined by using X-Ray Diffraction (XRD), Electron Probe Micro-Analyzer (EPMA), UV-Vis-NIR experiment, and X-ray Absorption Near Edge Structure (XANES) methods. XRD results were used to confirm the composition of synthetic corundums to be Al_2O_3 (Figure 19) while EPMA observations indicate the type and amount of metal oxides within the samples (Tables 2, 5, 8). UV-Vis-NIR measurements further show the absorption patterns of radiation as a function of wavelength due to its interaction with metal impurities in different oxidation states (Figures 22, 26, 30). In addition, XANES experiments were used to confirm the oxidation state of metals by observing the *K*-edge absorption and coordination of the structure (Figures 23, 27, 31). The cause of color in red, blue, and yellow synthetic corundums are discussed in the following sections.

5.1 Red synthetic corundum

5.1.1 Type and oxidation state of trace elements

Results from EPMA, UV-Vis-NIR, and XANES experiments indicate that Cr^{3+} is the major contributing factor to red color in synthetic corundums. The presence of V^{3+} in minor amount further gives the purple hue in some samples R5. In particular, EPMA results show a strong correlation between atomic proportion and the red shade (Table 3). Sample R1 has the highest atomic proportion of Cr, which leads to a deep red color. Samples R2, R3, and R4 have a moderate atomic proportion of Cr, which gives the pinkish red color. Interestingly, sample R5 has the lowest atomic proportion of Cr and the highest amount of V, which gives the purplish red color. UV-Vis-NIR results show consistent absorption patterns of Cr^{3+} in all samples. In general, the first absorption peak is present around 400-410 nm while the second peak is detected around 500-580 nm. The observation of Cr^{3+} absorption peaks is comparable with the absorption peaks of red synthetic corundums (Schmetzer and Peretti, 1999; Schmetzer and Peretti, 2000) and natural corundums (Emmett et al., 2003; Schwarz et al., 2008; Shen and Lu, 2018) in previous studies. Some Cr^{3+} absorption peaks in this study are slightly shift

from other studies (Table 4) possibly due to the small sample size, which creates a gap between the sample and the slit. Therefore some light rays, which do not pass through the sample, directly reach the signal detector, causing the slight shift of absorption spectra (Kantakapun, 2017). The measurement can thus be only measured in one axis (O-rays).

In addition to Cr^{3+} , V^{3+} is another important trace element in purplish red samples, particularly sample R5. The range of visible light is around 400-700 nm (Newton, 1952) and appears in different colors when transmitted through different mediums or known as 'transmitted light'. The color spectrum can be mapped into the circle known as 'the color wheel' or complementary color (Figure 32) (Clark, 2014), which indicates that the transmitted color (or transmitted light) is opposite color in the color wheel of the absorbed spectrum. The range of light absorption is an approximated value as it is a continuous electromagnetic spectrum (Table 32) (Bruno and Svoronos, 2005). The range of 1st absorption peak (~393-399 nm) in red samples is slightly below the range of visible light and less likely contributed to the coloration (Figure 22). The 2nd absorption peak in red samples is around (552-580) (Figure 22), which indicates the absorption of green-yellow range (Figure 32) and the transmission of red-purple color. Thus, red samples with higher absorption values (e.g. 550-600 nm) appear as dark red or purple.

The presence of V^{3+} is clearly visible at 558 nm in sample R5, which is similar to the detection of V^{3+} in synthetic corundum from 500 nm and 600 nm (Schmetzer and Peretti, 2000). The presence of Cr^{3+} is further confirmed by the detection absorption edge at 6009-6010 eV, which coincides with Cr_2O_3 standard in XANES experiments. Previous studies report the same values of absorption edge at 6010 eV and the shape of absorption edge is closely similar to this study (Gaudry et al., 2005; Tromp andMoulin andReid and Evans, 2007; Wongkokua andPongkrapan andDararutana andT-Thienprasert and Wathanakul, 2009). Therefore, it can be summarized that Cr^{3+} is the major contributing factor to red color while V^{3+} is the main cause of purple color in red synthetic corundums.

Table 11 The range of absorption color in visible light

Wavelength (nm)	Absorption color
400	Violet
450	Indigo
480	Blue
490	Blue-green
530	Green
570	Yellow-green
600	orange
650	red

Available from: faculty.sites.uci.edu

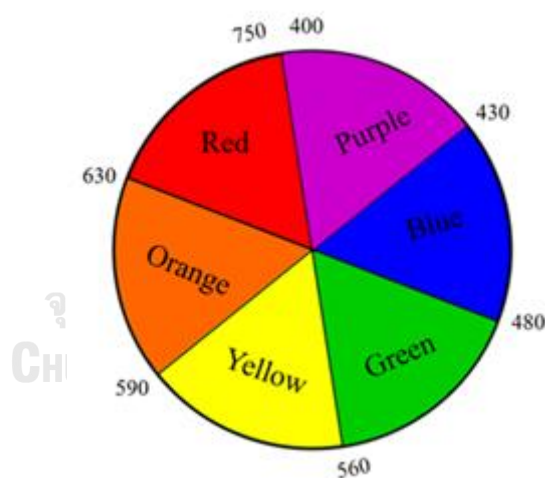


Figure 32 Complementary wheel Available from: faculty.sites.uci.edu

5.1.2 Cause of red color

In pure corundum (Al_2O_3), all electrons are paired and there is no light absorption. During corundum synthesis process, aluminum oxide and chromium oxide are mixed and heated, allowing some aluminum atoms to be substituted by chromium atoms. In general, corundum structure has negatively charged oxygen ions surround the aluminum ions, which normally donate three electrons to create covalent bond

with oxygen. In order to remain the same charge balance, chromium atom thus must donate three electrons to become Cr^{3+} and replace Al^{3+} in corundum structure (Figure 33). The substitution by Cr^{3+} further leads to the distortion of regular octahedral site in Al_2O_3 and changes the Al-O bonding properties (Figure 34).

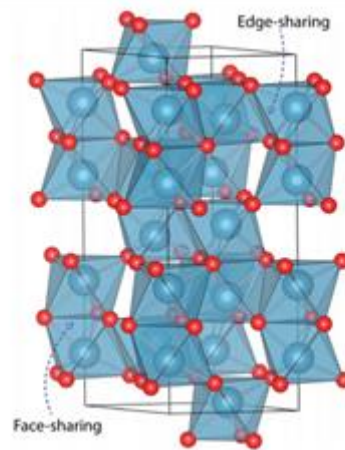


Figure 33 The structure of corundum: blue circle represents Al atom and red circle represents O atom (Bristow et al., 2014).

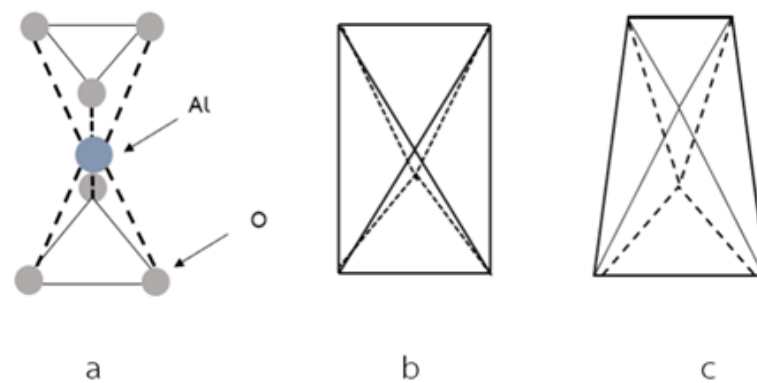


Figure 34 The corundum structure of corundum: (a) Al_2O_3 in octahedral structure (b) regular octahedral (c) irregular octahedral (Nassau, 1987).

In Al^{3+} , there are no partially filled energy levels or orbitals or unpaired electrons. However, in Cr^{3+} there are unpaired electrons, which can be excited and cause the absorption of certain wavelengths of light, resulting in color. These unpaired electrons in Cr^{3+} absorbs in the blue range around 400 nm and the green color around 550 nm and transmit the red color (Berlien et al., 2012). This phenomenon can be

explained by the field theory (Nassau, 1980), which involves the splitting of d -orbitals of Cr. When the Cr^{3+} substituted for Al^{3+} in corundum structure, ligand in the structure requires more energy to receive unpaired electron in d -orbitals of Cr^{3+} . This leads to splitting in the d -orbitals energy levels of Cr^{3+} and having energy gap between low energy (d_{xy}, d_{yz}, d_{zx}) and high energy ($d_x^2-d_y^2, d_z^2$) (Figure 35). Therefore, the unpaired electrons of Cr^{3+} can move from the ground state (low energy) to excited state (high energy) which requires certain energy for the unpaired electron to change its state. The energy absorbs the light in the range of green and blue, as a result, the corundum shows red color (Nassau, 1978; Rückamp et al., 2005).

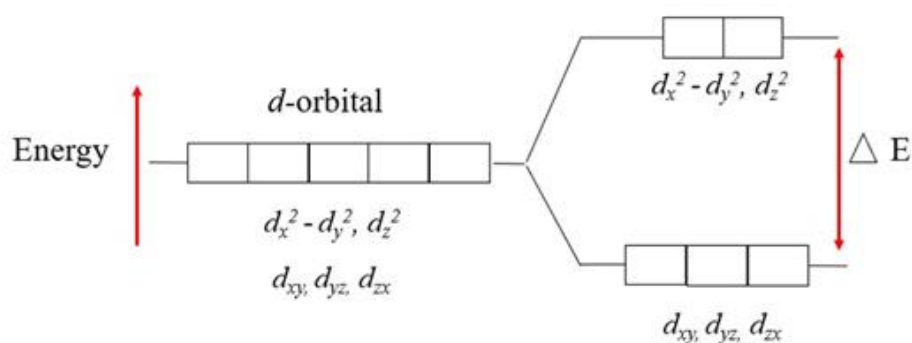


Figure 35 The splitting of d -orbitals in octahedral structure. Available from: chemistry.stackexchange.com

In addition to Cr^{3+} , V^{3+} was found in EPMA and UV-Vis-NIR experiments. A study by Deer (2011) suggests that the coloration of Cr^{3+} provides the red color in ruby and in some case V^{3+} produce the violet in corundum (Deer, 2011). The cause of violet color in corundum occurs due to V^{3+} substituted for Al^{3+} (Zaw and Sutherland and Yui and Meffre and Thu, 2015). In V^{3+} bearing corundum, V^{3+} substituted for Al^{3+} and distorted octahedral site in the crystal structure which has a same process as Cr^{3+} . Thus the cause of color of V^{3+} bearing corundum is the crystal field theory (Burns, 1993). The absorption of Cr^{3+} is in range of green that makes the appearance of the red color. While V^{3+} has absorption in the regions of yellow that causes the purple-blue color (Anderson and Payne and Mitchell, 1998). In some cases, V^{3+} and Cr^{3+} can be found

together in corundum and the cause of color involving these elements are also known as the alexandrite effect (Deer, 2011; Nassau, 1978).

Alexandrite is well known as the pleochroism gemstone that the color change under the difference light (daylight and incandescent light). The absorption spectra in alexandrite are quite different from ruby due to the bands absorption of V (Anderson and Payne and Mitchell, 1998). Previous studies suggest that the color change from grayish-green to reddish-violet in corundum caused by the presence of V^{3+} is known as the alexandrite effect (Gübelin and Schmetzer, 1982; Schmetzer and Peretti, 2000). The alexandrite effect is caused by a high absorption range in red and blue green spectra. In this study, sample R5 shows alexandrite effect which has bluish purple color in daylight and changes to red in incandescent light. In daylight, the blue shortwave is predominant and the human eyes are sensitive to the green light, resulting in blue-green color in gemstone. Similarly, in incandescent light, the longwave component is predominant and the human eyes perceive red color thus in incandescent light the alexandrite shows red color (Gübelin and Schmetzer, 1982). When applying incandescent light to sample R5, the color changes from purplish red to red color. Although the observation of color change in this study is different from previous studies, it highlights the significance of V^{3+} in corundum (Figure 36).



Figure 36 Color change apparent in the red synthetic corundum sample (R5): (a) side view in daylight, (b) top view showing bluish purple in daylight, and (c) top view showing purplish red in incandescent light.

5.1.3 Comparison with previous studies

All experimental results indicate that Cr^{3+} is the main cause of red color while V^{3+} affects the color change in red synthetic corundums. In general, natural red corundums has Cr^{3+} is the cause of color (Fritsch and Rossman, 1987; Sutherland and Zaw and Meffre and Yui and Thu, 2014; Zaw and Sutherland and Yui and Meffre and Thu, 2015). Similarly, Cr^{3+} is the cause of color in red synthetic corundum (Schmetzer and Peretti, 1999; Thomas and Mashkovtsev and Smirnov and Maltsev, 1997; Wongkookua and Pongkrapan and Dararutana and T-Thienprasert and Wathanakul, 2009). The previous study suggested that the amount of V^{3+} between natural and synthetic red corundum is different (Muhlmeister and Emmanue and Shigley and Devouard and Laurs, 1998). The result from comparison of V^{3+} in natural and synthetic corundum shows that the natural red corundum has higher V^{3+} than synthetic corundum (Figure 37). In this study, the result shows that the amount of V is fairly consistent with synthetic corundum in previous study except in some sample (R5). Moreover, the previous study shows V^{3+} is the cause of color change in corundum both natural and synthetic (Fritsch and Rossman, 1987; Schmetzer and Peretti, 1999; Zaw and Sutherland and Yui and Meffre and Thu, 2015). When comparison between natural and synthetic red corundum. It can summarize Cr^{3+} is the cause of color in red synthetic samples and V^{3+} is the main element to produce purple shade and leading to the color change in synthetic sample R5. There are consistent with previous study (Table 12).

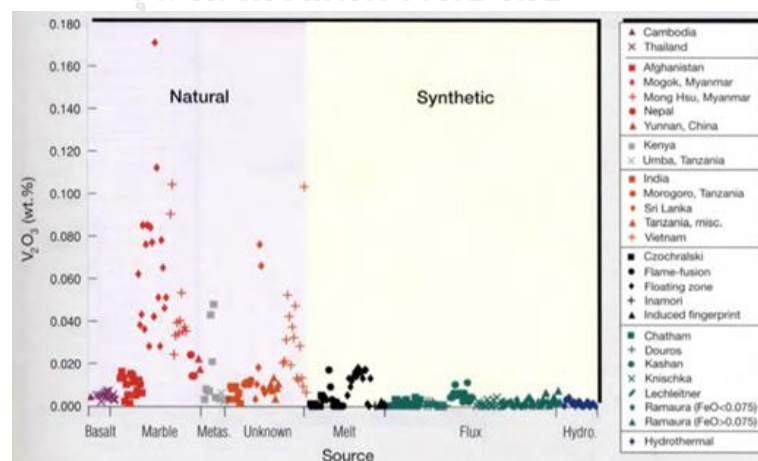


Figure 37 Comparison the amount of V^{3+} in red corundum between natural and synthetic (Muhlmeister et al., 1998).

Table 12 Comparison the oxidation state of trace elements in red synthetic corundum samples between previous studies and this study.

Color	Type	Cause of color	Remarks
Red, Pinkish red	Synthetic	Cr ³⁺	This study
Purplish red and color change	Synthetic	V ³⁺	This study
Red	Natural	Cr ³⁺	Sutherland et al., 2014
Red, Pinkish red	Natural	Cr ³⁺	Zaw, 2014
Red	Natural	Cr ³⁺	Fritsch and Rossman, 1987
Red	Synthetic	Cr ³⁺	Schmetzer et al., 1999
Red	Synthetic	Cr ³⁺	Thomas et al., 1997
Red	Synthetic	Cr ³⁺	Wongkokua et al., 2009
Color change	Natural	V ³⁺	Fritsch and Rossman, 1987
Color change	Natural	V ³⁺	Zaw, 2015
Color change	Synthetic	V ³⁺	Schmetzer et al., 2000

5.2 Blue synthetic corundum

5.2.1 Type and oxidation state of trace elements

The results of EPMA, UV-Vis-NIR, and XANES show that Ti⁴⁺ is a dominant element in blue synthetic corundum, while the blue coloration also requires the presence of Fe. The EPMA experiment may shows a relationship between the atomic proportion of elements and its blue shade. Sample B1, B2, and B4, which have the amounts of Ti at 0.0016, 0.0015, and 0.0012, respectively, appear pale blue color. Sample B3, has the amount of Ti at 0.0015 shows blue color and sample B5, which has the lowest amount of Ti at 0.0010, shows deep blue color (Table 6). Thus, the Ti contents are not directly related to the intensity of the stone's blue coloration. The fact that the shade of color possibly relates to the amount of trace element. Higher amount of specific trace elements tends to give the more intense color of corundum (Itten, 1970). Nonetheless, the EPMA results suggest that Fe affects the shade of blue corundum. The sample B4 shows the palest blue color and has the least amount of

Fe (Table 4.5). Assuming that the amount of Fe in all samples detected by EPMA is Fe^{2+} , the lowest amount of Fe^{2+} thus leads to the lightest shade of blue synthetic corundum. The samples B1, B2, and B3 have similar amount of Fe at 0.0002 (Table 6) and show more comparable shade of blue. Despite having similar amount of Fe to other samples, sample B5 appears dark blue which may be due to the difference of sample thicknesses or the reason explained below.

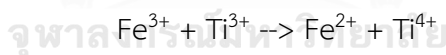
In general, the absorption band in blue corundum is around 570-700 nm and 680-750 nm which represents Ti^{4+} - Fe^{2+} pair in natural corundum that show in the previous studies (Amphon and Thanasuthipitak, 2016; Emmett et al., 2003; Shen and Lu, 2018; Sutherland and Schwarz and Jobbins and Coenraads and Webb, 1998). This study shows the range of 1st absorption peak around 380-400 nm (Figure 26) that represent Fe^{3+} (Emmett et al., 2003; Shen and Lu, 2018) in blue samples is less likely contributed to coloration due to the range of absorptions are below the range of visible light. While the range of 2nd absorption band at around 576-590 nm (Figure 26) represents pair of Ti^{4+} - Fe^{2+} (Amphon and Thanasuthipitak, 2016; Shen and Lu, 2018; Sutherland and Schwarz and Jobbins and Coenraads and Webb, 1998). The absorption of blue samples trends toward the longer wavelength around 600 nm which indicates the absorption range of yellow-orange color and transmission is blue color (Table 11).

From the results of UV-Vis-NIR, the amount of Fe in blue synthetic samples can possibly be both Fe^{2+} and Fe^{3+} . For examples, sample B4 has a clear peak of Fe^{3+} at 1st absorption that makes it less likely to be Fe^{2+} , combined with the EPMA experiment that shows less amount of Fe. As such the sample B4 gives the pale blue. On the other hand, sample B5 has unclearly peak at the 1st absorption that represents Fe^{3+} . Thus, this makes Fe in sample B5 to be Fe^{2+} rather than Fe^{3+} , that affect the sample B5 to be deep blue color. As for the samples B1, B2, and B3, they have the same amounts of Fe. It was found that samples B1 and B2 have a similar pale blue color. When compare the 1st absorption peak that represents of Fe^{3+} , the sample B2 is more intense than the sample B1. When comparing between samples B3 and B1, the 1st absorption peak of sample B1 is higher than sample B3. In addition, the thickness of sample may affect to the shade of color that the reason why sample B3 has intenser color than samples B1 and B2.

EPMA results show that Ti has the highest amount in blue samples thus Ti was selected to measure in XANES technique. The result shows that the detection absorption edge at 4987-4989 eV fairly consistent with standard of Ti^{4+} (Figure 27). The previous study suggests that the absorption edge at 4985 eV in blue corundum represents the oxidation state of Ti^{4+} (Gaudry et al., 2005; Wongrawang and Monarumit and Thammajak and Wathanakul and Wongkokua, 2016). Although the value of absorption has slightly different, these small discrepancy is probably due to the error of the tool in the experiment. However, the results in this study fairly consistent with the previous works.

5.2.2 Cause of blue color

Normally, pure corundum is colorless mineral. The color of corundum can occur due to impurities in structure. A study by Burn (1981) suggest that charge transfer between two ions can cause the energy absorption. When the energy required for that transition is equivalent to the energy in the range of visible light, then the color is produced (Nassau, 2001). Blue synthetic corundums in this study contain both Ti and Fe impurities. There can exist in two valence states and can be paired in two forms: $Fe^{2+}-Ti^{4+}$ and $Fe^{3+}-Ti^{3+}$. When in neighbouring lattice sites, charge transfer between Fe and Ti can occur:



This process is known as intervalence charge transfer (IVCT) (Burns, 1981; Kane, 1982; Nassau, 1980). The IVCT are normally induced by incident light in the wavelength between 400 to 2000 nm (Burns, 1981). In order for IVCT to occur, the interacting cations such as Fe and Ti must be adjacent to one another in corundum structure (Figure 37). The IVCT are thus observed between transition metals in coordination sites sharing edges or faces. The distance between Fe and Ti are approximately 2.65 angstrom in the C axis (Figure 38) (Loeffler and Burns, 1976; Nassau, 1978). The distance, of Fe and Ti cause the electron transfer in the corundum structure and $Fe^{2+}-Ti^{4+}$, which has lower energy change to $Fe^{3+}-Ti^{3+}$ which has higher energy. The pair of Fe-Ti in IVCT process show the results in the absorption of energy approximately 670-690 nm or

equivalent to orange-red color (Loeffler and Burns, 1976; Nassau, 1987). Thus, corundum with Fe-Ti pairs appears blue.

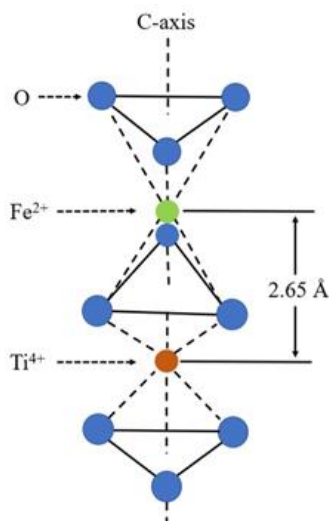


Figure 38 The Al site in corundum structure occupied by Fe²⁺ and Ti⁴⁺ (Nassau, 1987).

In general, the natural blue corundum has high amount of Fe than Ti (Emmett et al., 2003; Monarumit and Satitkune and Wongkokua, 2017) while the synthetic has amount of Ti higher than Fe (Emmett et al., 2003; Muhlmeister and Emmanue and Shigley and Devouard and Laurs, 1998). The difference between natural and synthetic blue corundums can be investigated by the amount of Fe and Ti. However, this study believes that the oxidation Ti⁴⁺-Fe²⁺ is the dominant element in blue synthetic samples and the cause of color in blue corundum is charge transfer.

5.2.3 Comparison with previous studies

From the result of this study, the blue synthetic corundum samples show high amount of Ti in EPMA experiment and clearly absorption of Ti⁴⁺-Fe²⁺ pair in UV-Vis-NIR method. The oxidation state of Ti⁴⁺ was confirmed by XANES technique. Normally, both natural and synthetic blue corundums show Ti⁴⁺-Fe²⁺ pair which is the cause of color (Emmett et al., 2003; Fritsch and Rossman, 1987; Nassau, 2001; Schmetzer and Peretti, 2000; Schwarz et al., 2008). In this study, in addition to Ti, a significant of Fe was found which has amount related to the shade of blue color in synthetic samples. Based on the previous study, Ti⁴⁺-Fe²⁺ pair can produce blue color in corundum (Table

13). From the results, it can be summarized and confirmed the pair of Ti^{4+} - Fe^{2+} is the cause of blue color in synthetic corundum samples.

Table 13 Comparison the oxidation state of trace elements in blue synthetic corundum samples between previous studies and this study.

Color	Type	Cause of color	Remarks
Blue	Synthetic	Ti^{4+} - Fe^{2+}	This study
Blue	Natural	Ti^{4+} - Fe^{2+}	Schwarz et al., 2008
Blue	Natural	Ti^{4+} - Fe^{2+}	Nassau, 2001
Blue	Natural	Ti^{4+} - Fe^{2+}	Schwarz et al., 2008
Blue	Synthetic	Ti^{4+} - Fe^{2+}	Schmetzer and Peretti, 2000
Blue	Synthetic	Ti^{4+} - Fe^{2+}	Emmett et al., 2003

5.3 Yellow synthetic corundum

5.3.1. Type and oxidation state of trace elements

The results of EPMA and UV-Vis-NIR experiment in this study suggests Cr and Ni are the dominant elements in yellow synthetic samples. From EPMA experiment, the atomic proportion of Cr has the highest amount in all samples followed by Ni. When considered together with UV-Vis-NIR results, it shows that the 1st absorption peak around 402-420 nm (Figure 30) in all samples, indicate the absorption of purple-blue color and the transmission of yellow-orange color. Sample Y1, Y2, and Y3 shows 2nd absorption peak at 570 nm, 531 nm, and 550 nm respectively (Figure 30), which indicates the absorption of green color and the transmission of red color. When two transmission color was combined (yellow and red) the resulting of samples show orangish yellow color.

Sample Y3, Y4, and Y5 have a similar shape of UV-Vis-NIR spectra. These spectra show the absorption at 300 nm to 420 nm. The shape of these spectra indicate significant trapped hole color center (Hughes and Manorotkul and Hughes, 2017; Pisutha-Arnond and Hager and Atichat and Wathanakul, 2006). The absorption around

380-420 nm also represents Ni^{2+} and Ni^{3+} (Thomas and Mashkovtsev and Smirnov and Maltsev, 1997). Unlike in samples Y3 and Y4, sample Y5 has a 2nd absorption at 550 nm, which represents Cr^{3+} (Emmett et al., 2003; Shen and Lu, 2018) and causes this sample to be orangish shade. While the absorption of samples Y3 and Y4 show relatively high absorption around 400-500 nm that possibly decreases the absorption of Cr^{3+} at 550 nm. The sample Y2 shows the 1st absorption at 399 nm that represents Ni^{2+} , Ni^{3+} , and Cr^{3+} while the 2nd absorption at 531 nm that represents Cr^{3+} . Sample Y2 detected the 2nd peak in UV-Vis-NIR experiment that represents Cr^{3+} combined with the large amount of Cr in EPMA experiment resulting in sample Y2 shows the orange shade more than the other samples. Although sample Y1 does not has the absorption that shows significant trapped hole color center, sample Y1 shows the absorption of Ni^{2+} , Ni^{3+} , and Cr^{3+} at 420 nm and 570 nm, respectively. Possibly the reason why the sample Y1 gives the pale yellow color.

5.3.2 Cause of yellow color

According to the result, the yellow samples have the orange shade because the high amount of Cr in all samples due to the Cr related to red shade in yellow corundum (Shor and Weldon, 2009). The cause of color can occur due to the defect of crystal, the previous study suggested that the cause of color in yellow corundum was 'color center' (Nassau, 1978). The color center was divided into two situations: the first is when the crystal has the vacancy of electron, called 'electron color center', and the trace element substituted for the main element in the structure. The second is when radiation ejects one of a pair of electrons, the crystal has the 'hole' called 'hole color center' (Fritsch and Rossman, 1998; Nassau, 1978; Nassau, 2001; Tilley, 2013). The color center can be divided into two cases, unstable and stable yellow color. The unstable yellow color center produce by irradiation will fade upon heating the stone (Emmett and Douthit, 1993; Pisutha-Armond and Hager and Atichat and Wathanakul, 2006). The stable yellow color can be caused by trapped-hole color center by Mg^{2+} in oxygen vacancy or the hole. The hole occurs by the reduction condition in the crystal growth or the heat treated in a reduction atmosphere. The hole trapped by Mg^{2+} is stable, resulting in high absorption in range of blue, which lead

to yellow color in corundum. This causes of color in synthetic corundum with high amount of Mg^{2+} impurity (Emmett et al., 2003; Pisutha-Arnond and Hager and Atichat and Wathanakul, 2006). In this study, Mg was found negligible by the EPMA experiments. Thus, the cause of yellow color by Mg^{2+} trapped hole color center is unlikely in our yellow samples.

Apart from the color center the previous study also suggested that Fe^{3+} could produce stable yellow color (Nassau, 1980, 1987). The crystal field theory by $Fe^{3+}-Fe^{3+}$ pair can produce pale yellow color in corundum as shown in the absorption peak at 388 nm and the broadband at 540, 700, and 1050 nm (Deer, 2011; Emmett et al., 2003). The stable yellow color produced by Fe^{3+} is usually found in natural corundum and the color will not fade when they were heated.

In this study, these absorptions were not detected that cannot define the absorption of $Fe^{3+}-Fe^{3+}$ pair. Emmett et al., (2003) suggested that Ni could exist in corundum because Ni has the multivalence states. Ni could suppress the formation of trapped-hole color centers in yellow corundum (Emmett et al., 2003). The coloration of Ni trapped hole color center possibly has the same process as trapped hole color center by Mg^{2+} . The previous study suggests that Ni^{3+} can produce yellow color in synthetic corundums by controlling the oxidation-reduction in growth process (Thomas and Mashkovtsev and Smirnov and Maltsev, 1997). However, in this study the results of EPMA, show the high amount of Ni. In addition, Ni can be detected the absorption in UV-Vis-NIR experiment. Thus, this study suggests that the cause of color in yellow synthetic samples is likely due to Ni in yellow synthetic corundum samples.

5.3.3 Comparison with previous studies

In general, natural corundums show the oxidation state of Fe^{3+} , $Fe^{3+}-Fe^{3+}$ pair and Mg^{2+} are cause of color in yellow corundum (Emmett et al., 2003; Schmetzer and Peretti, 1999). While in synthetic corundums, the yellow color are caused by Ni^{3+} , Mg^{2+} , and Fe^{3+} (Pisutha-Arnond and Hager and Atichat and Wathanakul, 2006; Schmetzer and Peretti, 1999; Schmetzer and Peretti, 2000; Thomas and Mashkovtsev and Smirnov and Maltsev, 1997). The previous studies indicated the oxidation states of trace elements in natural and synthetic yellow corundum are vary. This study was found that the

spectra of yellow samples (Y3, Y4, and Y5) in UV-Vis-NIR experiment (Figure 39b) are fairly consistent with UV-Vis-NIR absorbance spectra of yellow synthetic corundum by Mg^{2+} trapped hole paired with Fe^{3+} (Hughes and Manorotkul and Hughes, 2017) (Figure 39a). However, Mg^{2+} was not detected in this study, the previous study suggested that small amount of Ni can produce yellow color in synthetic corundum (Schmetzer and Peretti, 1999; Thomas and Mashkovtsev and Smirnov and Maltsev, 1997). Although, the oxidation state of Ni was not measured in this study because the Ni standard was not available in the XANES laboratory. A significant amount of Ni was detected in the EPMA experiments that could relate to the absorption spectra detected by the UV-Vis-NIR experiment. Thus, this study suggests that Ni is possibly the cause of yellow color in synthetic corundum samples.

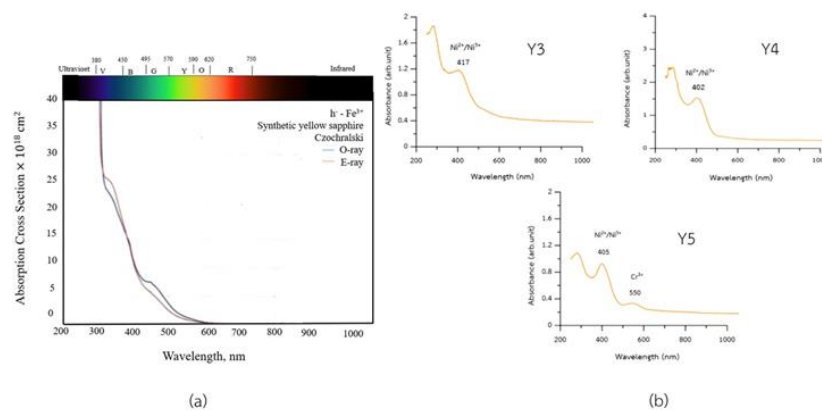


Figure 39 (a) The spectrum of yellow synthetic corundum by trapped hole involving Mg^{2+} and Fe^{3+} (Hughes et al., 2017) (b) the spectrum of yellow samples (Y3, Y4, and Y5)

Table 14 Comparison the oxidation state of trace elements in yellow synthetic corundum samples between previous studies and this study.

Color	Type	Cause of color	Remarks
Yellow	Synthetic	Ni ²⁺ , Ni ³⁺	This study
Pale yellow	Natural	Fe ³⁺	Schmetzer and Peretti, 1999
Yellow	Natural	Fe ³⁺ -Fe ²⁺	Emmett et al., 2003
Orangish yellow	Natural	Mg ²⁺	Emmett et al., 2003
Yellow	Synthetic	Ni ³⁺	Schmetzer and Peretti, 1999
Yellow	Synthetic	Ni ³⁺	Thomas et al., 1997
Yellow	Synthetic	Mg ²⁺	Pisutha-Armond, 2006
Yellow	Synthetic	Fe ³⁺	Schmetzer and Peretti, 2000

Chapter 6

Conclusion

This study is aimed to determine the type and oxidation state of trace elements in red, blue, and yellow synthetic corundum samples. Based on EPMA, UV-Vis-NIR, and XANES analyses, results show distinctive characteristics of trace elements and suggest the cause of color in the samples.

6.1 Red synthetic corundums

6.1.1 Cr^{3+} is the main cause of red color in corundum due to the highest amount in EPMA experiment, strong absorption of Cr^{3+} in UV-Vis-NIR and the oxidation state was confirmed by XANES. The results of all experiments show clearly that oxidation state of Cr is Cr^{3+} in synthetic corundum samples.

6.1.2 V^{3+} is the importance element to provide purple shade in red corundum and promotes the color change effect from bluish purple color in daylight to red in incandescent light.

6.1.3 The cause of color in red synthetic corundum samples are the crystal field theory by Cr^{3+} .

6.2 Blue synthetic corundum samples

6.2.1 In the blue samples, Ti^{4+} and Fe^{2+} is the main impurity, Ti shows highest amount in EPMA experiment. Although Fe was not measured the oxidation state, the result shows the absorption of $\text{Ti}^{4+}\text{-Fe}^{2+}$ pair was clearly presented in the UV-Vis-NIR experiment.

6.2.2 This study believes that Ti^{4+} and Fe^{2+} is the important elements involving the cause of blue color in synthetic corundum. From the results of EPMA, UV-Vis-NIR and XANES experiment, the blue color in synthetic corundum samples can be occurred due to $\text{Ti}^{4+}\text{-Fe}^{2+}$ pair in corundum structure. The ions transformation of each element can be transferred from $\text{Ti}^{4+}\text{-Fe}^{2+}$ to $\text{Ti}^{3+}\text{-Fe}^{3+}$, which cause the light absorption in range of orange to red and gives blue color. It can summarize that Ti^{4+} and Fe^{2+} is the

important elements to create blue color in synthetic corundum samples by electrons charge transfer process.

6.3 Yellow synthetic corundum samples

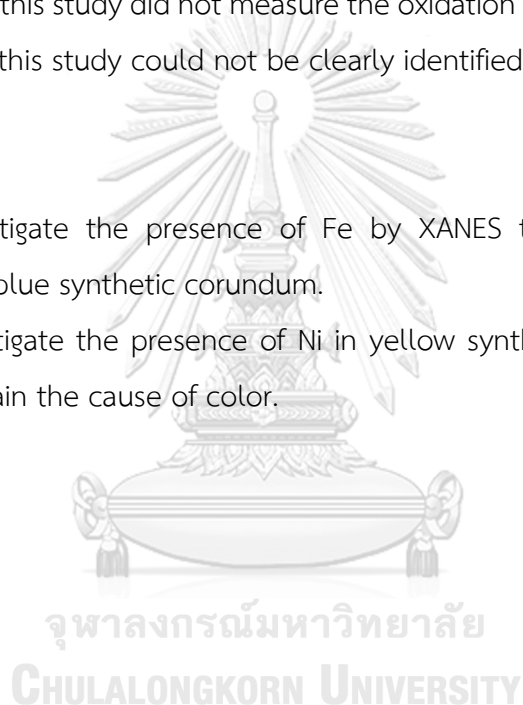
6.3.1 The studied results of yellow synthetic corundums suggest that Ni is element that may cause the yellow color in the synthetic samples.

6.3.2 The cause of color in yellow synthetic corundums may occur in the case of electrons trapped hole color center by Ni under controlling the oxidation-reduction process. However, this study did not measure the oxidation state of Ni. Thus, the cause of yellow color in this study could not be clearly identified.

6.4 Further study

6.4.1 Investigate the presence of Fe by XANES technique to confirm the oxidation state in blue synthetic corundum.

6.4.2 Investigate the presence of Ni in yellow synthetic corundum by XANES technique to explain the cause of color.



APPENDIX

APPENDIX A

EPMA data of red samples

Samples	BeO	Al ₂ O ₃	Cr ₂ O ₃	FeO	MgO	Ga ₂ O ₃	TiO ₂	V ₂ O ₃	NiO	Total	Spots
R1	0.000	98.763	0.730	0.000	0.000	0.000	0.010	0.031	0.011	99.545	1
	0.000	98.686	0.721	0.003	0.000	0.018	0.018	0.021	0.008	99.475	2
	0.000	99.630	0.618	0.000	0.000	0.025	0.008	0.000	0.023	100.304	3
	0.000	99.228	0.725	0.018	0.000	0.053	0.006	0.002	0.026	100.058	4
	0.000	98.850	0.580	0.000	0.000	0.034	0.059	0.000	0.000	99.523	5
	0.000	99.802	0.725	0.000	0.000	0.005	0.004	0.005	0.000	100.541	6
R2	0.000	99.003	0.214	0.007	0.000	0.003	0.015	0.021	0.014	99.277	1
	0.000	98.676	0.255	0.010	0.000	0.000	0.021	0.014	0.000	98.976	2
	0.000	99.379	0.213	0.008	0.000	0.016	0.021	0.000	0.010	99.647	3
	0.000	99.327	0.265	0.000	0.000	0.022	0.036	0.000	0.000	99.650	4
	0.000	99.109	0.180	0.000	0.000	0.063	0.004	0.023	0.000	99.379	5
	0.000	99.337	0.194	0.000	0.000	0.007	0.012	0.000	0.013	99.563	6
R3	0.000	99.488	0.242	0.009	0.006	0.045	0.017	0.000	0.025	99.832	1
	0.000	98.842	0.218	0.000	0.000	0.000	0.011	0.032	0.019	99.122	2
	0.000	98.788	0.221	0.008	0.000	0.000	0.016	0.000	0.004	99.037	3
	0.000	98.754	0.186	0.000	0.000	0.047	0.005	0.010	0.000	99.002	4
	0.000	98.871	0.161	0.012	0.000	0.059	0.000	0.014	0.000	99.117	5
	0.000	99.000	0.165	0.000	0.000	0.000	0.006	0.000	0.011	99.182	6
R4	0.000	98.830	0.331	0.017	0.000	0.005	0.000	0.000	0.006	99.189	1
	0.000	98.672	0.457	0.012	0.000	0.045	0.000	0.000	0.009	99.195	2
	0.000	99.163	0.570	0.000	0.000	0.000	0.032	0.000	0.000	99.765	3
	0.000	99.347	0.444	0.000	0.000	0.019	0.029	0.027	0.000	99.866	4
	0.000	99.155	0.463	0.005	0.000	0.039	0.018	0.000	0.000	99.680	5
	0.000	98.782	0.534	0.016	0.000	0.000	0.025	0.000	0.000	99.357	6
R5	0.000	99.458	0.074	0.050	0.000	0.000	0.035	0.695	0.030	100.342	1
	0.000	98.842	0.085	0.020	0.000	0.076	0.016	0.724	0.000	99.763	2
	0.000	99.577	0.056	0.000	0.001	0.066	0.000	0.596	0.037	100.333	3
	0.000	99.097	0.077	0.000	0.000	0.000	0.004	0.510	0.019	99.707	4
	0.000	98.616	0.082	0.004	0.000	0.030	0.036	0.586	0.026	99.380	5
	0.000	98.818	0.074	0.000	0.000	0.018	0.050	0.566	0.005	99.531	6

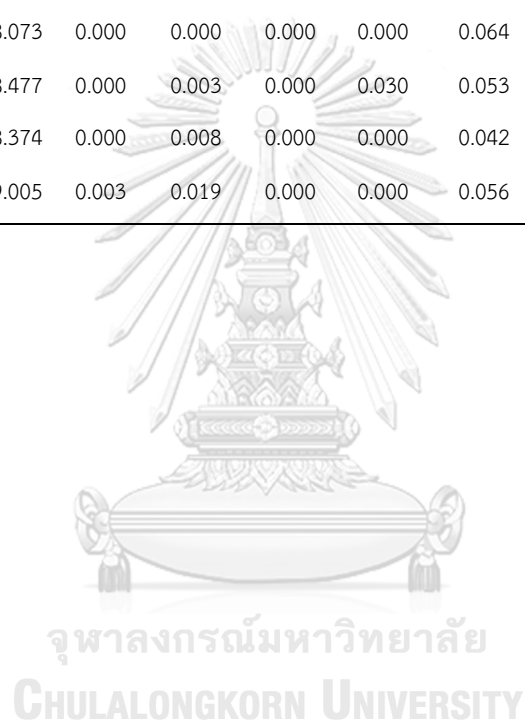
APPENDIX B

EPMA data of blue samples

Samples	BeO	Al ₂ O ₃	Cr ₂ O ₃	FeO	MgO	Ga ₂ O ₃	TiO ₂	V ₂ O ₃	NiO	Total	Spots
B1	0.000	98.214	0.000	0.015	0.000	0.029	0.096	0.000	0.000	98.354	1
	0.000	99.720	0.000	0.012	0.000	0.018	0.103	0.001	0.019	99.873	2
	0.000	98.822	0.019	0.040	0.000	0.091	0.141	0.004	0.000	99.117	3
	0.000	98.312	0.000	0.044	0.000	0.039	0.113	0.000	0.000	98.508	4
	0.000	99.209	0.000	0.006	0.000	0.000	0.149	0.000	0.000	99.364	5
	0.000	98.219	0.000	0.036	0.000	0.019	0.115	0.000	0.004	98.393	6
	0.000	99.010	0.023	0.000	0.000	0.071	0.140	0.049	0.039	99.332	7
	0.000	98.788	0.000	0.035	0.000	0.020	0.111	0.012	0.000	98.966	8
	0.000	99.529	0.000	0.008	0.000	0.050	0.137	0.000	0.029	99.753	9
	0.000	99.528	0.000	0.040	0.000	0.041	0.173	0.000	0.000	99.782	10
	0.000	98.002	0.000	0.011	0.004	0.028	0.149	0.007	0.000	98.201	11
	0.000	98.802	0.020	0.022	0.000	0.054	0.132	0.017	0.000	99.047	12
B2	0.000	98.794	0.032	0.010	0.000	0.026	0.084	0.000	0.021	98.967	1
	0.000	98.394	0.011	0.026	0.000	0.009	0.105	0.022	0.020	98.587	2
	0.000	98.517	0.000	0.000	0.000	0.026	0.088	0.005	0.000	98.636	3
	0.000	98.017	0.000	0.006	0.000	0.043	0.163	0.000	0.000	98.229	4
	0.000	98.751	0.000	0.005	0.000	0.000	0.146	0.000	0.022	98.924	5
	0.000	98.510	0.000	0.011	0.000	0.009	0.134	0.015	0.000	98.679	6
	0.000	98.589	0.000	0.010	0.000	0.000	0.055	0.007	0.000	98.661	7
	0.000	98.891	0.024	0.000	0.000	0.012	0.079	0.012	0.000	99.018	8
	0.000	98.438	0.000	0.000	0.000	0.039	0.025	0.000	0.004	98.506	9
	0.000	98.756	0.000	0.000	0.000	0.000	0.057	0.000	0.018	98.831	10
	0.000	98.464	0.007	0.007	0.000	0.015	0.024	0.000	0.000	98.517	11
	0.000	99.133	0.000	0.017	0.000	0.002	0.012	0.000	0.013	99.177	12

Samples	BeO	Al ₂ O ₃	Cr ₂ O ₃	FeO	MgO	Ga ₂ O ₃	TiO ₂	V ₂ O ₃	NiO	Total	Spots
B3	0.000	98.095	0.015	0.007	0.006	0.048	0.136	0.010	0.000	98.317	1
	0.000	98.502	0.009	0.007	0.000	0.067	0.132	0.027	0.038	98.782	2
	0.000	98.713	0.000	0.018	0.000	0.028	0.112	0.000	0.030	98.901	3
	0.000	98.379	0.006	0.007	0.002	0.029	0.150	0.009	0.044	98.626	4
	0.000	98.445	0.000	0.021	0.008	0.022	0.143	0.010	0.000	98.649	5
	0.000	98.013	0.005	0.001	0.000	0.000	0.124	0.012	0.000	98.155	6
	0.000	98.782	0.000	0.040	0.000	0.011	0.011	0.021	0.048	98.913	7
	0.000	99.290	0.000	0.017	0.000	0.047	0.067	0.000	0.030	99.451	8
	0.000	99.020	0.008	0.012	0.000	0.007	0.035	0.000	0.000	99.082	9
	0.000	99.120	0.046	0.000	0.000	0.000	0.074	0.012	0.034	99.286	10
	0.000	98.871	0.003	0.008	0.000	0.000	0.114	0.010	0.008	99.014	11
	0.000	98.921	0.014	0.002	0.000	0.087	0.057	0.027	0.000	99.108	12
B4	0.000	98.832	0.009	0.000	0.000	0.028	0.115	0.078	0.000	99.062	1
	0.000	98.902	0.003	0.012	0.000	0.011	0.106	0.051	0.000	99.085	2
	0.000	98.337	0.022	0.012	0.000	0.020	0.076	0.041	0.000	98.508	3
	0.000	98.740	0.000	0.033	0.000	0.045	0.100	0.090	0.034	99.042	4
	0.000	98.489	0.000	0.011	0.000	0.011	0.085	0.021	0.000	98.617	5
	0.000	98.507	0.006	0.003	0.000	0.016	0.103	0.073	0.000	98.708	6
	0.000	98.381	0.000	0.001	0.000	0.031	0.092	0.041	0.015	98.561	7
	0.000	98.373	0.025	0.000	0.000	0.000	0.059	0.096	0.000	98.553	8
	0.000	98.218	0.035	0.000	0.000	0.020	0.084	0.047	0.052	98.456	9
	0.000	98.646	0.000	0.000	0.000	0.008	0.292	0.065	0.011	99.022	10
	0.000	98.858	0.010	0.007	0.004	0.000	0.102	0.031	0.000	99.012	11
	0.000	98.692	0.055	0.000	0.000	0.000	0.097	0.064	0.000	98.908	12

Samples	BeO	Al ₂ O ₃	Cr ₂ O ₃	FeO	MgO	Ga ₂ O ₃	TiO ₂	V ₂ O ₃	NiO	Total	Spots
B5	0.000	99.142	0.000	0.005	0.001	0.040	0.071	0.044	0.089	99.392	1
	0.000	98.947	0.000	0.000	0.000	0.021	0.067	0.054	0.234	99.323	2
	0.000	98.578	0.000	0.020	0.000	0.022	0.055	0.059	0.512	99.246	3
	0.000	99.293	0.001	0.000	0.000	0.049	0.109	0.054	0.033	99.539	4
	0.000	99.031	0.000	0.013	0.001	0.000	0.117	0.048	0.000	99.210	5
	0.000	99.074	0.000	0.014	0.000	0.000	0.105	0.041	0.039	99.273	6
	0.000	99.449	0.000	0.008	0.000	0.054	0.078	0.032	0.032	99.653	7
	0.000	98.565	0.012	0.024	0.000	0.049	0.074	0.037	0.016	98.777	8
	0.000	98.073	0.000	0.000	0.000	0.000	0.064	0.063	0.012	98.212	9
	0.000	98.477	0.000	0.003	0.000	0.030	0.053	0.088	0.000	98.651	10
	0.000	98.374	0.000	0.008	0.000	0.000	0.042	0.040	0.009	98.473	11
	0.000	99.005	0.003	0.019	0.000	0.000	0.056	0.017	0.022	99.122	12



APPENDIX C

Spots selected of blue samples

Samples	BeO	Al ₂ O ₃	Cr ₂ O ₃	FeO	MgO	Ga ₂ O ₃	TiO ₂	V ₂ O ₃	NiO	Total	Spots
B1	0.000	98.214	0.000	0.015	0.000	0.029	0.096	0.000	0.000	98.354	1
	0.000	99.720	0.000	0.012	0.000	0.018	0.103	0.001	0.019	99.873	2
	0.000	99.209	0.000	0.006	0.000	0.000	0.149	0.000	0.000	99.364	5
	0.000	99.529	0.000	0.008	0.000	0.050	0.137	0.000	0.029	99.753	9
	0.000	98.002	0.000	0.011	0.004	0.028	0.149	0.007	0.000	98.201	11
	0.000	98.802	0.020	0.022	0.000	0.054	0.132	0.017	0.000	99.047	12
B2	0.000	98.794	0.032	0.010	0.000	0.026	0.084	0.000	0.021	98.967	1
	0.000	98.394	0.011	0.026	0.000	0.009	0.105	0.022	0.020	98.587	2
	0.000	98.017	0.000	0.006	0.000	0.043	0.163	0.000	0.000	98.229	4
	0.000	98.751	0.000	0.005	0.000	0.000	0.146	0.000	0.022	98.924	5
	0.000	98.510	0.000	0.011	0.000	0.009	0.134	0.015	0.000	98.679	6
	0.000	98.589	0.000	0.010	0.000	0.000	0.055	0.007	0.000	98.661	7
B3	0.000	98.095	0.015	0.007	0.006	0.048	0.136	0.010	0.000	98.317	1
	0.000	98.502	0.009	0.007	0.000	0.067	0.132	0.027	0.038	98.782	2
	0.000	98.713	0.000	0.018	0.000	0.028	0.112	0.000	0.030	98.901	3
	0.000	98.445	0.000	0.021	0.008	0.022	0.143	0.010	0.000	98.626	5
	0.000	99.290	0.000	0.017	0.000	0.047	0.067	0.000	0.030	99.451	8
	0.000	98.871	0.003	0.008	0.000	0.000	0.114	0.010	0.008	99.014	11
B4	0.000	98.902	0.003	0.012	0.000	0.011	0.106	0.051	0.000	99.085	2
	0.000	98.337	0.022	0.012	0.000	0.020	0.076	0.041	0.000	98.508	3
	0.000	98.489	0.000	0.011	0.000	0.011	0.085	0.021	0.000	98.617	5
	0.000	98.507	0.006	0.003	0.000	0.016	0.103	0.073	0.000	98.708	6
	0.000	98.381	0.000	0.001	0.000	0.031	0.092	0.041	0.015	98.561	7
	0.000	98.858	0.010	0.007	0.004	0.000	0.102	0.031	0.000	99.012	11
B5	0.000	99.031	0.000	0.013	0.001	0.000	0.117	0.048	0.000	99.210	5
	0.000	99.074	0.000	0.014	0.000	0.000	0.105	0.041	0.039	99.273	6
	0.000	99.449	0.000	0.008	0.000	0.054	0.078	0.032	0.032	99.653	7
	0.000	98.565	0.012	0.024	0.000	0.049	0.074	0.037	0.016	98.777	8
	0.000	98.374	0.000	0.008	0.000	0.000	0.042	0.040	0.009	98.473	11
	0.000	99.005	0.003	0.019	0.000	0.000	0.056	0.017	0.022	99.122	12

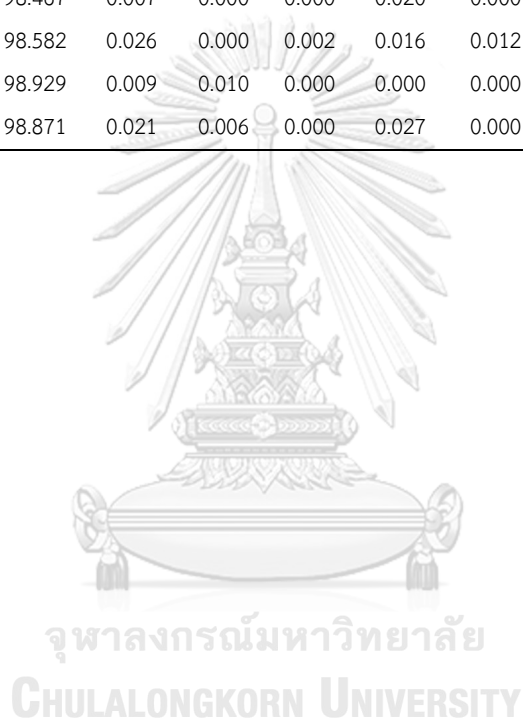
APPENDIX D

EPMA data of yellow samples

Samples	BeO	Al ₂ O ₃	Cr ₂ O ₃	FeO	MgO	Ga ₂ O ₃	TiO ₂	V ₂ O ₃	NiO	Total	Spots
Y1	0.000	99.216	0.000	0.000	0.000	0.052	0.004	0.000	0.062	99.334	1
	0.000	98.185	0.050	0.000	0.002	0.033	0.009	0.000	0.000	98.279	2
	0.000	98.480	0.042	0.007	0.000	0.013	0.000	0.000	0.060	98.602	3
	0.000	99.593	0.038	0.014	0.000	0.000	0.012	0.000	0.008	99.665	4
	0.000	99.031	0.058	0.001	0.000	0.034	0.001	0.000	0.021	99.146	5
	0.000	98.756	0.005	0.025	0.000	0.000	0.001	0.006	0.018	98.811	6
	0.000	98.017	0.000	0.009	0.000	0.061	0.016	0.023	0.012	98.138	7
	0.000	98.702	0.010	0.000	0.000	0.012	0.000	0.016	0.000	98.740	8
	0.000	98.954	0.010	0.003	0.000	0.000	0.025	0.000	0.003	98.995	9
	0.000	99.025	0.001	0.021	0.000	0.000	0.005	0.001	0.017	99.070	10
	0.000	99.936	0.003	0.015	0.000	0.004	0.004	0.028	0.009	99.999	11
	0.000	98.526	0.030	0.000	0.000	0.023	0.011	0.010	0.000	98.600	12
Y2	0.000	98.108	0.059	0.000	0.000	0.007	0.014	0.000	0.000	98.188	1
	0.000	98.451	0.072	0.016	0.000	0.000	0.000	0.000	0.000	98.539	2
	0.000	99.575	0.072	0.000	0.004	0.002	0.002	0.004	0.032	99.691	3
	0.000	98.549	0.011	0.000	0.004	0.000	0.000	0.009	0.000	98.573	4
	0.000	99.549	0.000	0.000	0.000	0.000	0.001	0.000	0.011	99.561	5
	0.000	99.906	0.107	0.000	0.000	0.014	0.000	0.005	0.011	100.043	6
	0.000	99.920	0.061	0.000	0.000	0.000	0.000	0.019	0.004	100.004	7
	0.000	98.907	0.060	0.000	0.000	0.038	0.010	0.000	0.004	99.019	8
	0.000	98.721	0.043	0.000	0.000	0.005	0.010	0.006	0.006	98.791	9
	0.000	98.690	0.038	0.030	0.000	0.065	0.002	0.018	0.000	98.843	10
	0.000	99.069	0.129	0.000	0.005	0.003	0.000	0.000	0.022	99.228	11
	0.000	98.345	0.040	0.013	0.000	0.036	0.000	0.000	0.022	98.456	12

Samples	BeO	Al ₂ O ₃	Cr ₂ O ₃	FeO	MgO	Ga ₂ O ₃	TiO ₂	V ₂ O ₃	NiO	Total	Spots
Y3	0.000	98.329	0.023	0.000	0.002	0.041	0.000	0.005	0.000	98.400	1
	0.000	98.162	0.028	0.000	0.000	0.000	0.000	0.000	0.026	98.216	2
	0.000	98.472	0.039	0.018	0.003	0.034	0.001	0.000	0.024	98.591	3
	0.000	98.189	0.074	0.000	0.000	0.027	0.000	0.000	0.028	98.318	4
	0.000	98.298	0.072	0.000	0.000	0.032	0.083	0.000	0.005	98.490	5
	0.000	99.807	0.043	0.003	0.000	0.042	0.000	0.000	0.017	99.912	6
	0.000	98.211	0.069	0.015	0.000	0.027	0.002	0.000	0.009	98.333	7
	0.000	98.113	0.020	0.015	0.000	0.005	0.001	0.016	0.000	98.170	8
	0.000	98.895	0.025	0.000	0.000	0.025	0.003	0.002	0.020	98.970	9
	0.000	98.536	0.007	0.000	0.000	0.001	0.005	0.001	0.000	98.550	10
	0.000	98.109	0.000	0.000	0.012	0.055	0.000	0.005	0.000	98.181	11
	0.000	98.232	0.022	0.000	0.000	0.026	0.000	0.000	0.000	98.280	12
Y4	0.000	98.853	0.028	0.000	0.007	0.032	0.000	0.010	0.000	98.930	1
	0.000	98.912	0.032	0.013	0.000	0.074	0.000	0.000	0.027	99.058	2
	0.000	98.432	0.071	0.000	0.000	0.054	0.002	0.002	0.022	98.583	3
	0.000	98.475	0.006	0.000	0.003	0.000	0.010	0.000	0.000	98.494	4
	0.000	98.191	0.040	0.000	0.000	0.000	0.022	0.000	0.020	98.273	5
	0.000	98.853	0.028	0.000	0.007	0.032	0.000	0.010	0.000	98.930	6
	0.000	98.636	0.035	0.000	0.000	0.016	0.020	0.000	0.017	98.724	7
	0.000	98.982	0.030	0.000	0.000	0.018	0.000	0.000	0.036	99.066	8
	0.000	98.441	0.037	0.000	0.000	0.028	0.000	0.000	0.000	98.506	9
	0.000	98.442	0.026	0.007	0.000	0.024	0.024	0.000	0.000	98.523	10
	0.000	98.664	0.002	0.000	0.000	0.000	0.027	0.002	0.016	98.711	11
	0.000	98.591	0.019	0.019	0.015	0.054	0.000	0.000	0.044	98.742	12

Samples	BeO	Al ₂ O ₃	Cr ₂ O ₃	FeO	MgO	Ga ₂ O ₃	TiO ₂	V ₂ O ₃	NiO	Total	Spots
Y5	0.000	98.295	0.047	0.000	0.000	0.018	0.000	0.000	0.037	98.397	1
	0.000	97.430	0.011	0.023	0.006	0.047	1.634	0.001	0.031	99.183	2
	0.000	98.373	0.019	0.000	0.000	0.000	0.000	0.010	0.041	98.443	3
	0.000	98.518	0.023	0.000	0.000	0.037	0.165	0.005	0.017	98.765	4
	0.000	98.830	0.030	0.000	0.004	0.048	0.000	0.000	0.038	98.950	5
	0.000	98.275	0.020	0.000	0.000	0.066	0.021	0.000	0.034	98.416	6
	0.000	98.857	0.047	0.001	0.008	0.009	0.000	0.000	0.025	98.947	7
	0.000	98.372	0.025	0.000	0.000	0.031	0.002	0.000	0.015	98.445	8
	0.000	98.467	0.007	0.000	0.000	0.020	0.000	0.000	0.006	98.500	9
	0.000	98.582	0.026	0.000	0.002	0.016	0.012	0.001	0.042	98.681	10
	0.000	98.929	0.009	0.010	0.000	0.000	0.000	0.000	0.000	98.948	11
	0.000	98.871	0.021	0.006	0.000	0.027	0.000	0.000	0.000	98.925	12



APPENDIX E

Spots selected of yellow samples

Samples	BeO	Al ₂ O ₃	Cr ₂ O ₃	FeO	MgO	Ga ₂ O ₃	TiO ₂	V ₂ O ₃	NiO	Total	Spots
Y1	0.000	99.216	0.000	0.000	0.000	0.052	0.004	0.000	0.062	99.334	1
	0.000	98.480	0.042	0.007	0.000	0.013	0.000	0.000	0.060	98.602	3
	0.000	99.031	0.058	0.001	0.000	0.034	0.001	0.000	0.021	99.146	5
	0.000	98.756	0.005	0.025	0.000	0.000	0.001	0.006	0.018	98.811	6
	0.000	99.025	0.001	0.021	0.000	0.000	0.005	0.001	0.017	99.070	10
	0.000	99.936	0.003	0.015	0.000	0.004	0.004	0.028	0.009	99.999	11
Y2	0.000	98.451	0.072	0.016	0.000	0.000	0.000	0.000	0.000	98.539	2
	0.000	99.549	0.000	0.000	0.000	0.000	0.001	0.000	0.011	99.561	5
	0.000	99.906	0.107	0.000	0.000	0.014	0.000	0.005	0.011	100.043	6
	0.000	99.920	0.061	0.000	0.000	0.000	0.000	0.019	0.004	100.004	7
	0.000	99.069	0.129	0.000	0.005	0.003	0.000	0.000	0.022	99.228	11
	0.000	98.345	0.040	0.013	0.000	0.036	0.000	0.000	0.022	98.456	12
Y3	0.000	98.162	0.028	0.000	0.000	0.000	0.000	0.000	0.026	98.216	2
	0.000	98.472	0.039	0.018	0.003	0.034	0.001	0.000	0.024	98.591	3
	0.000	99.807	0.043	0.003	0.000	0.042	0.000	0.000	0.017	99.912	6
	0.000	98.211	0.069	0.015	0.000	0.027	0.002	0.000	0.009	98.333	7
	0.000	98.113	0.020	0.015	0.000	0.005	0.001	0.016	0.000	98.170	8
	0.000	98.895	0.025	0.000	0.000	0.025	0.003	0.002	0.020	98.970	9
Y4	0.000	98.912	0.032	0.013	0.000	0.074	0.000	0.000	0.027	99.058	2
	0.000	98.432	0.071	0.000	0.000	0.054	0.002	0.002	0.022	98.583	3
	0.000	98.191	0.040	0.000	0.000	0.000	0.022	0.000	0.020	98.273	5
	0.000	98.636	0.035	0.000	0.000	0.016	0.020	0.000	0.017	98.724	7
	0.000	98.442	0.026	0.007	0.000	0.024	0.024	0.000	0.000	98.523	10
	0.000	98.664	0.002	0.000	0.000	0.000	0.027	0.002	0.016	98.711	11
Y5	0.000	98.295	0.047	0.000	0.000	0.018	0.000	0.000	0.037	98.397	1
	0.000	98.857	0.047	0.001	0.008	0.009	0.000	0.000	0.025	98.947	7
	0.000	98.372	0.025	0.000	0.000	0.031	0.002	0.000	0.015	99.445	8
	0.000	98.467	0.007	0.000	0.000	0.020	0.000	0.000	0.006	98.500	9
	0.000	98.929	0.009	0.010	0.000	0.000	0.000	0.000	0.000	98.948	11
	0.000	98.871	0.021	0.006	0.000	0.027	0.000	0.000	0.000	98.925	12

REFERENCES

- Amphon, R., and Thanasuthipitak, P. 2016. Gemological and spectroscopic properties of blue sapphires from Den Chai district, Prachinburi province. Suranaree Journal of Science & Technology 23: 141-145.
- Anderson, B., Payne, C.J., and Mitchell, R.K. 1998. The spectroscopy and gemmology. In pp. 80. Gemstone Press
- Batanova, V.G., Sobolev, A.V., and Magnin, V. 2018. Trace element analysis by EPMA in geosciences: detection limit, precision and accuracy. IOP Conference Series: Materials Science and Engineering 012001.
- Berlien, H.P., Breuer, H., Müller, G.J., Krasner, N., Okunata, T., and Sliney, D. 2012. Applied laser medicine. In pp. 57-58. Springer Science & Business Media.
- Bhale, J., Sharma, P., Mishra, A., and Parsai, N. 2015. XANES study of copper (II) mixed ligand complexes of alpha-aminonitrile. International Journal of Mathematics and Physical Sciences Research 2: 203-210.
- Bourikas, K., Hiemstra, T., and Van Riemsdijk, W.H. 2001. Ion pair formation and primary charging behavior of titanium oxide (anatase and rutile). Langmuir 17: 749-756.
- Bruno, T.J., and Svoronos, P.D. 2005. CRC handbook of fundamental spectroscopic correlation charts. In pp. 1-17. CRC Press.
- Bunaciu, A.A., Udriștioiu, E.G., and Aboul-Enein, H.Y. 2015. X-ray diffraction: instrumentation and applications. Critical Reviews in Analytical Chemistry 45: 289-299.
- Burns, R.G. 1981. Intervalence transitions in mixed valence minerals of iron and titanium. Annual Review of Earth and Planetary Sciences 9: 345-383.
- Burns, R.G. 1993. Mineralogical applications of crystal field theory. In pp. 209-211. Cambridge University Press.
- Calligaro, T., Poirot, J.P., and Querre, G. 1999. Trace element fingerprinting of jewellery rubies by external beam PIXE. Nuclear Instruments and Methods in Physics Research Section B: Beam Interactions with Materials and Atoms 150: 628-634.

- Carr, R.R., and Nisevich, S.D. 1977. Altering the appearance of corundum crystals. In pp. 1-5. Patent and Trademark Office: Washington, DC: U.S. Patent and Trademark Office.
- Chatterjee, N. 2012. Electron microprobe analysis. [Online]. Available from: ocw.mit.edu
- Clark, J. 2014. The visible spectrum and color. [Online]. Available from: chem.libretexts.org [Aug 19, 2014]
- Deer, W.A. 2011. Rock-forming minerals. In pp. 65-69. Geological Society of London.
- Duroc-Danner, J.M. 2002. A comparison between a flux grown synthetic ruby and an untreated natural ruby. Journal of Gemmology 28: 137-142.
- Emmett, J.L., and Douthit, R. 1993. Heat treating the sapphires. Gems & Gemology 29: 250-272.
- Emmett, J.L., et al. 2003. Beryllium diffusion of ruby and sapphire. Gems & Gemology 39: 84-135.
- Ferguson, J., and Fielding, P.E. 1971. The origins of the colors of yellow, green and blue sapphires. Chemical Physics Letters 10: 262-265.
- Fritsch, E., and Rossman, G.R. 1987. An update on color in gems part 1: introduction and colors caused by dispersed metal ions. Gems & Gemology 23: 126-139.
- Fritsch, E., and Rossman, G.R. 1998. An update on color in gems part 2: colors involving multiple atoms and color centers. Gems & Gemology spring: 3-13.
- Gaudry, E., et al. 2005. Structural relaxations around Ti, Cr and Fe impurities in α -Al₂O₃ probed by x-ray absorption near edge structure combined with first-principles calculations. Journal of Physics 17: 54-64.
- Gorghinian, A., Mottana, A., Rossi, A., Oltean, F.M., Esposito, A., and Marcelli, A. 2013. Investigating the colour of spinel: 1. red gem-quality spinels (“balas”) from Ratnapura (Sri Lanka). Rendiconti Lincei 24: 127-140.
- Grynberg, R., Sengwaketse, M., and Motswapong, M. 2014. Synthetic gem quality diamonds and their potential impact on the Botswana economy. The Global Diamond Industry 251-290.
- Gübelin, E., and Schmetzer, K. 1982. Gemstones with alexandrite effect. Gems & Gemology 18: 197-203.

- Harlow, G.E., and Bender, W. 2013. A study of ruby (corundum) compositions from the Mogok belt, Myanmar: searching for chemical fingerprints. American Mineralogist 98: 1120-1132.
- Henderson, G.S., De Groot, F.M., and Moulton, B.J. 2014. X-ray absorption near-edge structure (XANES) spectroscopy. Mineralogy and Geochemistry 78: 75-138.
- Hughes, R.W. 1997. Ruby & sapphire. RWH Publishing.
- Hughes, R.W., Manorotkul, W., and Hughes, E.B. 2017. Ruby & sapphire: a gemologist's guide. In pp. 130. RWH Publishing/Lotus Publishing.
- Itten, J. 1970. The elements of color. In pp. 1-14. John Wiley & Sons.
- Kadleiková, M., Breza, J., and Veselý, M. 2001. Raman spectra of synthetic sapphire. Microelectronics Journal 32: 955-958.
- Kane, R.E. 1982. The gemological properties of Chatham flux growth synthetic orange sapphire and synthetic blue sapphire. Gems & Gemology 18: 140-153.
- Kanouo, N.S., et al. 2016. Trace elements in corundum, chrysoberyl, and zircon: Application to mineral exploration and provenance study of the western Mamfe gem clastic deposits (SW Cameroon, Central Africa). Journal of African Earth Science 113: 35-50.
- Kantakapun, K. 2017. UV-Vis spectrophotometer. [Online]. Available from: chem.eng.psu.ac.th
- Keck, P.H., Levin, S.B., Broder, J., and Lieberman, R. 1954. Crystal growth by the tip fusion method. Review of Scientific Instruments 25: 298-299.
- Klysubun, W. 2017. X-ray absorption spectroscopy (XANES and EXAFS). [Online]. Available from: slri.or.th [13 January 2017]
- Kurlov, V.N. 2016. Sapphire: properties, growth, and applications. In pp. 1-11. Reference Module in Materials Science and Materials Engineering: Oxford.
- Kurlov, V.N., Rossolenko, S.N., Abrosimov, N.V., and Lebbou, K. 2010. Shaped crystal growth. In pp. 277-354. Springer Science & Business Media.
- Lancashire, R.J. 2019. Crystal Field Theory. [Online]. Available from: chem.libretexts.org

- Laurs, B.M., Devouard, B., Shigley, J.E., Fritsch, E., and Muhlmeister, S. 1998. Separating natural and synthetic rubies on the basis of trace-element chemistry. Gems & Gemology 34: 80-101.
- Loeffler, B.M., and Burns, R.G. 1976. Shedding light on the color of gems and minerals: the selective absorption of light according to wavelength—the result of various electronic processes whose energies correspond to certain wavelengths of visible light—gives minerals their distinctive hues. American Scientist 64: 636-647.
- Lu, R. 2013. Yellow synthetic sapphire colored by trapped-hole mechanism. Gems & Gemology 49: 50-51.
- Martin, G., and Pretzel, B. 1991. UV-Vis-NIR spectroscopy: what is it and what does it do. V&A Conservation Journal 1: 13-14.
- Mila, F., et al. 2000. Orbitally degenerate spin-1 model for insulating V_2O_3 . Physical Review Letters 85: 1-5.
- Monarumit, N., Satitkune, S., and Wongkokua, W. 2017. Role of ilmenite micro-inclusion on Fe oxidation states of natural sapphires. Journal of Physics: Conference Series 901: 012074.
- Monarumit, N., Wongkokua, W., and Satitkune, S. 2016. Fe^{2+} and Fe^{3+} oxidation states on natural sapphires probed by x-ray absorption spectroscopy. Procedia Computer Science 86: 180-183.
- Muhlmeister, S., Emmanue, F., Shigley, J.E., Devouard, B., and Laurs, B.M. 1998. Separating natural and synthetic rubies on the basis of trace-element chemistry. Gems & Gemology 34: 80-101.
- Mungchamnankit, A., Kittiauchawal, T., Kaewkhao, J., and Limsuwan, P. 2012. The color change of natural green sapphires by heat treatment. Procedia Engineering 32: 950-955.
- Na-Phattalung, S., Limpijumnong, S., T-Thienprasert, J., and Yu, J. 2018. Magnetic states and intervalence charge transfer of Ti and Fe defects in α - Al_2O_3 : the origin of the blue in sapphire. Acta Materialia 143: 248-256.

- Nassau, K. 1972. Dr. AVL Verneuil and the synthesis of ruby and sapphire. Journal of Crystal Growth 12-14: 12-18.
- Nassau, K. 1978. The origin of color in minerals. American Mineralogist 63: 219-229.
- Nassau, K. 1980. The causes of color. In pp. 124-155. Freeman.
- Nassau, K. 1987. The fifteen causes of color: the physics and chemistry of color. Color Research & Application 12: 4-26.
- Nassau, K. 1990. Synthetic gem materials in the 1980s. Gems & Gemology spring: 50-63.
- Nassau, K. 2001. The colour of metal compounds. Color Research & Application 26: 173-174.
- Nassau, K., and Valente, G.K. 1987. The seven types of yellow sapphire and their stability to light. Gems & Gemology winter: 222-231.
- Newton, I. 1952. Opticks. In pp. 215-218. Courier Corporation.
- Nikolskaya, L.N., Terekhova, V.M., and Samoilovich, M.I. 1978. On the origin of natural sapphire color. Physical Chemistry of Minerals 3: 213-224.
- Parikh, P., et al. 2002. Comparative study of the electronic structure of natural and synthetic rubies using XAFS and EDAX analyses Bulletin of Materials Science 25: 653-656.
- Peretti, A., and Günther, D. 2002. The color enhancement of fancy sapphires with a new heat-treatment technique (Part A): Inducing color zoning by internal migration and formation of color center. Contributions to Gemology 11: 1-48.
- Pisutha-Armond, V., Hager, T., Atichart, W., and Wathanakul, P. 2006. The role of Be, Mg, Fe and Ti in causing colour in corundum. Journal of Gemmology 30: 131-143.
- Pisutha-Armond, V., Sutthirat, C., Artichart, W., Wathanakul, P., and Suksawee, N. 2012. Corundum treatments and the causes of color. SWU Sci. J. 28: 1-12.
- Rückamp, R., et al. 2005. Optical study of orbital excitations in transition-metal oxides. Journal of Physics 7: 144.
- Saeseaw, S., Pardieu, V., Weeramonkhonlert, V., Sangsawong, S., and Moyal, J. 2015. An analysis of synthetic ruby overgrowth on corundum. [Online]. Available from: giathai.net [10 june 2015]

- Schmetzer, K., and Peretti, A. 1999. Some diagnostic features of russian hydrothermal synthetic rubies and sapphires. Gems & Gemology 35: 17-28.
- Schmetzer, K., and Peretti, A. 2000. Characterization of a group of experimental Russian hydrothermal synthetic sapphire. Journal of Gemmology 27: 1-7.
- Schwarz, D., et al. 2008. Rubies and sapphires from Winza, Central Tanzania. Gems & Gemology 44: 322-347.
- Shen, C., and Lu, R. 2018. The color origin of gem diaspore: correlation to corundum. Gems & Gemology 54: 47-56.
- Shor, R., and Weldon, R. 2009. Ruby and sapphire production and distribution: a quarter century of change. Gems & Gemology 45: 236-259.
- Smith, H.G.F. 2000. Alexandrite gemstone buyer and jewelry collector guide. [Online]. Available from: alexandrite.net
- Soonthorntantikul, W., Atikarnsakul, U., and Weeramonkhonlert, V. 2016. Update on spectroscopy of “Gold Sheen” sapphires. Gems & Gemology 52: 413-414.
- Subashini, B., and Govindarajan, G. 2017. Introduction to crystal growth techniques International Journal of Engineering and Techniques 3: 1-5.
- Sun, Z., Palke, A.C., and Renfro, N. 2015. Vanadium and chromium bearing pink pyrope garnet: characterization and quantitative colorimetric analysis. Gems & Gemology 51: 348-369.
- Sutherland, F., Zaw, K., Meffre, S., Yui, T.F., and Thu, K. 2014. Advances in trace element “fingerprinting” of gem corundum, ruby and sapphire, Mogok area, Myanmar Minerals 5: 61-79.
- Sutherland, F.L., Schwarz, D., Jobbins, E.A., Coenraads, R.R., and Webb, G. 1998. Distinctive gem corundum suites from discrete basalt fields: a comparative study of Barrington, Australia, and West Pailin, Cambodia, gemfields. Gems & Gemology 26: 65-85.
- Thomas, V.G., Mashkovtsev, R.I., Smirnov, S.Z., and Maltsev, V.S. 1997. Tairus hydrothermal synthetic sapphires doped with nickel and chromium. Gems & Gemology 33: 188-202.
- Tilley, R.J.D. 2013. color centers Encyclopedia of Color Science and Technology 223: 1-9.

- Tromp, M., Moulin, J., Reid, G., and Evans, J. 2007. Cr K-Edge XANES spectroscopy: ligand and oxidation state dependence-what is oxidation state. *AIP Conference Proceedings* 882: 699-701.
- Ueltzen, M. 1993. The Verneuil flame fusion process. *Journal of Crystal Growth* 132: 315-328.
- Verneuil, A. 1904. Reproduction artificielle du rubis par fusion. *Nature (Paris)* 32: 77.
- Wang, H.A., Lee, C.H., Kroger, F.A., and Cox, R.T. 1983. Point defects in α -Al₂O₃:Mg studied by electrical conductivity, optical absorption, and ESR. *Physical Review* 27: 3821-3841.
- Weldon, R. 2002. *An introduction to synthetic gem materials*. [Online]. Available from: gia.edu
- Winchell, H. 1944. Orientation of synthetic corundum for jewel bearings. *American Mineralogist: Journal of Earth and Planetary Materials* 29: 399-414.
- Wongkokua, W., Pongkrapan, S., Dararutana, P., T-Thienprasert, J., and Wathanakul, P. 2009. X-ray absorption near-edge structure of chromium ions in α -Al₂O₃. *Journal of Physics* 185: 1-4.
- Wongrawang, P., Monarumit, N., Thammajak, N., Wathanakul, P., and Wongkokua, W. 2016. Oxidation states of Fe and Ti in blue sapphire. *Materials Research Express* 3: 1-7.
- Zaw, K., Sutherland, L., Yui, T.F., Meffre, S., and Thu, K. 2015. Vanadium-rich ruby and sapphire within Mogok gemfield, Myanmar: implications for gem color and genesis. *Mineralium Deposita* 50: 35-39.



จุฬาลงกรณ์มหาวิทยาลัย
CHULALONGKORN UNIVERSITY

VITA

NAME Ontima Yamchuti

DATE OF BIRTH 29 May 1991

PLACE OF BIRTH Bangkok

INSTITUTIONS ATTENDED 2006 Benjamarachalai school, Bangkok (high school)
2009 Department of physics, Faculty of Science, Silpakorn University

HOME ADDRESS 543/21 Jarunsanitwong road, Bangkhunsri, Bangkoknoi, Bangkok 10700, Thailand

PUBLICATION Yamchuti, O., Kanitpanyacharoen, W., Sutthirat, C., Klysuban, W., and Amonpattarakit, P. 2018. OXIDATION STATES OF TRACE ELEMENTS IN SYNTHETIC CORUNDUM in The 44th Congress on Science and Technology of Thailand (STT 44) pp. 659-668. Bangkok International Trade & Exhibition Centre (BITEC) Thailand The Science Society of Thailand Under the Patronage of His Majesty the King